The University of New South Wales

School of Mechanical and Manufacturing Engineering

An Investigation into the Damping of a V8 Supercar

Jarrod Biti

3132411

Bachelor of Engineering (Mechanical)

Supervisor: Dr Nicole Kessissoglou

Industry Supervisor: Mr Danny Nowlan

October 2008

Abstract

The effect that the choice of suspension dampers has on a V8 Supercar's performance is an often misunderstood area. The increasing competitiveness of the V8 Supercar category and the reduced opportunities for testing mean that the team that can optimise their damper setup the quickest is likely to have a large advantage across the entire race meeting. In the past the selection of dampers was done empirically. The increasing availability of computational power means that numerical simulation is now a viable method of optimising a vehicle before it arrives at the track. This thesis outlines the development of the equations of motion for some simple vehicle models. It then demonstrates how these equations can be solved to estimate the road holding performance of a race car. Use is made of the ChassisSim race car simulation package to complete a more detailed analysis. The use of lap time optimisation, and damper histogram analysis are studied, and a comparison between these two methods presented. Although results for one particular vehicle have been studied, the focus throughout is to demonstrate numerical and computational techniques that can be used to optimise a V8 Supercar's dampers. A degree of generality has been maintained while analysing these techniques so that they can be applied to a variety of different categories of race cars. It was found that different techniques give different results. It is the job of the vehicle's engineer to be able to interpret which of these results is most important for a given set of circumstances.

Declaration of Originality

I, the undersigned declare that I am the sole author of this work, and that any content taken from other sources has been fully cited.

.....

Jarrod Biti

24th October, 2008

Acknowledgements

Completing this thesis, and indeed my entire degree has not always been an easy journey. There are many people who have made the completion of my degree possible, and I would like to thank them here.

My supervisor, Dr Nicole Kessissoglou, who has not only provided invaluable advice, but also taken time out of her maternity leave to provide me assistance.

Mr Danny Nowlan, Director of ChassisSim Technologies, for not only suggesting the detailed aims and objectives of this thesis, but also providing me with much technical assistance, career advice and insight into the global motor racing industry.

Barry Ryan of Perkins Engineering, who provided the initial motivation for this thesis.

Mum, Dad, Granny and Grandpa, for your love, advice and for always being so supportive. Without all of your sacrifices, I would never have been able to attend Goldstein College, where I met the many lifelong friends who have made the journey so enjoyable.

My family, including Cassie, Liam, Alexander, Nan and Pop, whose love, support and humour have kept me motivated to achieve my goals.

All of my closest friends, for not only providing a lot of laughs and moral support, but also for helping edit, cooking dinner when I have been too busy and providing help with computer problems.

And especially, Kristine, who has been with me since the beginning of my Mechanical Engineering degree. Thank you for all of the good times that we have shared, and for being so patient and so supportive throughout my studies. I love you, and I look forward to our future together.

From the bottom of my heart, a huge thank you to everyone for all of your help, love and support. Completing my degree would simply not have been possible without you.

Jarrod

October 2008

Table of Contents

List of Figures

List of Tables

List of Symbols

a	roughness of the road
A	amplitude of harmonic motion
$[A]$	combined mass, stiffness, damping matrix
$a_{lat_{max}}$	maximum lateral acceleration
$a_{m,n}$	element m, n of combined mass, stiffness, damping matrix
b	wavelength distribution of road
BPV	bypass velocity
BPV_{shock}	bypass velocity of the shoc absorber

BPV_{wheel}	bypass velocity as it applies to the wheel
c	damping coefficient
c_s	damping coefficient of suspension
c_{s1}	damping coefficient of suspension at front
c_{s2}	damping coefficient of suspension at rear
c_{shock}	damping coefficient of actual shock absorber
c_t	damping coefficient of tyre
c_{t1}	damping coefficient of tyre at front
c_{t2}	damping coefficient of tyre at rear
c_{wheel}	damping coefficient as it applies to the centre of wheel hub
CdF	linear damping coefficient at front
CdR	linear damping coefficient at rear
CoG	centre of gravity
$CoGH$	height of centre of gravity
CPL	contact patch load variation
DRF	linear damping ratio at front
DRR	linear damping ratio at rear
f	frequency
F	force
f_n	centre frequency of band n
g	gravitational constant
$G(f)$	power spectral density of road profile
h	width of frequency band
H	displacement between centre of gravity height and roll centre height

$\left\|H_{\frac{1}{4}}(\omega)\right\|$	frequency response function of quarter car sprung mass
$\bar{H}_{f_n}$	mean value of frequency response function in frequency band with centre frequency f_n
$\|H_{SDOF}(\omega)\|$	frequency response function of single degree of freedom system
$\|H_u(\omega)\|$	frequency response function of unsprung mass
$I_{1/2}$	mass moment of inertia of sprung mass about the axis of pitching motions
k	spring rate
k_s	spring rate of suspension
k_{s1}	spring rate of suspension at front
k_{s2}	spring rate of suspension at rear
k_{spring}	spring rate of the actual spring
k_t	spring rate of tyre
k_{t1}	spring rate of tyre at front
k_{t2}	spring rate of tyre at rear
k_{wheel}	spring rate as it applies to the centre of the wheel hub
l_B	lateral distance between rear suspension mounts and centre of gravity of chassis
l_F	lateral distance between front suspension mounts and centre of gravity of chassis
m	mass
$m_{1/2}$	half car chassis mass
$m_{1/4}$	quarter car chassis mass

m_T	total mass of vehicle
m_u	unsprung mass of wheel and suspension linkages
m_{uB}	unsprung mass of rear wheel and suspension linkages
m_{uF}	unsprung mass of front wheel and suspension linkages
MR	motion ratio of suspension
MR_B	motion ratio of rear suspension
MR_F	motion ratio of front suspension
R	non-dimensional measure of road holding performance
RC	roll centre
RCH	height of roll centre
t	time
T	track witdth
$t_{0\rightarrow max}$	time from zero to maximum lateral acceleration
V	velocity
x	damper displacement
$\dot{x}_{peak}$	peak damper velocity
z	vertical displacement
$\bar{Z}^2$	mean square displacement
$\bar{Z}_{1,f_n}$	RMS displacement of road profile in frequency band with centre frequency f_n
$\bar{Z}_{2,f_n}$	RMS displacement of wheel motion in frequency band with centre frequency f_n
z_i	vertical displacement about position number i
Z_i	amplitude of harmonic vertical displacement about position number i

$\dot{\Delta}_{FD_{max}}$	maximum front damper velocity due to body roll
Δ_L	deflection of left spring
Δ_R	deflection of right spring
$\dot{\Delta}_{RD_{max}}$	maximum rear damper velocity due to body roll
η	tyre efficiency
θ	pitch of sprung mass
θ_{roll}	angle of roll of sprung mass about centreline of vehicle
ζ	damping ratio
$\zeta_{HS\ Bump}$	damping ratio in the high speed bump region of curve
$\zeta_{HS\ Rebound}$	damping ratio in the high speed rebound region of curve
$\zeta_{LS\ Bump}$	damping ratio in the low speed bump region of curve
$\zeta_{LS\ Rebound}$	damping ratio in the low speed rebound region of curve
$\bar{\sigma}$	RMS value of difference between amplitude of motion of the tyre and road profile displacements
ω	radian frequency

Chapter 1 – Introduction

1.1 Introduction to Damping on Race Cars

There are three main objectives involved in suspension design. These are:

- maximising road holding
- maximising passenger comfort
- minimising ‘rattle space’.

Unfortunately, these three objectives are often conflicting. The problem is made a little simpler when designing race car suspension, as the comfort of the passenger may be disregarded. Minimising rattle space is largely a consequence of suspension geometry, which is beyond the scope of this thesis. The main role of a suspension engineer at a race meeting is to tune the suspension in such a way as to maximise the road holding performance of the vehicle. One of the more difficult components in achieving this is the selection of the dampers. This will be the emphasis of this thesis.

To maximise road holding, a car’s suspension must allow its tyres to follow the road profile. This is often achieved by using what is known as ‘soft’ suspension, or using shock absorbers that employ a low damping coefficient. Another consideration in maximising the road holding of a vehicle is to minimise the body roll of the chassis. Typically, this can be achieved by employing ‘hard’ suspension with higher damping coefficients. Both of these techniques are aimed at reducing the load fluctuations between the tyre and the road.

Most modern race cars employ dampers with non linear characteristics, which are often specified on a graph of force versus velocity, known as the damper curve. These are non-linear, in that they usually employ two different damping coefficients, one in the low velocity region of the curve, and another in the high speed region. Typically, these will have a higher damping coefficient at low velocities where body roll tends to occur, and a lower damping coefficient at higher velocity, where road disturbances tend to occur [1]. The damping coefficient is also often higher in rebound, which occurs as the damper is extending.

The shape of these damper curves has developed over many years, mostly through empirical research. The reason for this is that it has always been cheaper and easier to take a trial and error approach to damper selection on race cars, than to try to model these mathematically. For example, when compared to the aviation industry, budgets and the consequence of faulty or misunderstood equipment on a race car are relatively low. This has meant that highly scientific analysis and computer simulation has until recently, been largely unjustified. However track days for testing of race cars are becoming extremely expensive and restrictions are often made on the number of these allowed per season by the sport's regulating authorities. These restrictions are put in place as a means of reducing the expense of owning a race car, but the end result is that the team that can arrive at the track with a car which is already close to optimal is going to be ahead for the entire racing weekend. Combined with an increasing availability of computational power, race car simulation packages are becoming a standard means for evaluating a car's performance.

1.2 Thesis Objectives

This thesis investigates the effect that the choice of dampers will have on a V8 supercar. The type of damper considered will be in compliance with Section C 9.4 of the "V8 Supercars Operations Manual Rules" [2], attached as Appendix A. Note particularly paragraph C 9.4.8:

"Only four (4) shock absorber characteristics that can be adjusted from the outside of each shock absorber are permitted, but this number does not include shock absorber gas pressure adjustment."

The four adjustments being referred to are:

1. Low speed bump damping coefficient (or damping ratio)
2. Low speed rebound damping coefficient (or damping ratio)
3. High speed bump damping coefficient (or damping ratio)
4. High speed rebound damping coefficient (or damping ratio).

These adjustments can be made independently for each of the four dampers on the vehicle. This thesis aims to select the most appropriate values for each of these four adjustable parameters. It also aims to outline a method of estimating the optimal damper characteristics, which can be used by V8 Supercar teams before they even arrive at the race track, and also to account for the changes in the vehicle's setup due to changing track conditions. This will therefore give these teams a big advantage for the entire race meeting.

Extensive use will be made of the race car simulation package *ChassisSim*. This is a simulation and testing package used by many professional race teams across a number of racing categories, including low downforce vehicles such as V8 Supercars, as well as high downforce categories such as Formula 3 and Formula 3000. The package has a number of toolboxes, which allow the investigation of different setups on the racecar's dynamic performance. Particular use will be made of:

- Seven post shaker rig, which uses a sweep of harmonic inputs of varying frequencies at the tyre, allowing the estimation of the frequency response functions of the various degrees of freedom of the system
- Lap time simulation, which assumes that the "perfect driver" is driving the vehicle at the limit of the tyre's traction at all times
- Optimisation toolbox, which varies specified parameters of the vehicle and uses a lap time estimation to find the optimal settings.

Although the concepts and examples provided in this thesis relate most directly to V8 supercars, a level of generality will be kept in the calculations so that the methods employed can be used on any other low downforce racing car, and to a lesser extent, high downforce vehicles.

1.3 Literature Review

1.3.1 V8 Supercars

V8 Supercars are an Australian touring car motor racing category. They are very loosely based on current model Ford Falcon and Holden Commodores, although aside from basic appearances, they bear very little in common with their commercial counterparts. The rules of the category are quite restrictive, placing a lot of emphasis on being able to "tune" the vehicle to the track conditions in order to be competitive.

As far as race cars go, V8 Supercars are rather peculiar, with many of their characteristics being far from optimal. For instance:

- The cars create only a small amount of downforce, meaning that much of the traction of the tyres must be created purely by mechanical grip
- They have a high unsprung mass, particularly at the rear wheels, which is undesirable as this mass cannot be easily controlled
- The rear suspension uses a live axle, which is inferior to the more common double wishbone style suspension
- In relative terms, the tyres are quite thin, meaning that throttle applications must be carefully controlled.

These factors make for vehicles which handle poorly in comparison to other categories of motorsport, but are extremely entertaining to watch. This is one of the reasons for the

increasing popularity of the category, but means that many compromises must be made by the vehicle's engineers in order to obtain the best performance of the vehicle, without prematurely destroying the tyres.

1.3.2 Dampers

The primary role of a damper on a vehicle is to oppose the undesirable motions of the suspended vehicle body and to control the oscillation of the sprung masses. As one of the most fundamental contributors to a vehicle's handling, dampers have been studied at great length. This began with the introduction of internal combustion engine driven vehicles in the late nineteenth century [3], when the increased speed available due to these engines made an undamped vehicle inherently unsafe. Since this time, dampers have undergone a number of significant transformations.

In modern vehicles, there are two major classifications of dampers, passive and active dampers. Passive damping systems function with fixed operating characteristics, such as damping coefficient. Although these characteristics may be non linear and can sometimes be adjusted by the operator, they will not change in real-time to adjust to the road conditions or the behaviour of a vehicle. This is in contrast to an active suspension system, where an adaptive control system is used to ensure that the optimum damping force is produced in real time.

A historical review of the development of active and semiactive suspension systems is presented by Karnopp [4]. Passive damping systems are still the more common system,

used on most family vehicles and even a large majority of race cars. The dampers considered in this paper are classified as passive dampers, as these are the only type of damper allowed under the rules of V8 Supercar Racing [2].

Damping on a V8 Supercar is provided by the means of an adjustable hydraulic shock absorber. This is the most common type of shock absorber used on race cars. The hydraulic shock absorber works by forcing a viscous fluid through small passageways and valves as the damper is either extended or compressed. By altering the configurations of these passages and valves, it is possible to vary the damping characteristics of a shock absorber. A typical hydraulic shock absorber configuration is shown in Figure 1-1.

Figure 1-2 shows the damping characteristics of a typical adjustable race car damper, as specified in the time domain. Features to note from this diagram are that there is a higher damping ratio ζ (steeper slope) in the low speed region of the damper curve compared to the damping ratio in the high speed region. This occurs in both bump and rebound. These represent the four allowable adjustments that can be made to the damper under the rules of V8 Supercar racing. The low speed movements are usually a result of undesirable body roll and weight transfer, which is controlled by the higher damping coefficient. On the other hand, high speed damper motions tend to be caused by inconsistencies in road profile, so a lower damping coefficient is employed to allow the tyre to maintain a consistent grip. This is achieved through the use of blow-off or pressure control valves [5]. It should also be noted that the rebound force of the damper is typically higher than the bump force.

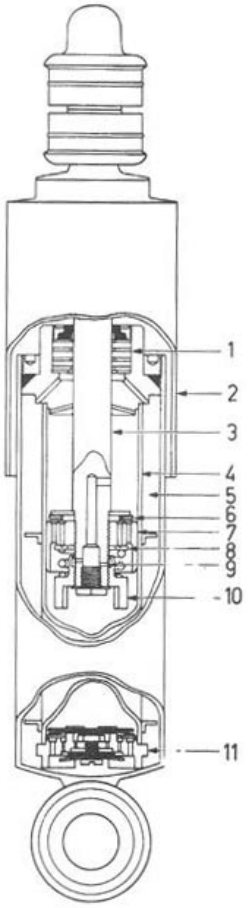

Figure 1-1: A double tube damper showing the following features - 1 seal; 2 shroud; 3 rod; 4 inner cylinder; 5 annular foot and gas chambers; 6 piston compression valve; 7 piston; 8 extension valve; 9 parallel hole feed; 10 adjuster; 11 foot valve. [3]

It can be observed that most dampers and essentially all race car dampers are non-linear and asymmetric. A linearisation technique that is most often used in the analysis of such dampers is to treat the damper as a series of piecewise linear functions [5], [6], [7]. Liu *et al.* [6] studied the accuracy of this model using the program ADAMS and found that although the piecewise linear model was sufficient an unsymmetrical hysteric loop could be used to more accurately and practically model a conventional damper.

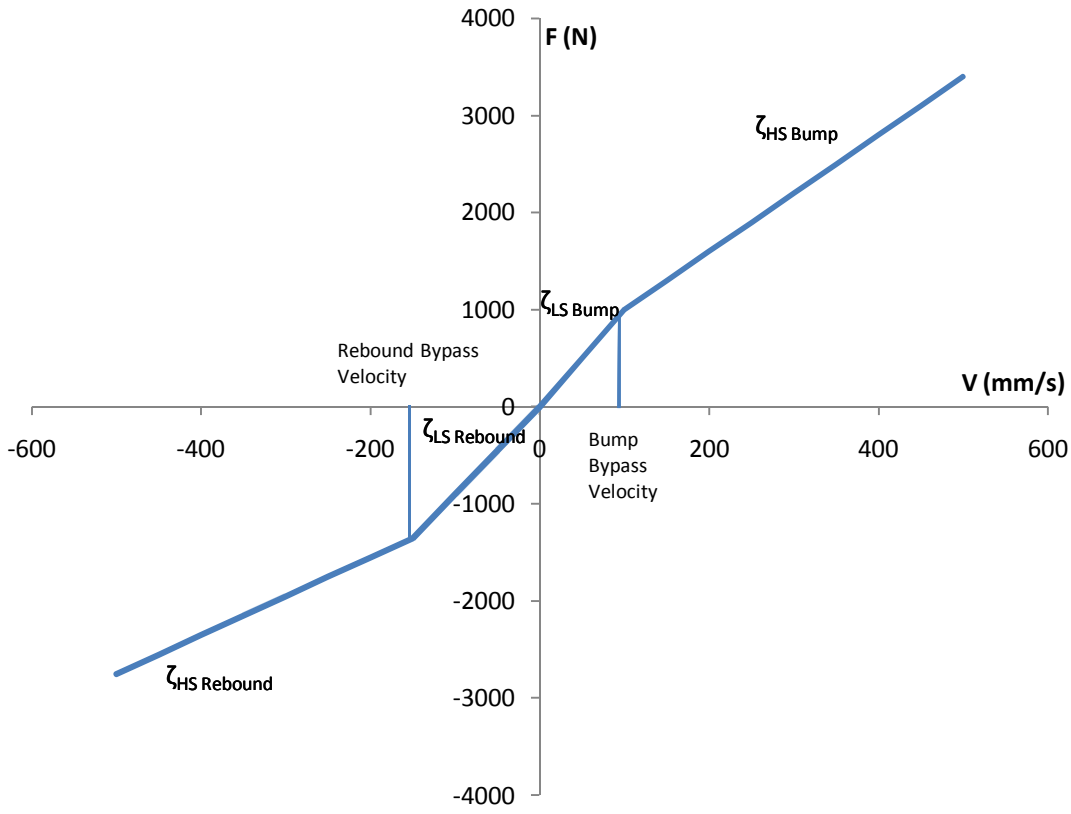

Figure 1-2: Typical race car damper characteristic [8].

The current conventional damper characteristics have been developed over years of empirical testing and data collection. This curve is accepted as being the best method of passively controlling the conflicting design problems of allowing the tyre to follow the road profile while minimising body roll. An explanation of why it is desirable to prevent body roll, but allow suspension movement is given in section 1.3.2.

As shown in Figure 1-2 the force provided by a damper is a function of the velocity of the damper movements. Laboratory testing of a damper usually involves a pure

sinusoidal input, using a set frequency and amplitude on a damper dynamometer [9]. The equation of motion for this system may be described in its most simple form by the following equation:

$$x = Asin(\omega t) \tag{1.1}$$

A conventional, velocity dependent damper is analysed by varying the frequency (ω) while holding stroke (A) constant. The damper force is measured at the peak velocity point of the harmonic displacement [10]. The peak velocity is given by:

$$\dot{x}_{peak} = 2\pi \times A \times \omega \tag{1.2}$$

Because the approaches to engineering a race car have developed over many years in a different manner to the more pure engineering subjects, race cars have developed their own nomenclature whose definitions are not strictly correct according to a purely vibration analysis study. The first of these peculiarities occurs around the term “damping ratio”. This term is still used in the way that it is generally intended, although for a race car some rather large assumptions are made in order to simplify the calculations. Firstly, the car may have a different damping ratio at each of its four “corners”. Each of the four corners can be represented by the two degree of freedom quarter car model shown in Figure 1-3 (an extended explanation of the treatment of this model is presented in section 2.2).

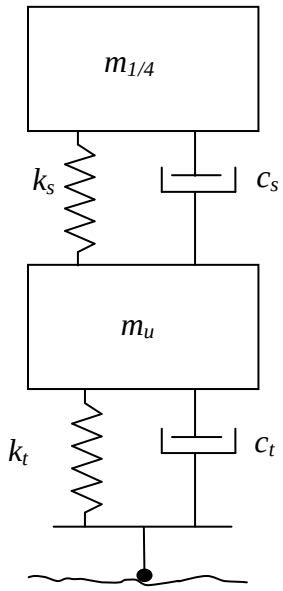

Figure 1-3: 2-DOF quarter car model

As explained by Nowlan [8], some assumptions may be made. These are:

- The damping of the tyre is negligible
- The spring rate of the tyre is much higher than the spring rate of the suspension elements
- The sprung mass of the vehicle body is much higher than the unsprung mass of the wheel and axle.

This leads to the following definition of damping ratio, which can be calculated individually at each corner:

$$\zeta = \frac{c_s}{2\sqrt{k_s m_{1/4}}} \tag{1.3}$$

In conventional vibration analysis the term “overdamped” refers to a system with a damping ratio greater than 1, while the term “underdamped” refers to a system with a damping ratio less than 1. For race car engineers these terms are used quite differently. “Overdamped” simply refers to a vehicle whose damping ratio is too high for optimal performance, and “underdamped” is a vehicle whose damping ratio is lower than optimal. Of course, the position of these optimal performance points is always the subject of debate, so these terms tend to be used in a subjective manner.

1.3.3 Suspension System

Vehicle suspension systems may be defined as being either independent or dependent suspension systems. An independent system is one where each wheel is free to move independently of the movements of the other wheels. In other words, in an independent suspension system, each wheel has its own degree of freedom. On the other hand, in a dependent suspension system, the movement of one wheel may be reliant upon the movement of another. Most high performance vehicles will employ an independent suspension system. The most common independent race car suspension geometry is the double wishbone suspension, as shown in Figure 1-4. This is what is used for the front suspension of a V8 Supercar.

V8 Supercar legislation requires the use of a dependent rear suspension known as a “live axle”. This suspension arrangement uses a solid or beam axle between the two rear wheels, which is located laterally by a Watt’s linkage, as shown in Figure 1-5. There are a number of handling disadvantages inherent in the use of a live axle. Most importantly,

each wheel cannot respond to bumps and other forces independently. The live rear axle also means an increase in the unsprung mass of the vehicle as the differential and drive shaft become part of this unsprung mass [11]. Large unsprung masses are undesirable for high performance handling of a vehicle, as the higher mass means that the wheels will resist following the contours of the road, resulting in a loss of available traction.

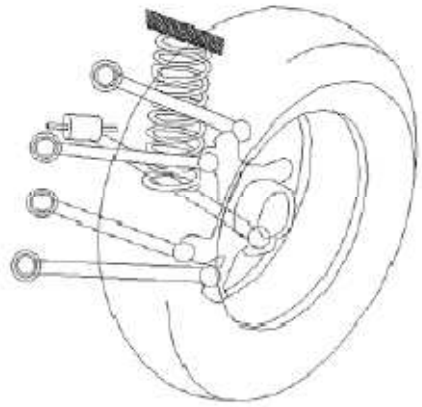

Figure 1-4: Double wishbone suspension [12].

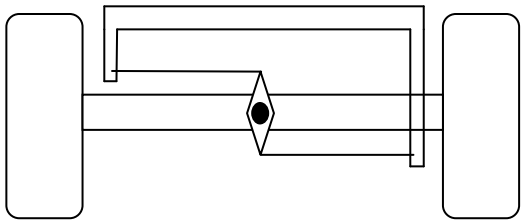

Figure 1-5: Live rear axle with Watt's linkage

Spring and damper analysis is most straightforward when the spring and damper are assumed to act vertically on the centre of the wheel hub. In reality, suspension geometry factors mean that this is unlikely to be the case, particularly in the case of double wishbone suspension. To specify the actual spring rate and damping coefficient required, the motion ratio of the suspension must be determined. The motion ratio can be defined as the number of units of contraction of the suspension elements for every unit of vertical displacement of the centre of the wheel hub. This leads to some important relations, the derivations of which have been described by Milliken [10]:

$$k_{wheel} = k_{spring} \times (MR)^2 \tag{1.4}$$

$$c_{wheel} = c_{shock} \times (MR)^2 \tag{1.5}$$

$$BPV_{wheel} = BPV_{spring} \div MR \tag{1.6}$$

where :

MR is the motion ratio of the suspension linkages

k_{wheel} is the spring rate as it applies at the centre of the wheel hub

k_{spring} is the spring rate as it applies at the spring itself

c_{wheel} is the damping coefficient as it applies at the centre of the wheel hub

c_{shock} is the damping coefficient as it applies at the actual shock absorber

BPV_{wheel} is the bypass velocity of the damper it applies at the centre of the wheel hub

BPV_{shock} is the bypass velocity of the damper it applies at the actual shock absorber

Using these relations, the spring and damper analysis can be performed by assuming that these components act at the centre of the wheel. This is known as a “wheel rate

model". Once the analysis is complete, the values found for the wheel rate model can simply be converted to the correct values for the actual spring and damper. For a double wishbone suspension, the motion ratio is normally a number less than 1, and for a live rear axle, the motion ratio can be approximated to be equal to 1.

When analysing the performance of a race car, one of the most important things to understand is the behaviour and performance of the tyre, as it is through the four tyres that all accelerating, braking and cornering forces must be transmitted. As can be seen in Figure 1-6 the traction available of a tyre is non-linear. Tyre efficiency can be defined as:

$$\eta = \frac{(Traction)}{(Vertical\ Load)} \times 100\% \tag{1.7}$$

The higher the vertical load on the tyre, the lower its efficiency. To maximise the amount of traction available to the car at any time, an even weight distribution must be present across all four tyres. Although it is possible to set-up the car in such a way that statically all four cornerweights of the car are equal, it is critical to minimise the dynamic weight transfer of the vehicle [11]. The road holding performance of a vehicle can be related to the standard deviation of the vertical load of the tyre to the road normalised with respect to the static value [13], [14]. A similar measure of the road holding performance of a race car was developed by Sugasawa *et al.* [15] and also presented by Milliken *et al.* [10]. Their method involves relating the road holding performance of the vehicle to the load fluctuation rate of the tyre. This method results

in a non-dimensional “evaluation criterion”, usually represented by the symbol R, which can be used to quantify the road holding performance of the vehicle.

The traction available to a vehicle, and therefore the magnitude of the accelerating, braking and cornering forces the tyres can transmit, is approximately equal to the sum of the traction available at the individual tyres [11]. Body roll induced weight transfer may increase the traction available at some of the tyres, but the loss of traction at the remaining tyres is greater than this gain, as illustrated in Figure 1-6, resulting in a net loss of performance of the vehicle.

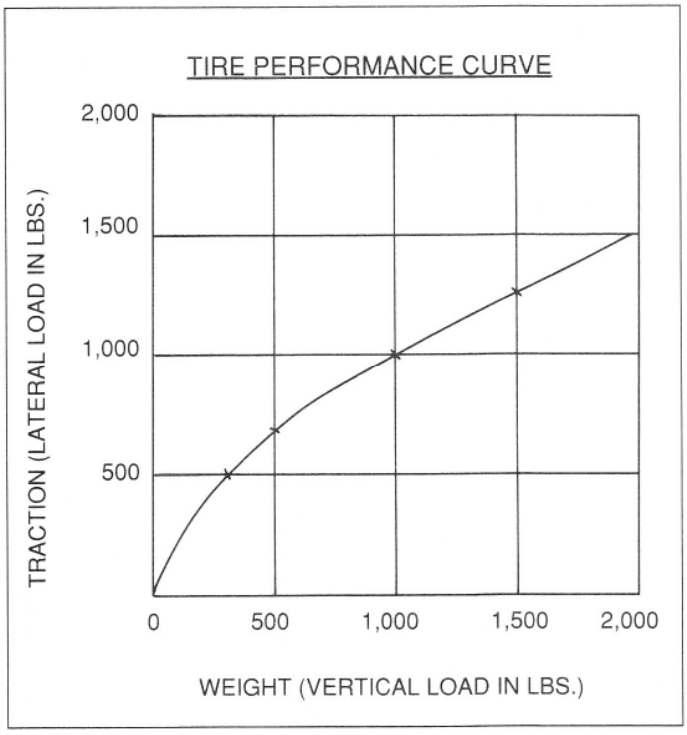

Figure 1-6: Typical race car tyre performance curve [11].

Variations in tyre load do not only occur due to weight transfer. They are also the result of displacements in the road profile. A tyre acts as a spring with negligible damping.

Any compression of this spring, whether it be due to an impulse load or a harmonic fluctuation, will create a harmonic oscillation in the tyre force. This oscillation of normal force will result in a net loss of traction for the vehicle.

What is also critical to note in this example is that when the tyre has traction to the road, the coefficient of friction between the road and tyre is the static value. Once traction has been broken, the coefficient of friction between the road and the tyre becomes the dynamic value, which is much lower. This means that once traction has been broken, the driver must slow the tyres down considerably in order to regain this traction.

It is known empirically that body roll tends to occur at a lower frequency than disturbances due to road profile. Further, there is a close relationship between frequency and peak velocity. This is what has led race car engineers over the years to employ the piecewise linear damper curve like the one in Figure 1-2. Using a higher damping ratio in the low speed region, the low frequency body roll of the vehicle can be controlled. Using a lower damping ratio in the high speed region will allow high frequency flexibility of the suspension to adequately follow the road profile [8].

1.3.4 Simulation in Racecar Design

The use of simulation in race car design is becoming increasingly common, and the accuracy of these simulations is greatly determined by the accuracy of the damper model [16]. Simulation may be mathematical, computational or physical. At the heart of

any race car dynamics simulation is the necessity for an accurate and realistic road profile input. This holds true whether the simulation is purely mathematical or physical as is the case for a seven post shaker rig. The information of the shape of the road profile is usually represented in the form of a power spectral density (PSD). Andrén [17] has conducted an extensive literature review on the use of PSD approximations in modelling road profiles. In his paper, Andrén has described the history and motivations for use of a PSD. He has also made comparisons between a number of different PSD models, and concluded spectral analysis to be a valid form of modelling the road profile. PSDs of road excitation are often determined by use of experimental data. Tamboli [18] found that this could be approximated to an exponentially decreasing curve.

Simulation is not always completed with the aid of a computer. Physical simulation of the dynamics of a race car is often achieved through the use of a seven post shaker rig. These rigs use seven actuators to simulate the dynamics of the vehicle. Four actuators operate at the wheels to simulate the road inputs. The other three are used to simulate the motions (including aerodynamic loads) of the sprung mass of the vehicle. Kowalczyk [19] studied the use of such seven post shaker rigs for the tuning of suspension systems. This study showed that the use of a seven post shaker rig allowed a greater understanding of the dynamics of a particular vehicle. It also found that many race teams do not have the resources to create fully non-linear simulations. In these vehicles the non-linear effects could be studied using the seven post shaker rig. Kelly *et al.* [20] came to a similar conclusion, finding the seven post shaker rig to be an important tool for helping engineers to set up their vehicles for specific tracks.

1.4 Thesis Layout

Chapter 1 provides background information on how and why damping is employed on V8 supercar. It also outlines the motivation and objectives of this thesis and the need for a race car to be properly tuned before arriving at the race track.

Chapter 2 is the development of the equations of motion necessary to model the dynamics of the vehicle.

Chapter 3 solves these equations to obtain the frequency response functions of a V8 supercar with typical vehicle parameters.

Chapter 4 uses the frequency response functions and the concept of “evaluation criterion” to obtain optimal damper properties for this system.

Chapter 5 is an introduction to the use of computer simulation in race car optimisation, and a demonstration of how the concept of “contact patch load” may be used to determine optimal damper characteristics.

Chapter 6 introduces non-linear damping and the concept of a bypass velocity, and uses both “lap time analysis” and “damper histogram analysis” to find the optimal shape of a V8 Supercar, non linear damper curve.

Chapter 7 compares the results obtained via the different methods of analysis, and explains some of the causes for discrepancy between these results.

Chapter 8 provides conclusions, and also some suggestions of where future work could be carried out within a similar area of study.

Chapter 2 – Dynamic Modelling of Vehicles and Dampers

To begin the study of the effect of damping coefficient on the performance of a racecar, it is first necessary to develop the equations of motion of the vehicle. Even a simplified vehicle model can require quite a complex analysis. This chapter begins with some basic vehicle dynamics concepts, and then builds upon these to create a more complete and accurate vehicle dynamics model.

2.1 Spring Mass Damper Subject to Base Excitation

The first model to be studied is the single degree of freedom spring-mass-damper system as shown in Figure 2-1. This system undergoes a forcing input due to displacement of the base. The single degree of freedom system is often studied due to its relative simplicity. In this case, the system may be thought of to represent a simplified model of the motion of a vehicle's chassis, given an identical simultaneous displacement of all four wheels. Because of its simplicity, this single degree of freedom model can be used to begin to derive the equations of motion for the more complicated systems to follow.

A free body diagram of this system is given in Figure 2-2. The degree of freedom of this system is the vertical displacement z_2 of mass m. The mass is supported by a spring with stiffness k and a damper with damping coefficient c. Displacements z_1 and z_2 are measured about their static equilibrium positions.

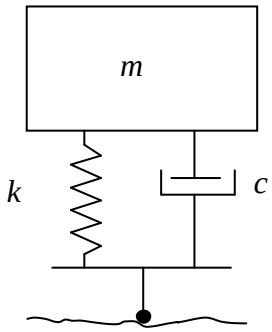

Figure 2-1: Single degree of freedom spring-mass-damper system

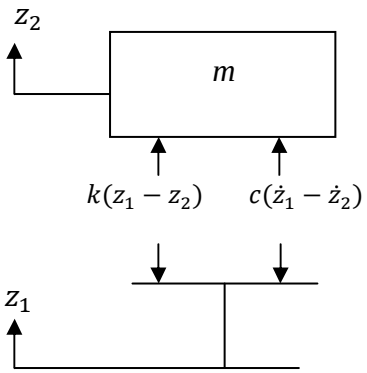

Figure 2-2: Free body diagram of SDOF spring-mass-damper system

Using Newton's second law of motion, the equation of motion of the system is given by:

$$m\ddot{z}_2 + c\dot{z}_2 + kz_2 = c\dot{z}_1 + kz_1 \tag{2.1}$$

If the motion of the base is harmonic then the motion of the output, that is, mass m, must also be harmonic. The output will have an identical frequency to the input, but will

likely have a different amplitude. The output is also likely to be out of phase with the input.

Assuming harmonic motion of base and the masses, and the displacements in complex notation can be represented as:

$$z_i(t) = Z_i e^{j\omega t} \quad i = 1,2 \tag{2.2}$$

where ω represents the radian frequency. Therefore:

$$\dot{z}_i(t) = Z_i j\omega e^{j\omega t} \quad i = 1,2 \tag{2.3}$$

$$\ddot{z}_i(t) = -Z_i \omega^2 e^{j\omega t} \quad i = 1,2 \tag{2.4}$$

For this study, the primary concern is in regard to the amplitude of motion of the various degrees of freedom of a system. It is necessary to determine how this amplitude varies with respect to the frequency of the system. Some phase lag will also exist. This is defined as the phase difference between the input to the system and the motion of its degrees of freedom. Because the road holding performance relies primarily on the amplitude of the motion of the masses, phase lag is of minor concern and is thus disregarded. Substituting equations (2.2), (2.3) and (2.4) into equation (2.1), the equation of motion of the single degree of freedom spring- mass-damper system may now be represented as:

$$[-m\omega^2 + j\omega c + k]Z_2 = [j\omega c + k]Z_1 \tag{2.5}$$

The frequency response function (FRF) of a system is a measure of the amplitude of an output of the system relative to its input, for a given frequency.

The FRF ($|H_{SDOF}(\omega)|$) of the base excited, single degree of freedom spring-mass-damper system may be obtained by manipulation of equation (2.5) as described in equations (2.6) to (2.13).

$$|H_{SDOF}(\omega)| = \left|\frac{Z_2}{Z_1}\right| \tag{2.6}$$

$$H_{SDOF}(\omega) = \frac{[j\omega c + k]}{[-m\omega^2 + j\omega c + k]} \tag{2.7}$$

Rationalising:

$$H_{SDOF}(\omega) = \frac{[k + j\omega c]}{[k - m\omega^2 + j\omega c]}.\frac{[k - m\omega^2 - j\omega c]}{[k - m\omega^2 - j\omega c]} \tag{2.8}$$

$$H_{SDOF}(\omega) = (k + j\omega c).\frac{(k - m\omega^2 - j\omega c)}{(k - m\omega^2)^2 + (c\omega)^2} \tag{2.9}$$

$$H_{SDOF}(\omega) = (k + j\omega c)\left[\frac{(k - m\omega^2)}{(k - m\omega^2)^2 + (c\omega)^2} - \frac{(j\omega c)}{(k - m\omega^2)^2 + (c\omega)^2}\right] \tag{2.10}$$

Making use of the property $|a + jb| = \sqrt{a^2 + b^2}$

$$|H_{SDOF}(\omega)| = \sqrt{k^2 + (\omega c)^2}.\sqrt{\left[\frac{k - m\omega^2}{(k - m\omega^2)^2 + (c\omega)^2}\right]^2 + \left[\frac{\omega c}{(k - m\omega^2)^2 + (c\omega)^2}\right]^2} \quad (2.11)$$

$$|H_{SDOF}(\omega)| = \sqrt{k^2 + (\omega c)^2}.\sqrt{\frac{[(k - m\omega^2)^2 + (\omega c)^2]}{[(k - m\omega^2)^2 + (c\omega)^2]^2}} \quad (2.12)$$

The final FRF of this system becomes:

$$|H_{SDOF}(\omega)| = \sqrt{\frac{k^2 + (\omega c)^2}{[(k - m\omega^2)^2 + (c\omega)^2]}} \quad (2.13)$$

This process may be simplified by using the MATLAB *'abs'* function, to return the complex modulus of equation (2.7).

2.2 Quarter Car Model

Although for most practical purposes, the single degree of freedom vehicle representation is too simplistic to be completely meaningful, its results, and the method of derivation of these results are a necessary building block when studying more complicated systems. The next simplest model to study is the two degree of freedom (2-DOF) system given in Figure 2-3. This is also known as the quarter car model, as it may

be thought of a representing the dynamics of a quarter of the car (for example, the front left quarter). The advantage of the 2-DOF quarter car model is that while still a relatively simple system to analyse, it allows a good approximation of the motion of both the chassis and the wheels of a vehicle.

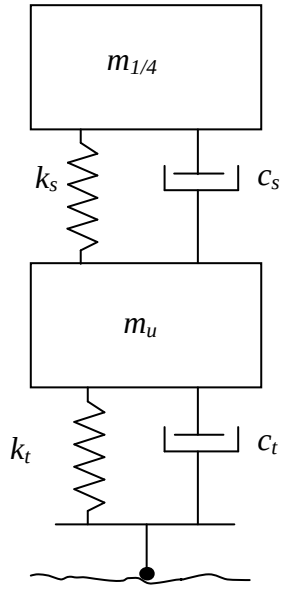

Figure 2-3: 2-DOF quarter car model

A free body diagram of the quarter car model is given in Figure 2-4. The degrees of freedom of this system are the vertical displacements z_2 and z_3 of masses m_u and $m_{1/4}$ respectively. The system is subjected to base excitation which is defined by the displacement z_1. Displacements z_1, z_2 and z_3 are measured relative to their static equilibrium positions. m_u represents the unsprung mass, which for this model is the mass of the wheel, tyre and a proportion of the suspension linkages, while $m_{1/4}$ refers to the sprung mass, in this case, the remaining mass of the suspension linkages, and a quarter of the mass of the chassis. k_s and k_t refer to the spring rate of the suspension

elements and spring rate of the tyre respectively, while c_s and c_t refer to the damping coefficient of the suspension elements and tyre.

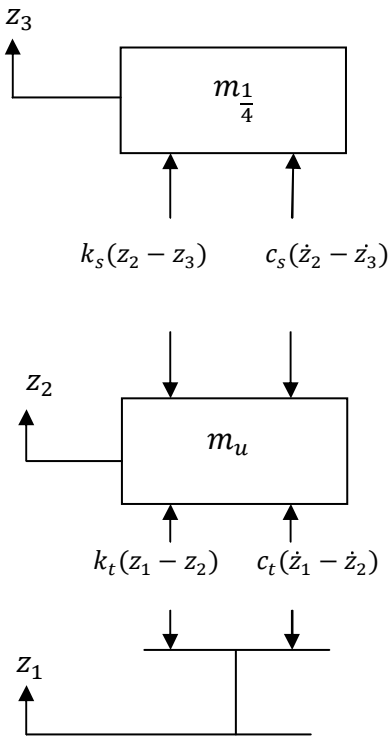

Figure 2-4: Free body diagram of 2-DOF quarter car model

Using Newton's second law of motion, the equations of motion for this system become:

$$m_u\ddot{z}_2 = k_t(z_1 - z_2) + c_t(\dot{z}_1 - \dot{z}_2) - k_s(z_2 - z_3) - c_s(\dot{z}_2 - \dot{z}_3) \quad (2.14)$$

$$m_{1/4}\ddot{z}_3 = k_s(z_2 - z_3) + c_s(\dot{z}_2 - \dot{z}_3) \quad (2.15)$$

Rearranging this system into its output and input components gives:

$$m_u\ddot{z}_2 + k_t z_2 + c_t\dot{z}_2 + k_s z_2 - k_s z_3 + c_s\dot{z}_2 - c_s\dot{z}_3 = k_t z_1 + c_t\dot{z}_1 \quad (2.16)$$

$$m_{1/4}\ddot{z}_3 - k_s z_2 + k_s z_3 - c_s \dot{z}_2 + c_s \dot{z}_3 = 0 \tag{2.17}$$

Assuming harmonic motion of base and the masses

$$z_i(t) = Z_i e^{j\omega t} \quad i = 1,2,3 \tag{2.18}$$

$$\dot{z}_i(t) = Z_i j\omega e^{j\omega t} \quad i = 1,2,3 \tag{2.19}$$

$$\ddot{z}_i(t) = -Z_i \omega^2 e^{j\omega t} \quad i = 1,2,3 \tag{2.20}$$

where Z_i is the amplitude of harmonic motion.

$$\begin{bmatrix} -m_u\omega^2 + k_t + k_s + j\omega(c_t + c_s) & -k_s - c_s j\omega \\ -k_s - c_s j\omega & -m_{1/4}\omega^2 + k_s + c_s j\omega \end{bmatrix} \begin{bmatrix} Z_2 \\ Z_3 \end{bmatrix} = \begin{bmatrix} (k_t + j\omega c_t)Z_1 \\ 0 \end{bmatrix} \tag{2.21}$$

As was done in [21], the frequency response function of the sprung mass of the quarter car model may be defined as:

$$\left| H_{\frac{1}{4}}(\omega) \right| = \left| {Z_3}/{Z_1} \right| \tag{2.22}$$

And the frequency response function of the unsprung mass of the quarter car model may be defined as:

$$|H_u(\omega)| = \left| {Z_2}/{Z_1} \right| \tag{2.23}$$

Rewriting equation (2.21) as:

$$[A]\begin{bmatrix} Z_2 \\ Z_3 \end{bmatrix} = \begin{bmatrix} (k_t + j\omega c_t)Z_1 \\ 0 \end{bmatrix} \tag{2.24}$$

Each side of the equation can be multiplied by the inverse of $[A]$:

$$[A]^{-1}[A]\begin{bmatrix} Z_2 \\ Z_3 \end{bmatrix} = [A]^{-1}\begin{bmatrix} (k_t + j\omega c_t)Z_1 \\ 0 \end{bmatrix} \tag{2.25}$$

and therefore:

$$\begin{bmatrix} Z_2 \\ Z_3 \end{bmatrix} =$$

$$\frac{1}{detA}\begin{bmatrix} -m_{1/4}\omega^2 + k_s + c_s j\omega & k_s + c_s j\omega \\ k_s + c_s j\omega & -m_u\omega^2 + k_t + k_s + j\omega(c_t + c_s) \end{bmatrix}\begin{bmatrix} (k_t + j\omega c_t)Z_1 \\ 0 \end{bmatrix} \tag{2.26}$$

which becomes:

$$\begin{bmatrix} Z_2 \\ Z_3 \end{bmatrix} = \frac{1}{detA}\begin{bmatrix} (-m_{\frac{1}{4}}\omega^2 + k_s + c_s j\omega)(k_t + j\omega c_t)Z_1 \\ (k_s + c_s j\omega)(k_t + j\omega c_t)Z_1 \end{bmatrix} \tag{2.27}$$

where :

$$detA = \left(-m_u\omega^2 + k_t + k_s + j\omega(c_t + c_s)\right)\left(-m_{\frac{1}{4}}\omega^2 + k_s + c_s j\omega\right) - (k_s + c_s j\omega)^2 \tag{2.28}$$

Thereby resulting in the frequency response functions of the two degrees of freedom given by equations (2.29) and (2.30).

$$\left|H_{\frac{1}{4}}(\omega)\right| = \left|\frac{(k_s + c_s j\omega)(k_t + j\omega c_t)}{\left(-m_u\omega^2 + k_t + k_s + j\omega(c_t + c_s)\right)\left(-m_{\frac{1}{4}}\omega^2 + k_s + c_s j\omega\right) - (k_s + c_s j\omega)^2}\right| \tag{2.29}$$

$$|H_u(\omega)| = \left|\frac{(-m_{\frac{1}{4}}\omega^2 + k_s + c_s j\omega)(k_t + j\omega c_t)}{\left(-m_u\omega^2 + k_t + k_s + j\omega(c_t + c_s)\right)\left(-m_{\frac{1}{4}}\omega^2 + k_s + c_s j\omega\right) - (k_s + c_s j\omega)^2}\right| \tag{2.30}$$

2.3 Half Car Model

Building upon these models in levels of complexity, the next is the half car model as illustrated in Figure 2-5. It can represent the left half or right half of the car. This is a four degree of freedom system (4-DOF). This model is an improvement on the quarter car model as it allows consideration of potentially different responses between the front and rear unsprung masses, as well as the heaving and pitching motions of the vehicle.

These may occur due to differing unsprung masses, damping coefficients or spring rates at the front to the rear of the vehicle, or because the centre of gravity is forward or backwards of the centreline of the vehicle.

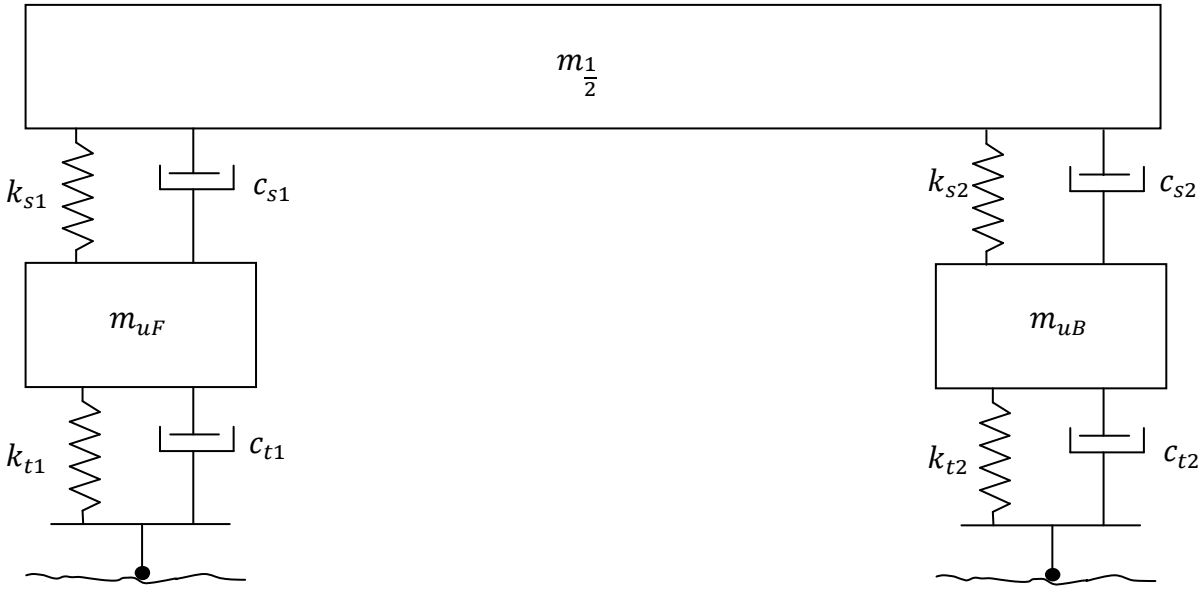

Figure 2-5: The half car model

A free body diagram of the half car model is given in Figure 2-6. Its four degrees of freedom include:

1. The vertical motion z_3 of the unsprung mass m_{uF}.
2. The vertical motion z_4 of the unsprung mass m_{uB}.
3. The vertical motion z_5 of the sprung mass $m_{1/4}$, known as *heave*.
4. The angular motion θ of the sprung mass, known as *pitch*.

Once again, this system is subject to base excitation, which is provided by the displacements z_1 and z_2. All displacements are measured about their static equilibrium

positions. It is assumed that the pitching motion θ, is small and therefore $\sin\ \theta = 0$ and $\cos\ \theta = 1$.

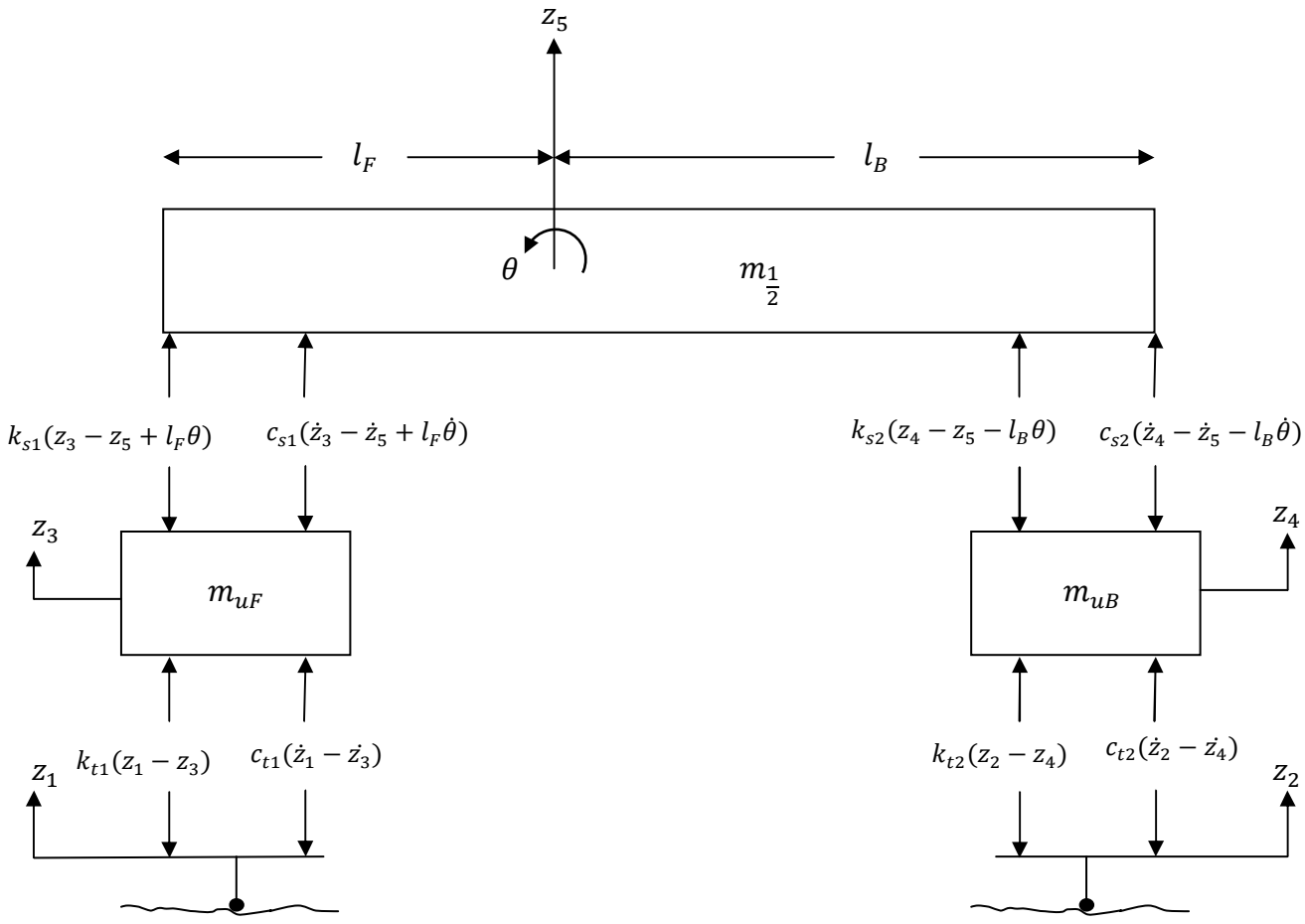

Figure 2-6: Free body diagram of 4-DOF half car model

Using Newton's second law of motion, the equations of motion of each of the four degrees of freedom may be defined as:

$$m_{uF}\ddot{z}_3 = k_{t1}(z_1 - z_3) + c_{t1}(\dot{z}_1 - \dot{z}_3) - k_{s1}(z_3 - z_5 + l_F\theta) - c_{s1}\left(\dot{z}_3 - \dot{z}_5 + l_F\dot{\theta}\right) \qquad (2.31)$$

$$m_{uB}\ddot{z}_4 = k_{t2}(z_2 - z_4) + c_{t2}(\dot{z}_2 - \dot{z}_4) - k_{s2}(z_4 - z_5 - l_B\theta) - c_{s2}\left(\dot{z}_4 - \dot{z}_5 - l_B\dot{\theta}\right) \tag{2.32}$$

$$m_{\frac{1}{2}}\ddot{z}_5 = k_{s1}(z_3 - z_5 + l_F\theta) + c_{s1}\left(\dot{z}_3 - \dot{z}_5 + l_F\dot{\theta}\right) + k_{s2}(z_4 - z_5 - l_B\theta) + c_{s2}\left(\dot{z}_4 - \dot{z}_5 - l_B\dot{\theta}\right) \tag{2.33}$$

$$I_{\frac{1}{2}}\ddot{\theta} = -k_{s1}l_F(z_3 - z_5 + l_F\theta) - c_{s1}l_F\left(\dot{z}_3 - \dot{z}_5 + l_F\dot{\theta}\right) + k_{s2}l_B(z_4 - z_5 - l_B\theta) + c_{s2}l_B\left(\dot{z}_4 - \dot{z}_5 - l_B\dot{\theta}\right) \tag{2.34}$$

Equations (2.31) to (2.34) may be separated into their output and input components

$$m_{uF}\ddot{z}_3 + k_{t1}z_3 + c_{t1}\dot{z}_3 + k_{s1}z_3 - k_{s1}z_5 + k_{s1}l_F\theta + c_{s1}\dot{z}_3 - c_{s1}\dot{z}_5 + c_{s1}l_F\dot{\theta} = k_{t1}z_1 + c_{t1}\dot{z}_1 \tag{2.35}$$

$$m_{uB}\ddot{z}_4 + k_{t2}z_4 + c_{t2}\dot{z}_4 + k_{t2}z_4 - k_{t2}z_5 - k_{s2}l_B\theta + c_{s2}\dot{z}_4 - c_{s2}\dot{z}_5 - c_{s2}l_B\dot{\theta} = k_{t2}z_2 + c_{t2}\dot{z}_2 \tag{2.36}$$

$$m_{\frac{1}{2}}\ddot{z}_5 - k_{s1}z_3 + k_{s1}z_5 - k_{s1}l_F\theta - c_{s1}\dot{z}_3 + c_{s1}\dot{z}_5 - c_{s1}l_F\dot{\theta} - k_{s2}z_4 + k_{s2}z_5 + k_{s2}l_B - c_{s2}\dot{z}_4 + c_{s2}\dot{z}_5 + c_{s2}l_B\dot{\theta} = 0 \tag{2.37}$$

$$I_{\frac{1}{2}}\ddot{\theta} + k_{s1}l_Fz_3 - k_{s1}l_Fz_5 + k_{s1}{l_F}^2\theta + c_{s1}l_F\dot{z}_3 - c_{s1}l_F\dot{z}_5 + c_{s1}{l_F}^2\dot{\theta} - k_{s2}l_Bz_4 + k_{s2}l_Bz_5 + k_{s2}{l_B}^2\theta - c_{s2}l_B\dot{z}_4 + c_{s2}l_B\dot{z}_5 + c_{s2}{l_B}^2\dot{\theta} = 0 \tag{2.38}$$

Assuming that the input displacements, and hence the motion of each of the degrees of freedom is harmonic:

$$z_i(t) = Z_i e^{j\omega t} \quad i = 1,2,3,4,5 \tag{2.39}$$

and hence:

$$\dot{z}_i(t) = Z_i j\omega e^{j\omega t} \quad i = 1,2,3,4,5 \tag{2.40}$$

$$\ddot{z}_i(t) = -Z_i \omega^2 e^{j\omega t} \quad i = 1,2,3,4,5 \tag{2.41}$$

where Z_i is the amplitude of harmonic motion.

Equations (2.35) to (2.41) may be further simplified by writing them in matrix form:

$$\begin{bmatrix} a_{1,1} & \cdots & a_{1,4} \\ \vdots & \ddots & \\ a_{4,1} & & a_{4,4} \end{bmatrix} \begin{bmatrix} Z_3 \\ Z_4 \\ Z_5 \\ \theta \end{bmatrix} = \begin{bmatrix} (k_{t1} + j\omega c_{t1})Z_1 \\ (k_{t2} + j\omega c_{t2})Z_2 \\ 0 \\ 0 \end{bmatrix} \tag{2.42}$$

where

$$a_{1,1} = -m_{uF}\omega^2 + k_{t1} + k_{s1} + j\omega(c_{t1} + c_{s1}) \tag{2.43}$$

$$a_{2,2} = -m_{uB}\omega^2 + k_{t2} + k_{s2} + j\omega(c_{t2} + c_{s2}) \tag{2.44}$$

$$a_{3,3} = -m_{\frac{1}{2}}\omega^2 + k_{s1} + k_{s2} + j\omega(c_{s1} + c_{s2}) \tag{2.45}$$

$$a_{4,4} = -I_{\frac{1}{2}}\omega^2 + k_{s1}{l_F}^2 + k_{s2}{l_B}^2 + j\omega(c_{s1}{l_F}^2 + c_{s2}{l_B}^2) \quad (2.46)$$

$$a_{2,1} = a_{1,2} = 0 \quad (2.47)$$

$$a_{3,1} = a_{1,3} = -k_{s1} - j\omega c_{s1} \quad (2.48)$$

$$a_{4,1} = a_{1,4} = k_{s1}l_F + j\omega c_{s1}l_F \quad (2.49)$$

$$a_{2,3} = a_{3,2} = -k_{s2} - j\omega c_{s2} \quad (2.50)$$

$$a_{2,4} = a_{4,2} = -k_{s2}l_B - j\omega c_{s2}l_B \quad (2.51)$$

$$a_{3,4} = a_{4,3} = -k_{s1}l_F + k_{s2}l_B + j\omega(c_{s2}l_B - c_{s1}l_F) \quad (2.52)$$

The motions z_1 and z_2 refer to the irregularity of the road profile. Because both wheels are driving over the same piece of road, it is assumed that Z_2 is equal to Z_1.

Therefore

$$\begin{bmatrix} a_{1,1} & \cdots & a_{1,4} \\ \vdots & \ddots & \\ a_{4,1} & & a_{4,4} \end{bmatrix} \begin{bmatrix} Z_3 \\ Z_4 \\ Z_5 \\ \theta \end{bmatrix} = \begin{bmatrix} f_1 Z_1 \\ f_2 Z_1 \\ 0 \\ 0 \end{bmatrix} \quad (2.53)$$

Where

$$f_1 = (k_{t1} + j\omega c_{t1}) \quad (2.54)$$

$$f_2 = (k_{t2} + j\omega c_{t2}) \quad (2.55)$$

MATLAB's symbolic toolbox was used in order to determine the frequency response functions from equation (2.53). These were found to be:

$$|H_{uF}(\omega)|$$

$$= \left|\frac{f_1(a_{2,2}a_{3,3}a_{4,4} - a_{2,2}a_{3,4}a_{4,3} - a_{3,2}a_{2,3}a_{4,4} + a_{3,2}a_{2,4}a_{4,3} + a_{4,2}a_{2,3}a_{3,4} - a_{4,2}a_{2,4}a_{3,3})}{D}\right. \tag{2.56}$$

$$\left. + \frac{f_2(a_{3,2}a_{1,3}a_{4,4} - a_{3,2}a_{1,4}a_{4,3} - a_{4,2}a_{1,3}a_{3,4} + a_{4,2}a_{1,4}a_{3,3})}{D}\right|$$

$$|H_{uB}(\omega)|$$

$$= \left|\frac{f_2(a_{1,1}a_{3,3}a_{4,4} - a_{1,1}a_{3,4}a_{4,3} - a_{3,1}a_{1,3}a_{4,4} + a_{3,1}a_{1,4}a_{4,3} + a_{4,1}a_{1,3}a_{3,4} + a_{4,1}a_{1,4}a_{3,3})}{D}\right. \tag{2.57}$$

$$\left. + \frac{f_1(a_{3,1}a_{2,3}a_{4,4} - a_{3,1}a_{2,4}a_{4,3} - a_{4,1}a_{2,3}a_{3,4} + a_{4,1}a_{2,4}a_{3,3})}{D}\right|$$

$$\left|H_{\frac{1}{2}}(\omega)\right| = \left|\frac{f_1(-a_{3,1}a_{2,2}a_{4,4} + a_{3,1}a_{2,4}a_{4,2} + a_{4,1}a_{2,2}a_{3,4} - a_{4,1}a_{2,4}a_{3,2)}}{D}\right. \tag{2.58}$$

$$\left. + \frac{f_2(-a_{1,1}a_{3,2}a_{4,4} + a_{1,1}a_{3,4}a_{4,2} - a_{3,1}a_{1,4}a_{4,2} + a_{4,1}a_{1,4}a_{3,2})}{D}\right|$$

$$|H_{\theta}(\omega)| = \left|\frac{f_1(a_{3,1}a_{2,2}a_{4,3} - a_{3,1}a_{2,3}a_{4,2} - a_{4,1}a_{2,2}a_{3,3} + a_{4,1}a_{2,3}a_{3,2)}}{D}\right. \tag{2.59}$$

$$\left. + \frac{f_2(a_{1,1}a_{3,2}a_{4,3} - a_{1,1}a_{3,3}a_{4,2} + a_{3,1}a_{1,3}a_{4,2} - a_{4,1}a_{1,3}a_{3,2)}}{D}\right|$$

where

$$
\begin{aligned}
D = {} & a_{1,1}a_{2,2}a_{3,3}a_{4,4} - a_{1,1}a_{2,2}a_{3,4}a_{4,3} - a_{1,1}a_{3,2}a_{2,3}a_{4,4} + a_{1,1}a_{3,2}a_{2,4}a_{4,3} \\
& + a_{1,1}a_{4,2}a_{2,3}a_{3,4} - a_{1,1}a_{4,2}a_{2,4}a_{3,3} - a_{3,1}a_{2,2}a_{1,3}a_{4,4} \\
& + a_{3,1}a_{2,2}a_{1,4}a_{4,3} + a_{3,1}a_{4,2}a_{1,3}a_{2,4} - a_{3,1}a_{4,2}a_{1,4}a_{2,3} \\
& + a_{4,1}a_{2,2}a_{1,3}a_{3,4} - a_{4,1}a_{2,2}a_{1,4}a_{3,3} - a_{4,1}a_{3,2}a_{1,3}a_{2,4} \\
& + a_{4,1}a_{3,2}a_{1,4}a_{2,3}
\end{aligned}
\tag{2.60}
$$

Now that the frequency response functions of the various models have been defined, they can be plotted in the frequency domain to determine the behaviour of the system when subjected to various harmonic inputs. The following chapters will create these plots for a typical V8 Supercar, and then demonstrate how these can be used to determine the road holding performance of the vehicle.

Chapter 3 – Computational Model of Vehicle

3.1 Typical V8 Supercar Parameters

The scope of this thesis concentrates on the effect of varying the damper settings for a particular vehicle. All other vehicle parameters will be considered constant. Typical values for these constants are given in Table 3-1. Unless otherwise specified, these are the values that will be used to obtain the results, and will be referred to as the "default V8 Supercar". For this thesis, the actual values of these parameters are not as important as the techniques that are presented.

Table 3-1: Typical V8 Supercar vehicle parameters

Vehicle Parameter	Value	Units	Description
$m_{\frac{1}{4}}$	345	kg	quarter car mass
$m_{\frac{1}{2}}$	630	kg	half car mass
m_{u1}	50	kg	unsprung mass, front
m_{u2}	83	kg	unsprung mass, rear
$I_{\frac{1}{2}}$	250	kg.m^2	moment of inertia of quarter car model about y-axis
l_F	1.3	m	distance between centre of gravity and front suspension mounts of half car model

l_B	1.5	m	distance between centre of gravity and rear suspension mounts of half car model
k_t	305000	$N.m^{-1}$	spring rate of tyre
c_t	0	$N.s.m^{-1}$	damping coefficient of tyre
k_{s1}	55000	$N.m^{-1}$	wheel rate, front
k_{s2}	55000	$N.m^{-1}$	wheel rate, rear
MR_F	0.63		motion ratio, front
MR_B	1		motion ratio, rear

3.2 Frequency response functions

Using the default V8 Supercar parameters, and the equations derived in Chapter 2 it is now possible to draw the frequency response function curves for the various degrees of freedom of the vehicle. This is achieved by solving the equations of motion simultaneously at each value of input frequency. These frequency response functions were created using MATLAB codes, examples of which may be found in Appendix B.1 and B.2.

The frequency response functions show the ratio of magnitude of output displacement versus the input displacement. In this case the output displacement can be any of the

degrees of freedom of the system being studied. The input to the system is the amplitude of road profile fluctuations.

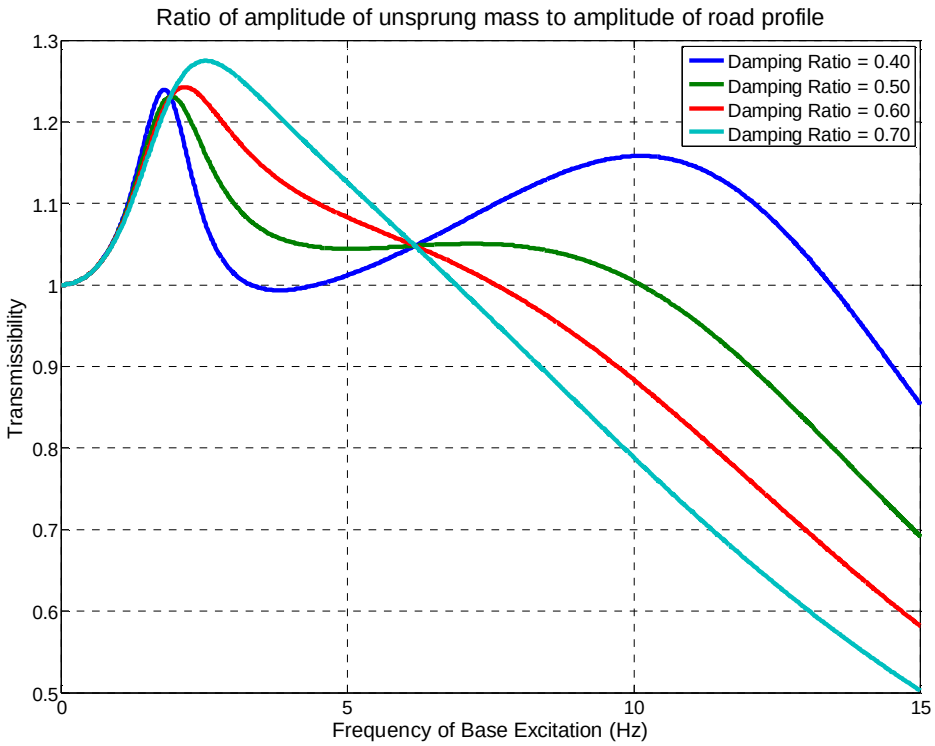

Figure 3-1: Frequency response function of the unsprung mass of the quarter car model

Figure 3-1 is the frequency response function of the unsprung mass for the 2-DOF quarter car model. Several different damping ratios have been plotted on the same axes to illustrate how the behaviour of the car may change due to different damping ratios. It is clearly visible in this graph that even a small change in damping ratio, from 0.4 to 0.7, can have a very drastic effect on the motion of the unsprung mass. In the frequency range between 0 and approximately 2 Hz, the different damping ratios have very little effect. In the region approximately between 2 and 6 Hz, the lower damping ratio (of 0.4) will result in a lower amplitude of displacement of the unsprung mass. In contrast, in the

region beyond 6 Hz, the higher damping ratio of 0.7 will result in less displacement of the unsprung mass. It can also be observed from this figure that with the higher damping ratios there is a single local maximum for the FRF curve. Lowering the damping ratio may add a second local maximum of approximately 11 Hz, and the height of this increases as the amount of damping in the system decreases.

The frequency response function of the sprung mass of the V8 supercar quarter car model is shown in Figure 3-2. It can be seen that there is a single peak in the FRF for all of the damping ratios examined. This peak occurs at approximately the same frequency regardless of the amount of damping applied. One important factor to note is that the lower the damping ratio, the higher the peak amplitude of the FRF. This figure confirms what is already commonly known. That is, that if the vehicle is subjected to random broadband input, most of the motion of the sprung mass will occur at a low frequency, and in order to control the movement of the sprung mass, a higher damping ratio is required.

The frequency response functions for the 4-DOF half car model can now be obtained. It is important to note that although the damping coefficient is set to be equal at both the front and the rear of the vehicle, the damping ratio will be different at the front to the back. This is due to the way that damping ratio has been defined in section 1.3.2. The sprung mass at the rear of the vehicle may differ from that at the front of the vehicle, resulting in different damping ratios for the same damping coefficient. Figure 3-3 through to Figure 3-6 show the frequency response functions of each of the four degrees of freedom of the half car model. The legends of these graphs indicate the amount of

damping, where CdF and CdR refer to the coefficient of damping at the front and the rear respectively, and DRF and DRR refer to the damping ratio at the front and rear respectively

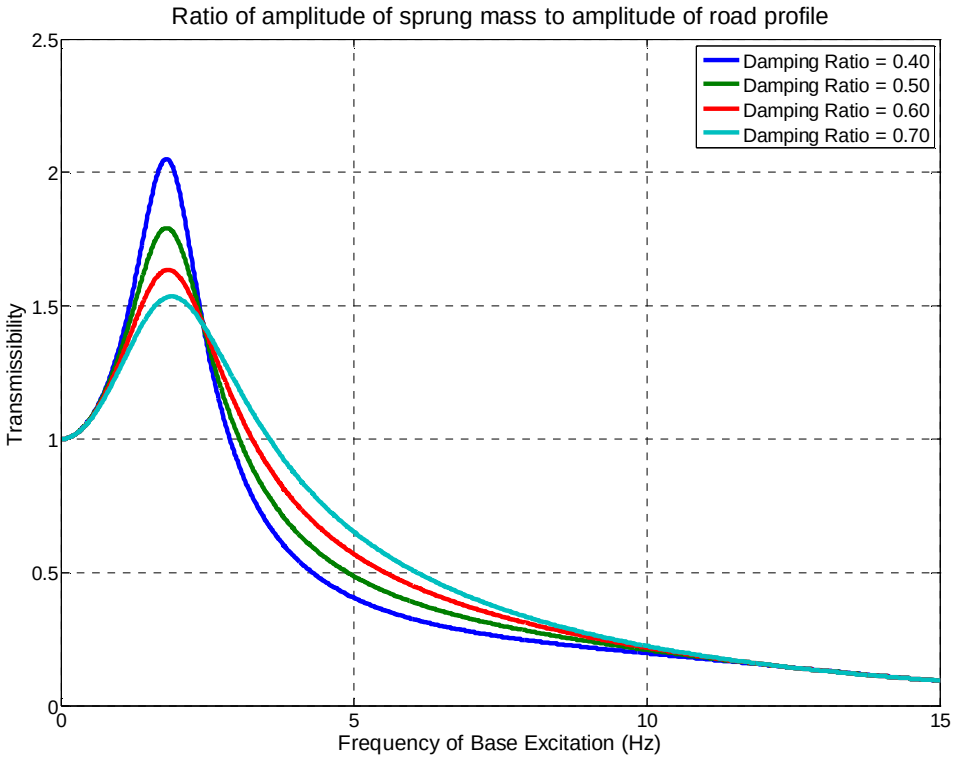

Figure 3-2: Frequency response function of the sprung mass of the quarter car model

Figure 3-3 is the frequency response function of the unsprung mass of the front of the vehicle. Similar to the 2-DOF system (Figure 3-1), there are three regions in this graph.

1. From 0 to 2 Hz, where there is no meaningful difference in the response of the system, due to varying damper properties.
2. From 2 to 6 Hz, where the response is highest from the more highly damped system.
3. Beyond 6 Hz, where the response is greatest from the lesser damped systems.

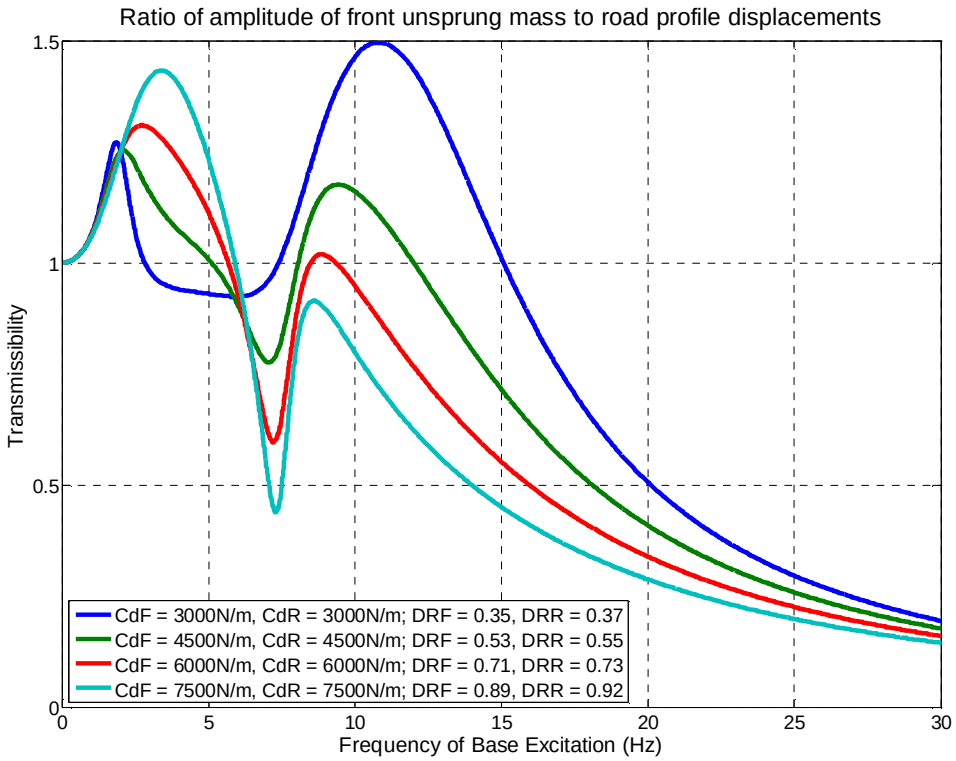

Figure 3-3:FRF for the front unsprung mass for the half car model

The response of the rear unsprung mass also follows similar relations, as shown in Figure 3-4. It should be noted that the only difference in the model between the front and rear of the vehicle is the mass distribution. In this example, the unsprung mass of the rear wheels is higher, and the sprung mass at the rear is lower when compared to the front of the car. This effects not only the magnitude of the displacements of the unsprung masses, but also the damped natural frequencies, where these peaks occur.

Figure 3-5 and Figure 3-6 show the frequency response functions for the heave and pitch modes of the sprung mass of the system respectively. The heave mode is the vertical displacement of the sprung mass, while the pitch mode refers to its angular displacement. The heave mode of the sprung mass of the 4-DOF system is very similar

in meaning to the sprung mass of the 2-DOF quarter car model shown in Figure 3-2, and the frequency response functions confirm this. In both cases, the peaks occur at approximately the same frequency. Also in both cases, the lower damping coefficients result in a higher peak transmissibility, and the effect of this can be profound.

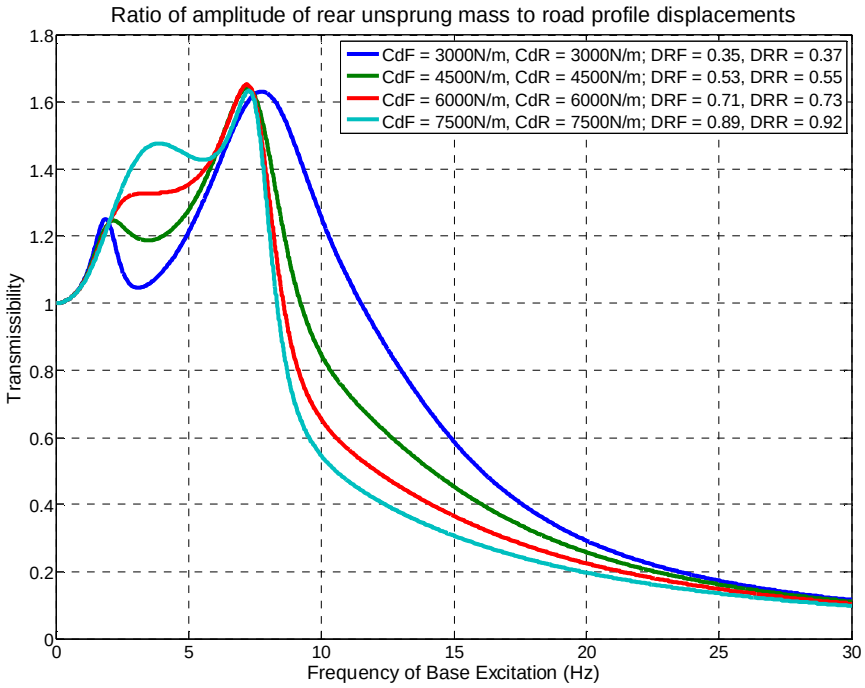

Figure 3-4: FRF for the rear unsprung mass for the half car model

Although it may be observed from Figure 3-5 that increasing the damping coefficients of the system will reduce the value of the peak heave response, it is evident from Figure 3-6 that the opposite is true when it comes to the pitching motion of the sprung mass. That is, increasing the damping coefficients of the system will increase the peak pitching response of the vehicle. Obviously, it is necessary to reach a compromise between these conflicting parameters. The following chapters will outline methods of quantitatively determining the best compromise.

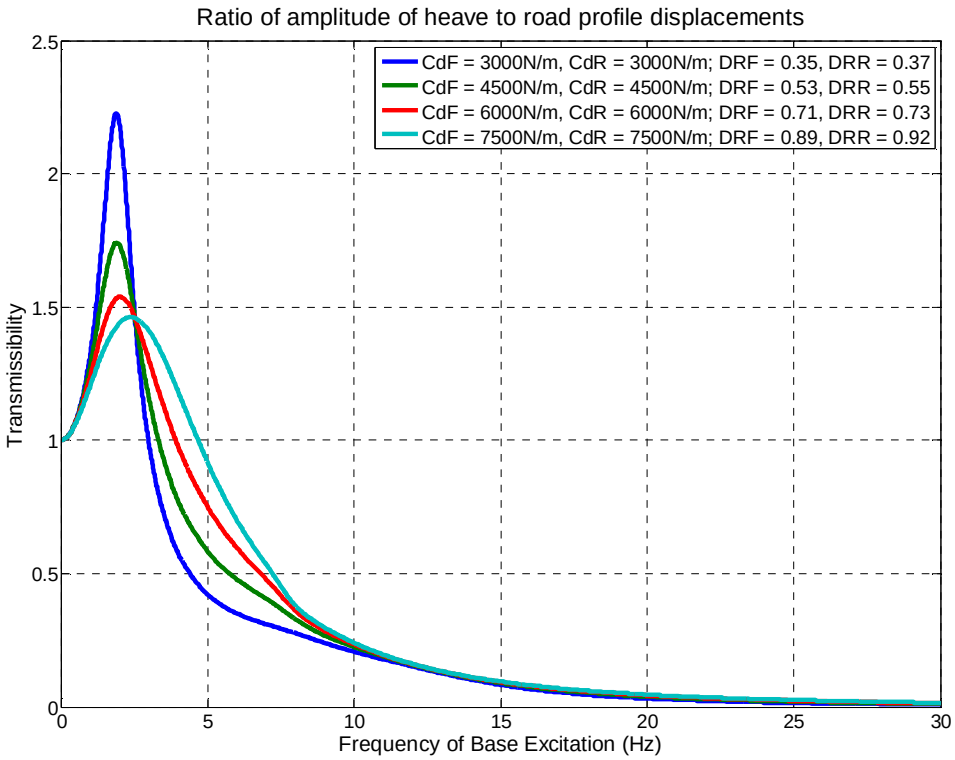

Figure 3-5: FRF for the heave motion of the sprung mass for the half car model

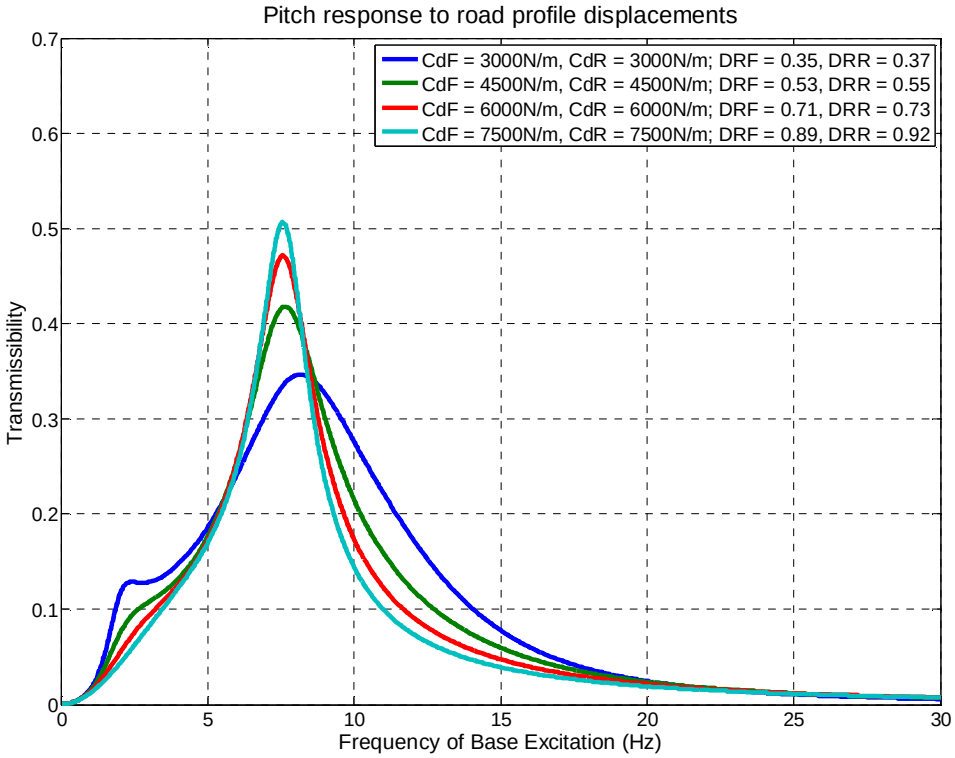

Figure 3-6: FRF for pitching motion of the sprung mass for the half car model

Chapter 4 – Tyre Load Fluctuations

4.1 Load Fluctuation Rate

It has been stated already in section 1.3.3 that the performance of a race car tyre is inversely proportional to the variation of its contact force with the road. There have been many attempts at quantifying the effect of tyre load fluctuations. The method used in this thesis to quantify the effect of tyre load fluctuations was developed by Sugasawa *et al.* [15]. They defined the evaluation criterion for the quarter car load fluctuation rate $R_{1/4}$ as being:

$$R_{\frac{1}{4}} = \frac{k_t}{\left(m_{\frac{1}{4}} + m_u\right) g} \bar{\sigma} \tag{4.1}$$

where:

k_t = the spring rate of the tyre

$m_{\frac{1}{4}}$ = the quarter car sprung mass

m_u = the unsprung mass

g = the gravitational constant

$\bar{\sigma}$ = the RMS value of $(Z_1 - Z_2)$

Z_1 = the amplitude of the road profile displacements

Z_2 = the amplitude of motion of the tyre

This equation allows a quantitative analysis of the effect of varying the vehicle parameters. By minimising the value of $R_{1/4}$ (or in the more general case R), the vehicle which has the lowest tyre load fluctuations can be obtained. This will result in higher average traction available to the tyres. Obtaining the values of Z_1 and Z_2 in this equation depends on not only the FRF of the system, but also requires some information about the shape of the road profile. This is usually given in the form of a power spectral density of the size of the road profile irregularities.

4.2 Power spectral density

It was mentioned in section 1.3.4 that in order to make quantitative comparisons between different vehicle setups, it is necessary to have a realistic profile of the road surface characteristics. This is most conveniently done by plotting the magnitude of displacement of the road profile in the frequency domain. This is known as the power spectral density (PSD) of the road surface. There have been many different attempts at creating a general PSD model for road profiles, and these have been studied at length by Andrén [17].

The comparison is to be made of the performance of the same vehicle with several different dampers over a generic stretch of road. Therefore, any realistic approximation of the PSD of the road profile will provide sufficient results to make a comparison between these different damper set-ups. Care must be taken in the interpretation of these results however, as race cars, and particularly V8 supercars, are required to compete on

roads with varying roughness and bump characteristics. The most appropriate damper for one PSD road profile is not necessarily the best for another road.

Another complicating factor is that most approximations of road profile are given in terms of spatial frequency of the road profile disturbances. Spatial frequency is the inverse of the wavelength. It may be thought of as the number of cycles or road profile fluctuations per distance travelled. The number of fluctuations per second is therefore dependent upon the velocity of the vehicle across this road profile. In order to convert spatial frequency into radian frequency, it is necessary to multiply the special frequency by $2\pi V$, where V is the velocity of the vehicle. The velocity of a V8 supercar is not constant and can vary anywhere up to 300 kilometres per hour. The PSD used by Tamboli *et al.* [18] will be used, as it simplifies the problem somewhat by assuming a constant velocity. This PSD has been defined as:

$$G(f) = ae^{(-bf)} \tag{4.2}$$

where

a describes the general roughness of the road

b describes the wavelength distribution

f refers to frequency (Hz)

Tamboli *et al.* [18] suggests the coefficients for PSD obtained in Table 4-1. These values are dependent upon both the quality of the road, and also the speed of the vehicle travelling on it. Neither of the two road types in Table 4-1 directly relate to a racing

circuit, however the highway driving is likely to be the better approximation of the two, and will therefore be used for comparing the different dampers.

Table 4-1: Coefficients of the PSD used by Tamboli [18].

Road type	a (m^2/Hz)	b
Highway	4.85×10^{-4}	0.19
City	23.0244×10^{-4}	0.213

The mean square displacement of the road irregularities may be found from the PSD:

$$\bar{Z}^2 = \int_0^\infty G(f)\, df \tag{4.3}$$

Equation (4.3) may be discretised to find the root mean square displacements in a given frequency band:

$$\bar{Z}_{1,f_n} = \sqrt{\int_{f_n-\frac{h}{2}}^{f_n+\frac{h}{2}} G(f)\, df} \tag{4.4}$$

where

$f_n =$ the centre frequency of the frequency band

$h =$ the width of the frequency band.

Equation (4.4) may be used to represent the amplitude of displacement, or irregularity of the road profile within each given frequency band. The mean value of the actual response of the vehicle must relate the amplitude of the road profile fluctuations to the frequency response of the vehicle in that same frequency band. The mean value of the FRF in each frequency band is given by equation (4.5).

$$\bar{H}_{f_n} = \frac{1}{h} \int_{f_n - \frac{h}{2}}^{f_n + \frac{h}{2}} |H_u(\omega)| df \tag{4.5}$$

where $\omega = 2\pi f$.

The amplitude of displacement of the unsprung mass can now be calculated for each frequency band.

$$\bar{Z}_{2,f_n} = \bar{Z}_{1,f_n} \times \bar{H}_{f_n} \tag{4.6}$$

Equations (4.4) and (4.6) can now be substituted into equation (4.1) and be rewritten as it is in equation (4.7). All of the information required to obtain the load fluctuation rate $R_{\frac{1}{4}}$ of the vehicle is now available.

$$R_{\frac{1}{4}} = \frac{k_t}{\left(m_{\frac{1}{4}} + m_u\right) g} \sqrt{\sum_{n=1}^{k} \left(\bar{Z}_{1,f_n} - \bar{Z}_{2,f_n}\right)^2} \tag{4.7}$$

4.3 Results of Evaluation Criterion Analysis

Using the expressions obtained in Chapter 2 and section 4.2, it is possible to analyse the effect of varying the level of damping on the vehicle. The definition of $R_{1/4}$ specifies that road holding performance is greatest when the value of $R_{1/4}$ is minimised. Using MATLAB, it is possible to obtain the value of road holding performance over a sweep of damping values. Examples of the MATLAB script used to obtain these graphs are found in Appendix B: MATLAB Script.3 and B.4.

Figure 4-1 graphs the value of $R_{1/4}$ versus coefficient of damping for the quarter car model of the default V8 Supercar. This indicates that a damping coefficient between 3500 and 4000 Ns/m will result in a vehicle that produces the highest average traction at the tyres. That is, at these damping coefficients, the $R_{1/4}$ value is minimised, indicating that tyre load fluctuations will be minimised. Also, the slope of the curve is steeper when the damping coefficient is below the optimal point, than when it is above the optimal damping point. This shows that the consequence of overdamping the car does not have as large a negative impact on performance as underdamping will.

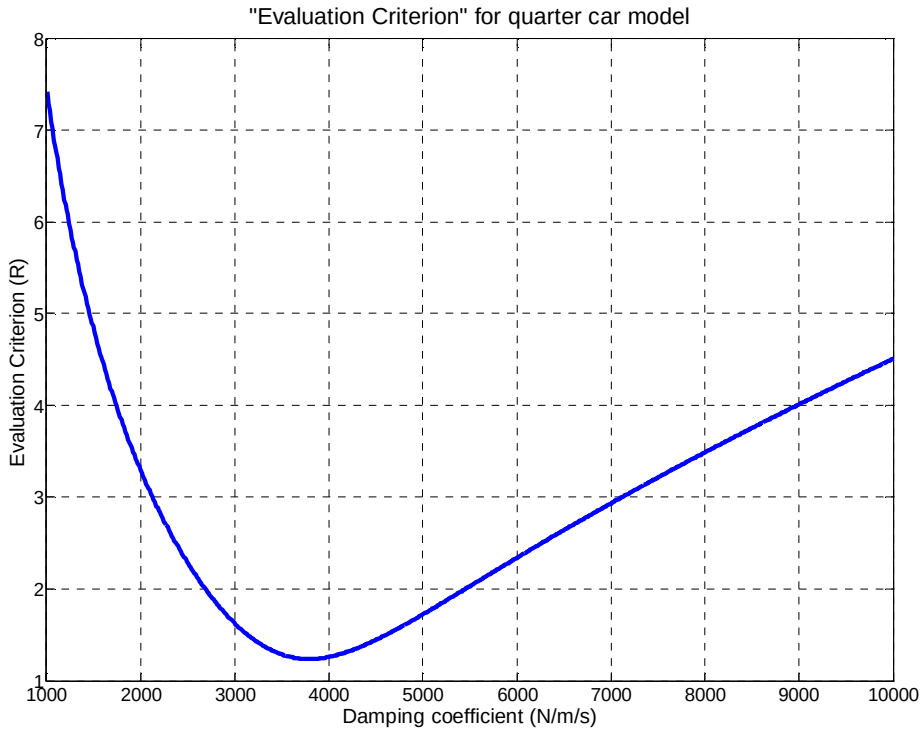

Figure 4-1: The effect of damping coefficient on the evaluation criterion for a V8 Supercar quarter car model

Figure 4-2 continues this analysis using the V8 Supercar 4-DOF half car model. In this figure, the damping coefficient at the front and the rear is assumed to be equal. Again, this model is solved using MATLAB, and in this case the tyre load fluctuations at both the front and rear wheel are calculated separately. It is evident that the ideal level of damping is different at the front to what it is at the rear. From here, it may be observed that to optimise the damping for the rear, a damping coefficient of 3250 Ns/m is ideal. In order to minimise the front tyre load fluctuations, a damping coefficient of 4000 Ns/m is ideal. As is the case for the quarter car model, the slope of the curve is steeper

in the region below optimal damping, indicating that the negative consequence of overdamping the vehicle is less than that of underdamping.

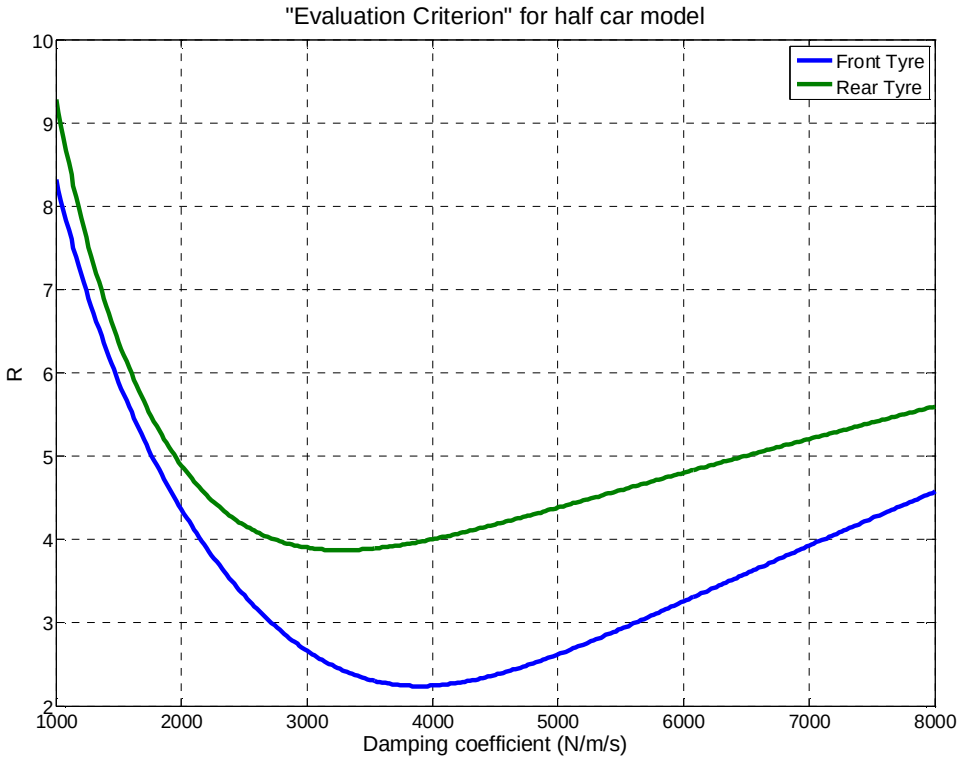

Figure 4-2: The evaluation criterion for V8 Supercar half car model, using the assumption that damping is equal at the front and rear

One thing that the analysis of Figure 4-2 does not take into consideration is the fact that the car can be engineered to use a different damping coefficient at the front to the rear of the vehicle. Observing that a damping coefficient of 3250 Ns/m is optimal for minimising the rear tyre load fluctuations, the rear dampers are set to this value. The damping coefficient at the front can then be examined to determine its optimal value, as is fone in Figure 4-3. From this figure the optimal damping at the front is now 4250

Ns/m. Further to this, the *R* value at the front tyre has lowered further to 2.125 as opposed to the value of 2.25 in the case of Figure 4-2. This represents a net improvement in performance for the vehicle.

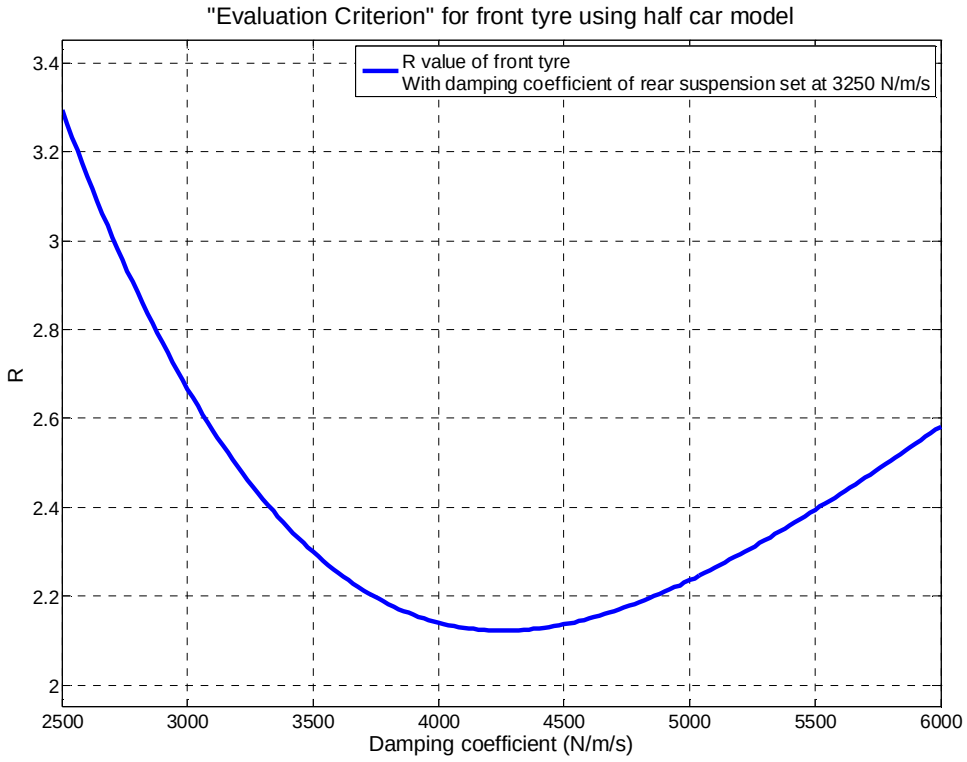

Figure 4-3: Evaluation criterion at front tyre, first iteration

The story doesn't end there, however. The motion at the rear unsprung mass is dependent upon the motion at the front unsprung mass, and vice versa. So the next step is to continue this as an iterative process by setting the front damping coefficient to the new found optimal value of 4250 Ns/m, and repeating the process for the rear tyre load fluctuations, as is done in Figure 4-4.

The first thing to note is that in Figure 4-2, the optimal damping coefficient for the rear was found to be 3250 Ns/m, and this resulted in an *R* value of 3.9 at the rear tyre. In Figure 4-4, the damping coefficient at the front of the vehicle has been further optimised, and this changed the optimal point of damping for the rear. Even so, if the rear was to be left at the value of 3250 Ns/m, the new value of *R* is 3.55. In other words, by improving the performance of the front of the car, the performance at the rear of the car has improved, even without making any change to the settings at the rear. This happens because the displacement fluctuations at the front of the vehicle transmit through the suspension, into the sprung mass of the vehicle, and ultimately to the rear tyre. So by reducing the tyre load fluctuations at the front, the tyre load fluctuations at the rear are also reduced.

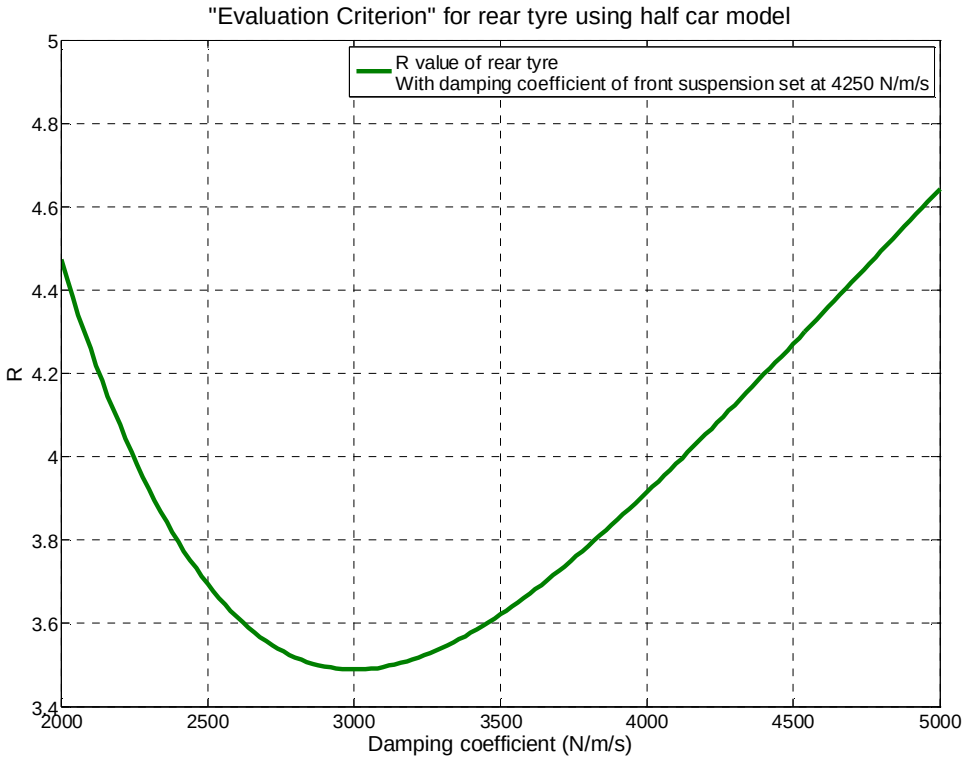

Figure 4-4: Evaluation criterion at rear tyre, second iteration

From Figure 4-4 the point of optimal damping for the rear of the vehicle can be read off as 3000 Ns/m, and this results in an *R* value of 3.5, which is a further improvement to the performance of the vehicle. This is again reiterated to observe how the new value at the rear of the car effects how the front of the car is performing. This analysis is shown in Figure 4-5, where it can be seen that the optimal damping coefficient still occurs at 4250 Ns/m, which is the same as it was before the modification to the rear was made, signalling the end of the iteration process. Once again, it can be observed that even though the optimal amount of damping has not changed, the degree of tyre load fluctuations have further decreased, down to a value of 2.1, due to the improved performance at the rear.

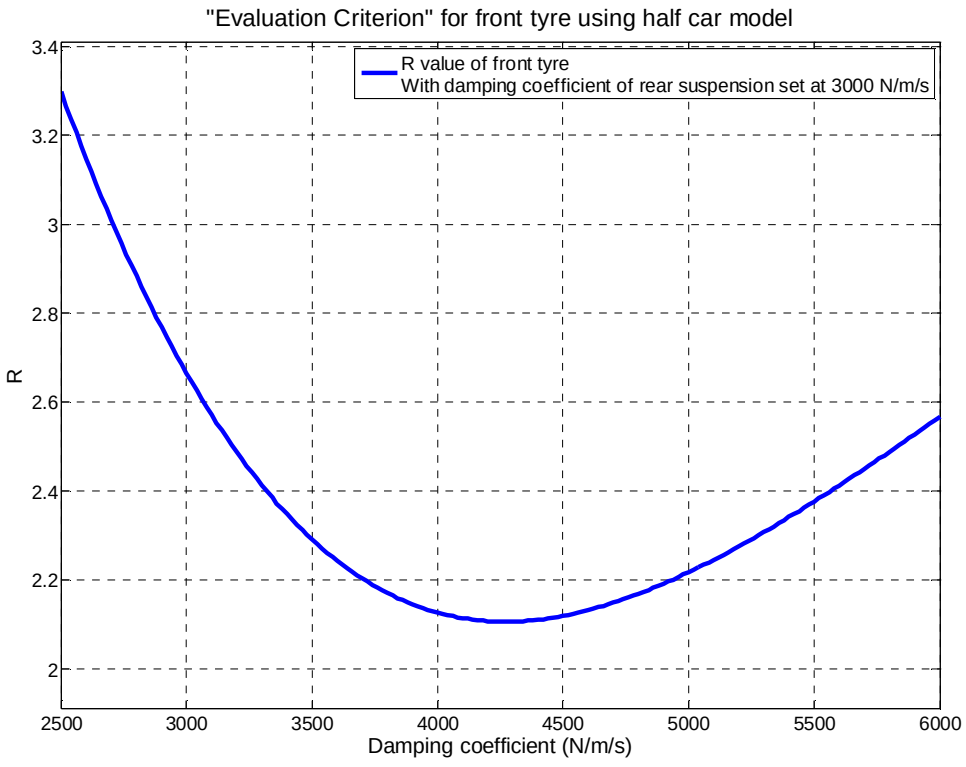

Figure 4-5: Evaluation criterion at front tyre, third iteration

The results of this iteration process are summarised in Table 4-2. From this the optimal damping coefficients at the front and rear are determined, assuming linear dampers and a road profile that is similar in character to highway driving. These optimal damping coefficients at the front and rear are 4250 Ns/m and 3000 Ns/m respectively.

Table 4-2: Summary of results of iterative process

Analysis	Optimal Damping Coefficient Front (Ns/m)	Optimal Damping Coefficient Rear (Ns/m)	Minimum *R* Front	Minimum *R* Rear
Equal damping coefficient front and rear	4000	3250	2.25	3.9
Optimise front, first iteration	4250	-	2.125	-
Optimise rear, second iteration	-	3000	-	3.5
Optimise front, third iteration	4250	-	2.1	-

Chapter 5 – ChassisSim

5.1 Introduction to ChassisSim

Race cars are extremely complicated machines, such that even in a tightly controlled category such as V8 Supercars, there are many variables other than the damper characteristics which can be modified by the engineers in order to obtain peak performance of the vehicle. These include, but are not limited to, the choice of springs, the size and shape of anti-roll bars, the amount of pressure in the tyres and the aerodynamic characteristics of the vehicle. Up until this point, many of these effects have not been considered. Although the optimisation of all these parameters is beyond the scope of this thesis, it is necessary to include their effects when analysing the dampers. To continue this analysis using only MATLAB would be extremely complicated. Instead, a vehicle dynamics simulation package can be used to make this analysis simpler.

ChassisSim is a race car dynamics simulation program which is being developed in Sydney by ChassisSim Technologies. It has a number of different analysis modes allowing an in-depth study of the vehicle's dynamics. These include

- Lap simulation, which provides traces of information about the vehicle over a simulated lap. This makes the assumption that the vehicle is being driven by the "perfect driver" who keeps the vehicle's tyres at the limit of traction at all times. This will also estimate a lap time for the track, although it is stated in the

documentation for the program that the focus of this toolbox should be on optimising the vehicle's dynamics, rather than the lap time itself.

- Optimisation toolbox, which allows the user to input upper and lower bounds for frequently altered parameters, such as coefficients of damping. The program then uses a lap time estimation to choose the optimum values for these parameters.
- A simulated seven post shaker rig, which is the computational manifestation of a physical seven post shaker rig described in section 1.3.4, and can be used to perform a similar analysis.

ChassisSim has several advantages over many other race car simulation packages, which makes it particularly suitable to this thesis. To begin with, it has a clear interface as shown in Figure 5-1, which does not require any three dimensional modelling to be conducted. Because the package is principally aimed at racecar engineers, the program is already loaded with generic racecar geometry, so it is just a matter of specifying the values of vehicle's various parameters.

Further to this, the program comes with a number of default vehicle models, one of these being a V8 Supercar. In competitive motorsport, obtaining the parameters of a race car is notoriously difficult, and this is particularly the case in V8 Supercars, where there are only a very small number of teams, and very little academic research being undertaken. Because ChassisSim contains a V8 Supercar model, this is an invaluable source of information on typical set-ups of the vehicle. Further to this, it means that analyses can very quickly be carried out, because any unknown parameters of the

vehicle can be left at their default values, allowing more time to be spent concentrating on the particular area of the vehicle that is being studied: in this case, dampers.

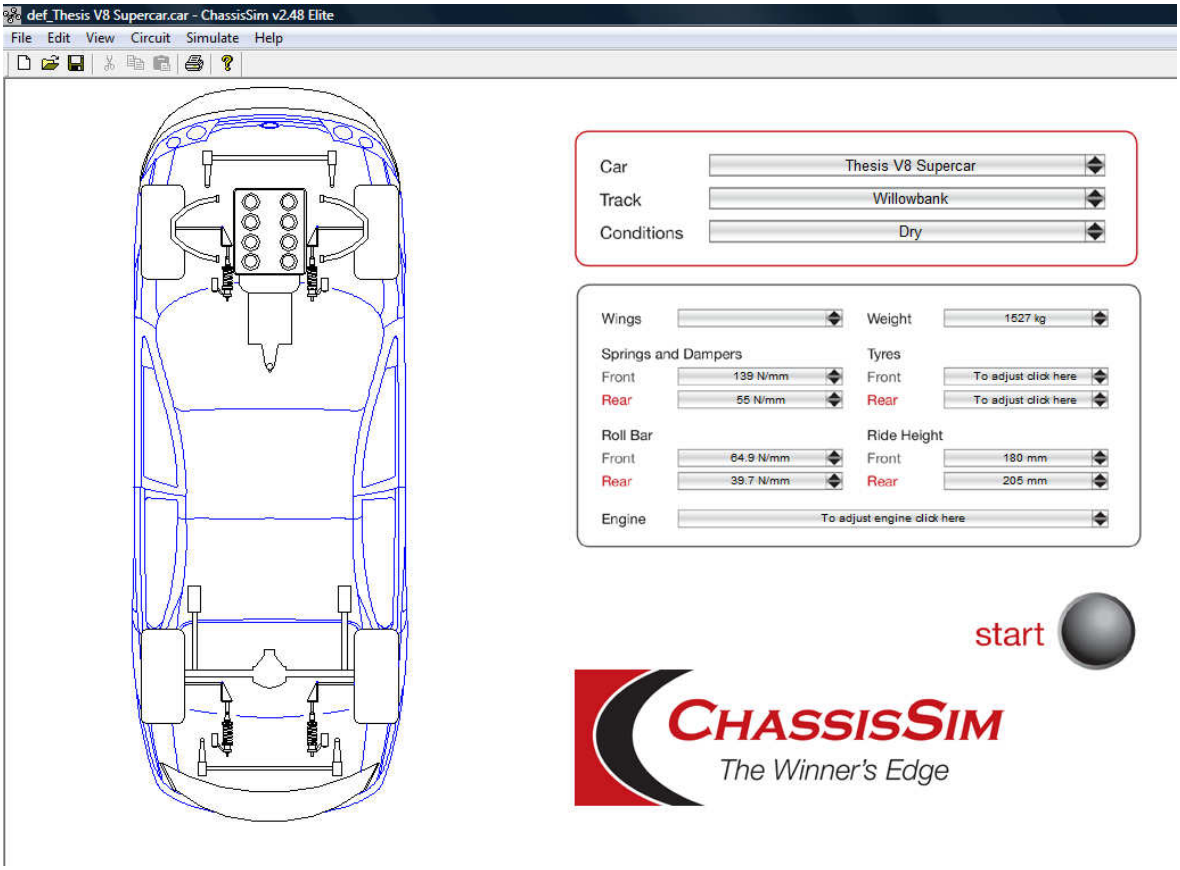

Figure 5-1: The ChassisSim interface

Section 4.2 covered the importance of using an accurate representation of road profile. Another benefit of ChassisSim is that it contains data of the bump profile and curvature for most Australian tracks that V8 Supercars compete on, allowing accurate simulations to be performed.

One final benefit of ChassisSim is that the results of its lap simulations are exportable into a number of programs, including MoTeC Interpreter, and MATLAB. MoTeC

Interpreter is a data analysis tool used by many V8 Supercar teams to interpret their telemetry and is used in section 6 of this thesis when determining bypass velocities. By exporting into MATLAB, further data manipulation can be performed, such as creating damper histograms, as is done in section 6.3 (these can alternatively be created in MoTeC Interpreter).

ChassisSim is already being used by many race teams across a number of categories including V8 Supercars, and has been shown to provide accurate results in simulating the dynamics of the vehicle. This means that although physical testing of results cannot be conducted on an actual vehicle due to the restrictions discussed in section 1.1, the results from this program can be used with confidence.

5.2 Seven Post Shaker Rig Analysis

The seven post shaker rig is a tool that is used by race teams in all categories throughout the world. They use seven actuators to excite the vehicle, and the response of the degrees of freedom of the vehicle are measured. Four of the actuators are used to simulate the road inputs to the tyres, while the remaining three are used to simulate the aero loads and accelerations of the sprung mass [22]. These rigs are important analysis tools, because they can be used to determine the frequency response functions of the many degrees of freedom of a racecar.

For a car which relies mostly on mechanical grip, as opposed to a high downforce vehicle, the most important analysis mode is the heave mode, where all four road inputs

move simultaneously [22]. This is not to be confused with the heave motion of the sprung mass. Mechanical grip is created by using the suspension to keep the tyres to the ground. High downforce vehicles rely on the use of wings and ground effects to increase the normal force of the tyre to the road. Because V8 Supercars are relatively low downforce vehicles relying on mechanical grip, the seven post rig analysis conducted in this thesis will be done in the heave mode.

The simulated seven post shaker rig also reports a contact patch load (CPL) value for both the front and the rear of the vehicle. CPL is a measure of the magnitude of fluctuation of force in the contact patch of the tyre. Although defined slightly differently, it is very similar in meaning to the evaluation criterion R of Chapter 4, and can be used in much the same way.

Figure 5-2 shows the seven post shaker rig interface in ChassisSim. Aside from the vehicle parameters, there are a few important values to specify for this analysis:

- Maximum frequency - chosen to be 16 Hz, as this is the default value. Any fluctuations occurring at frequencies higher than this are unlikely to have any physical meaning, and are therefore disregarded.
- Speed of the car - chosen to be 150 km/h, as this is representative of the speed that many of the transient manoeuvres, such as cornering and accelerating, will occur at.
- Maximum peak input velocity - 250 mm/s, as from logged data from a typical vehicle, most of the inputs into the tyre will happen at a velocity below this value.

The actual values used here are not critical, as long as they are appropriate estimations. It is critical, however, that these values remain constant across all the testing.

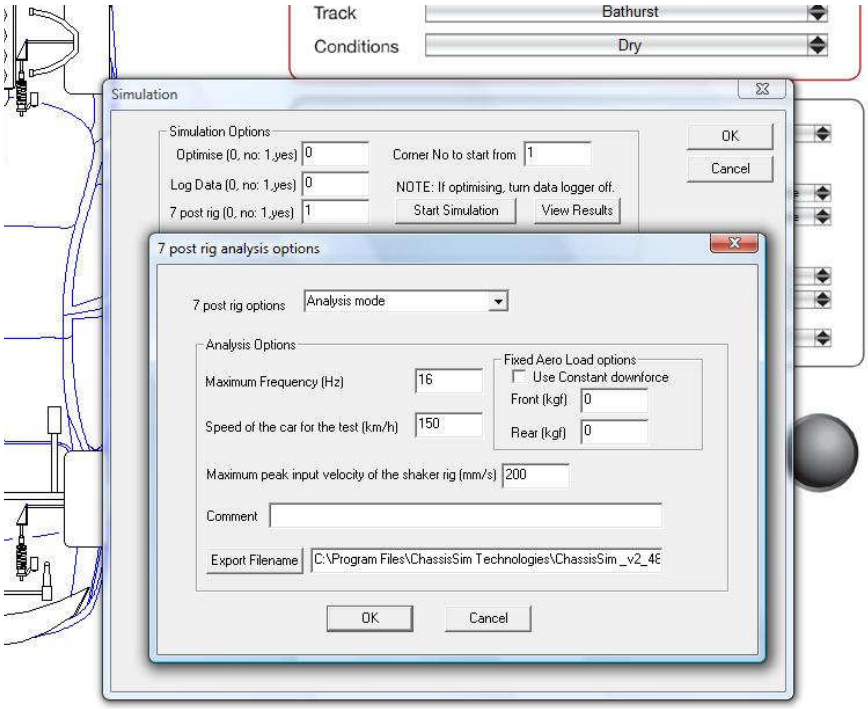

Figure 5-2: The ChassisSim seven post rig interface

The tests conducted using the simulated seven post shaker rig will follow a similar procedure to that of the evaluation criterion analysis of section 4.3. Firstly, the assumption is made that the dampers are linear, and both the front damper and the rear damper have the same damping coefficient. The seven post shaker rig simulation was completed for various damping values, and the results are plotted in Figure 5-3. Once again, the optimum damping coefficient is the one that minimises the value of CPL. The results are very similar in shape and characteristic to their counterpart results from Figure 4-2. That is, they follow a similar shape, and the slope on the overdamped side of

the curves is shallower than that on the underdamped side. Also, the CPL at the rear is higher than that at the front. The optimum CPL at the rear also happens at a lower damping coefficient than that of the optimum value at the front.

The results from ChassisSim do differ somewhat from the results of Figure 4-2, in that curves obtained from ChassisSim are translated further towards the left of the graph. From Figure 5-3, the first estimates of optimum damping coefficient can be read off as 2700 Ns/m at the front and 2300 Ns/m at the rear, giving CPL values of 129.6 and 132.2 respectively.

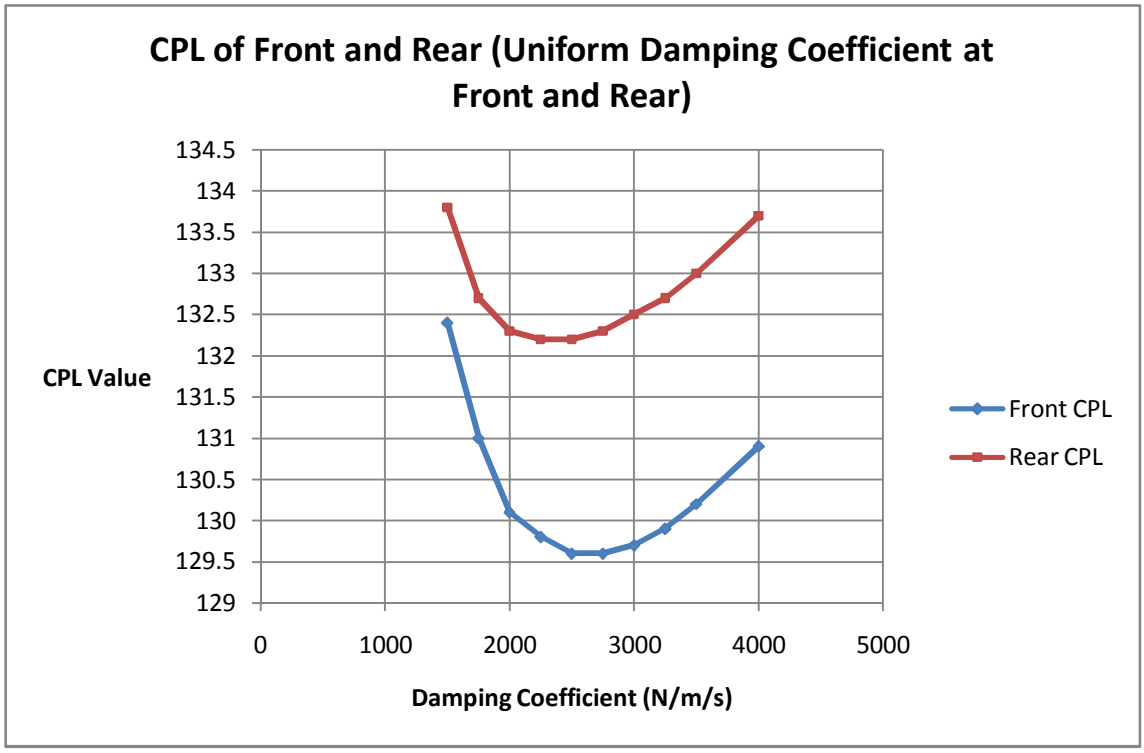

Figure 5-3: ChassisSim measurement of CPL for front and rear.

Following the procedure from section 4.3, the rear damper is set at 2300 Ns/m, and the effect of varying the front damping coefficient is plotted in Figure 5-4. From this it can

be seen that the new optimum front damping value is 3000 Ns/m as this minimises the value of CPL for the front damper to 129.5. Once again, improving the performance of the front of the vehicle has also improved that of the rear, as this now has an improved CPL value of 131.7.

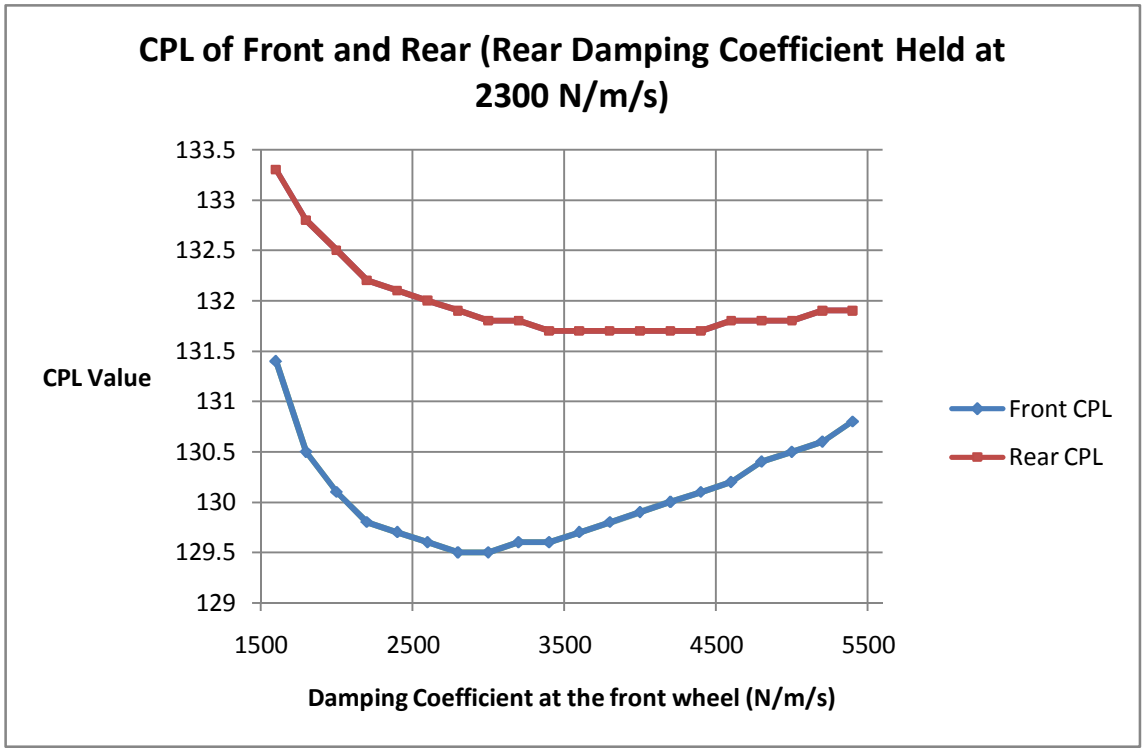

Figure 5-4: Effect of variation of front damper on CPL, first iteration

The process is again repeated, this time holding the front damper properties constant, and varying the rear, as shown in Figure 5-5. From this figure, there exists a range of values of damping coefficient that optimise the CPL at the rear. The value of 2000 Ns/m is chosen to be the best, because of the range, this damper coefficient results in the lowest CPL for the front as well as the rear. These CPLs are 131.6 and 129.5 for the rear and front respectively.

This is again iterated, holding the rear damping coefficient at 2000 Ns/m and the results are plotted in Figure 5-6. The new optimal damping at the front is 3200 Ns/m, giving CPLs of 129.6 and 131.5 at the front and rear respectively.

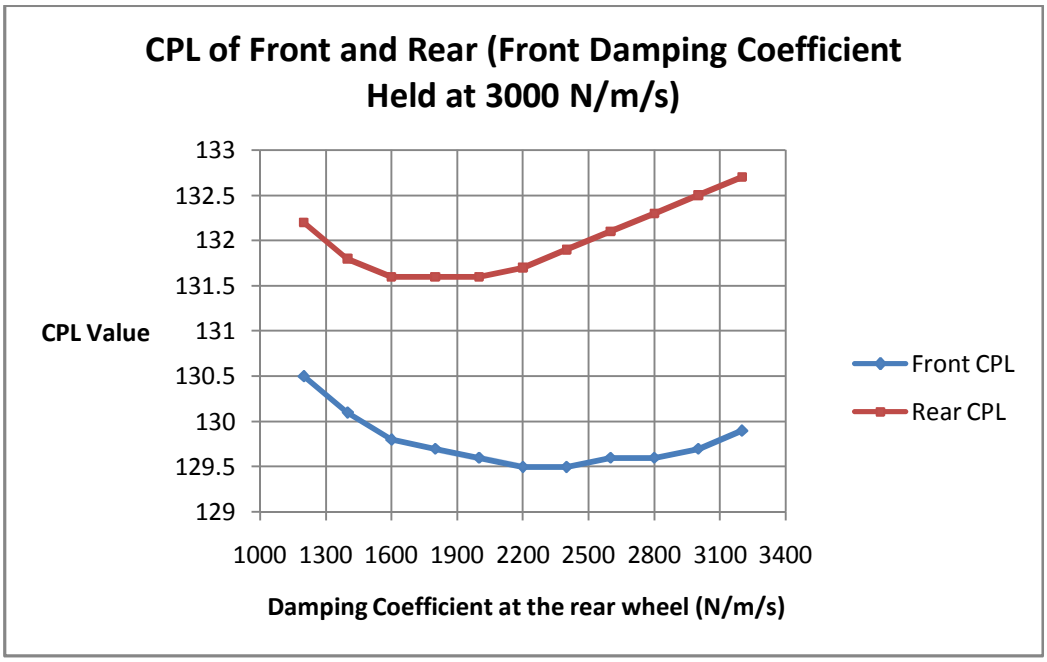

Figure 5-5: Effect of variation of rear damper on CPL, second iteration

A summary of results obtained by the simulated seven post shaker rig CPL analysis is given in Table 5-1. With each iteration, the size of the improvement in CPL value reduces, and by the third iteration the CPL at the front has actually increased slightly. When comparing the results obtained in this section with those from section 4.3, it can be seen that the optimum damping coefficients from the CPL analysis are approximately 1000 Ns/m lower than those found using the evaluation criterion. One of the reasons for this is that the CPL analysis uses a different sweep of sine waves than the *R*-value analysis. Further to this, the CPL analysis includes some more complicated effects such as aerodynamic loads.

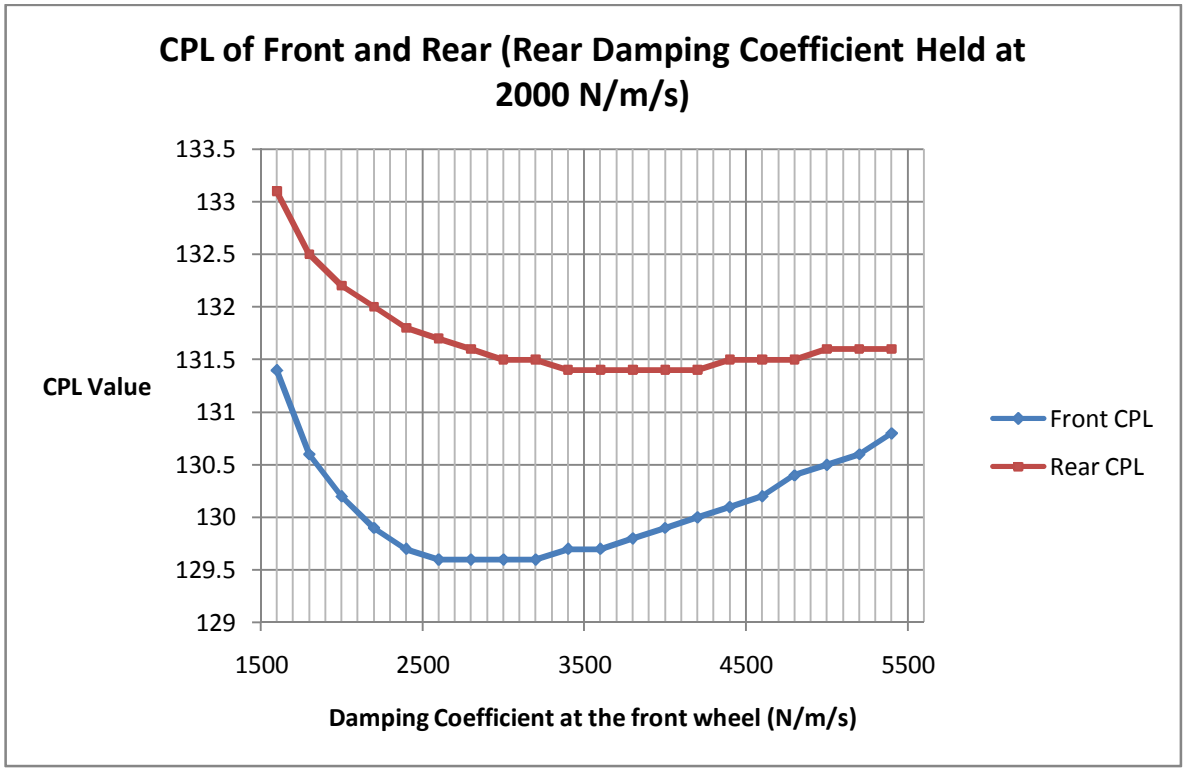

Figure 5-6: Effect of variation of front damper on CPL, third iteration

Table 5-1: Summary of results from seven post shaker rig CPL analysis

Analysis	Optimal Damping Coefficient Front (Nm/s)	Optimal Damping Coefficient Rear (Nm/s)	Minimum CPL Front	Minimum CPL Rear
Equal damping coefficient front and rear	2700	2300	129.6	132.2
Optimise front, first iteration	3000	2300	129.5	131.7
Optimise rear, second iteration	3000	2000	129.5	131.6
Optimise front, third iteration	3200	2000	129.6	131.5

These results will provide a sufficient starting point for the non linear analysis to follow.

Chapter 6 – Non-linear damping

6.1 Bypass Velocities

It was mentioned in section 1.3.1 that dampers are nonlinear. Typically, they will employ two different damping coefficients in “bump” (when the damper is contracting), and another two damping coefficients in “rebound” (when the damper is expanding). Usually, the low speed region of the damper curve, in both bump and rebound, utilises a higher coefficient of damping than the high speed region of the curve. The point at which the damping coefficient changes is known as the “knee” of the damper curve, and the velocity at the knee is known as the bypass velocity.

It has been stated already that the damper serves two contradicting purposes. It must be soft enough to allow sufficient movement for the tyre to follow the shape of the road profile, and impart a consistent normal force to the road, while at the same time be hard enough to prevent unwanted roll of the sprung mass of the vehicle.

It is known that the body roll of the vehicle tends to happen at a lower frequency than the excitation due to road profile. Because of the close relationship between frequency and velocity, this implies that damper motions due to body roll will occur at a lower velocity than those due to the road profile. Using this information, the bypass velocity of the damper can be set so that it acts somewhat like a filter. By setting a higher damping ratio in the low speed area of the curve to control the body roll of the vehicle,

and a lower damping ratio can be used in the high speed region of the curve to maximise road holding.

In order to select the optimum point for the bypass velocity, it is necessary to obtain an estimation of the maximum velocity of the damper that occurs due to body roll. This procedure is similar to that described by Nowlan [8]. It requires the use of logged data of the vehicle, which is shown in Figure 6-1. The lap shown in this figure was created by ChassisSim using standard values for a V8 Supercar, completing a simulated lap of Willowbank Raceway. The data was then exported into MoTeC Interpreter for more convenient viewing. From Figure 6-1 the maximum logged lateral acceleration ($a_{lat_{max}}$) of the vehicle and the time taken to reach this value ($t_{0\rightarrow max}$) may be determined. To ensure accuracy, the max values taken will not be the absolute maximums, rather the maximum values that occur in the linear range of the curve.

In order to perform the bypass velocity calculations, it is necessary to determine the location of the roll centre. The roll centre is used to determine the size of the moment arms of the forces on the vehicle. This is not an easy parameter to accurately determine, as it will change position as the vehicle traverses bumps or turns corners. Its location can be found by constructing a line between the tyre's contact patch and the instantaneous centre of the suspension elements. This is repeated on the other side of the vehicle, and the intersection of these two lines is defined as the vehicle's roll centre. The determination of this point for both symmetrical and asymmetrical suspension geometry is shown in Figure 6-2. For simplicity, in this thesis, the location of the roll

centre will be assumed to be constant. A realistic estimate will be taken for its height, and it is assumed that it is occurs along the centreline of the vehicle.

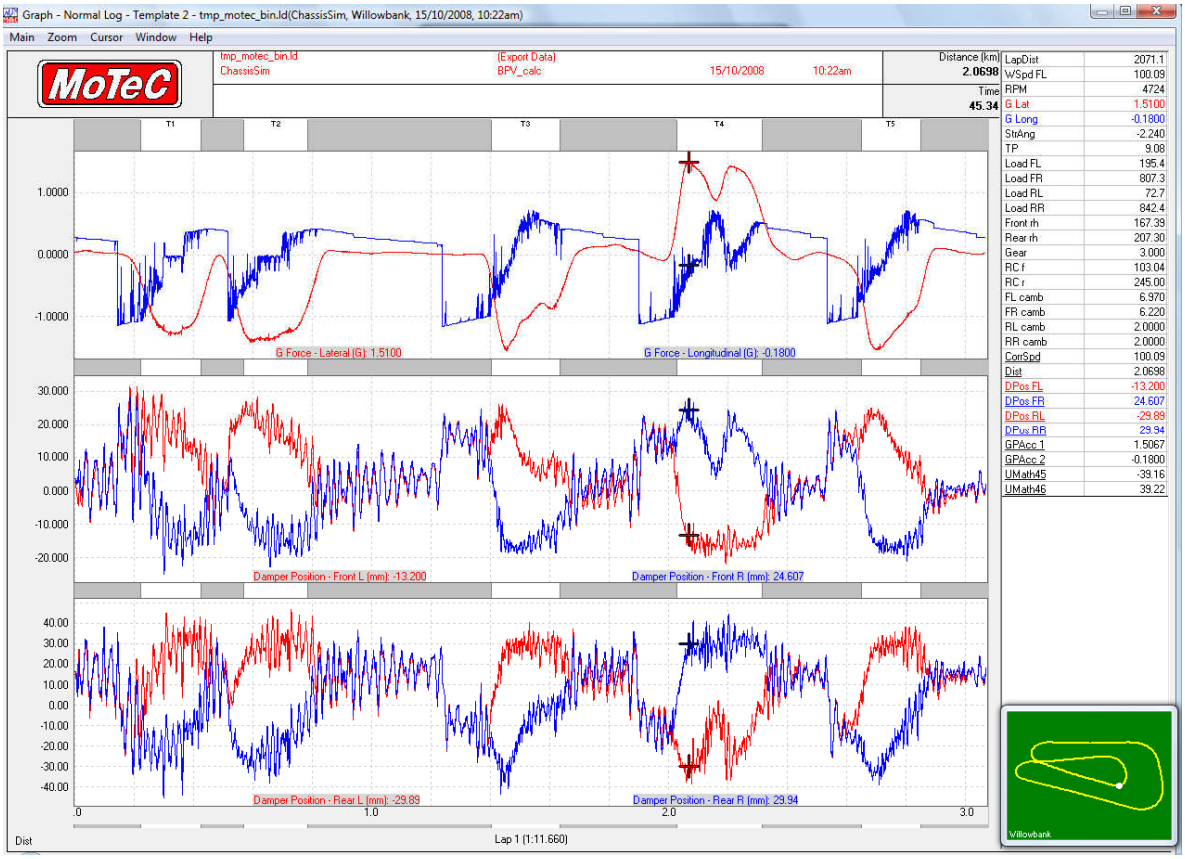

Figure 6-1: MoTeC Interpreter representation of a simulated lap of Willowbank Raceway

The diagram of the system used to determine the roll rate of the vehicle is shown in Figure 6-3. The corresponding free body diagram is given in Figure 6-4, with all forces shown in red. These can be used to determine the roll angle of the sprung mass per unit of g-force of lateral acceleration.

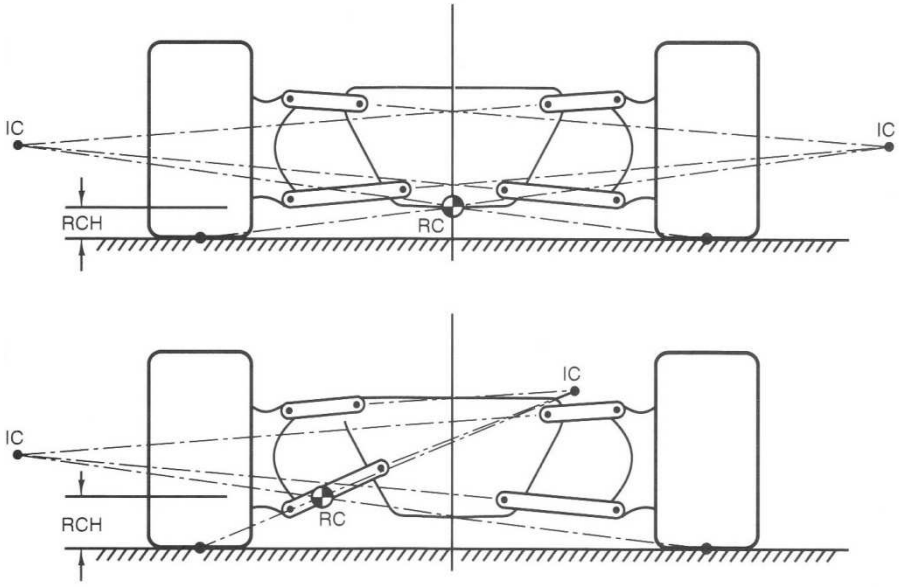

Figure 6-2: Determination of roll centre [10].

From Figure 6-1, the maximum lateral acceleration occurs at turn 4. The magnitude of this acceleration is 1.51g and it takes 1.8 seconds to reach this point from the point of 0g. These values are most easily found by running the cursor over the data in MoTeC Interpreter, and reading the values straight from the screen. A summary of the parameters used for the roll rate and bypass velocity calculation is given in Table 6-1. The tyres are assumed to be sufficiently stiff such that their deflection is negligible. Some further assumptions are that Δ_L and Δ_R equal zero in their static equilibrium position, and the effect that anti-roll bars have on spring rate has been neglected.

Table 6-1: Summary of parameters for roll rate calculations

Vehicle Parameter	Value	Units	Description
CoGH	0.495	m	height of centre of gravity
RCH	0.195	m	height of roll centre
m_T	1526	kg	total mass of the vehicle
T	1.6	m	the track of the vehicle
k_{s1}	55000	N.m^{-1}	wheel rate, front
k_{s2}	55000	N.m^{-1}	wheel rate, rear
$a_{lat_{max}}$	1.38	g	maximum lateral acceleration
$t_{0\rightarrow max}$	1.46	s	time from zero to max lateral acceleration

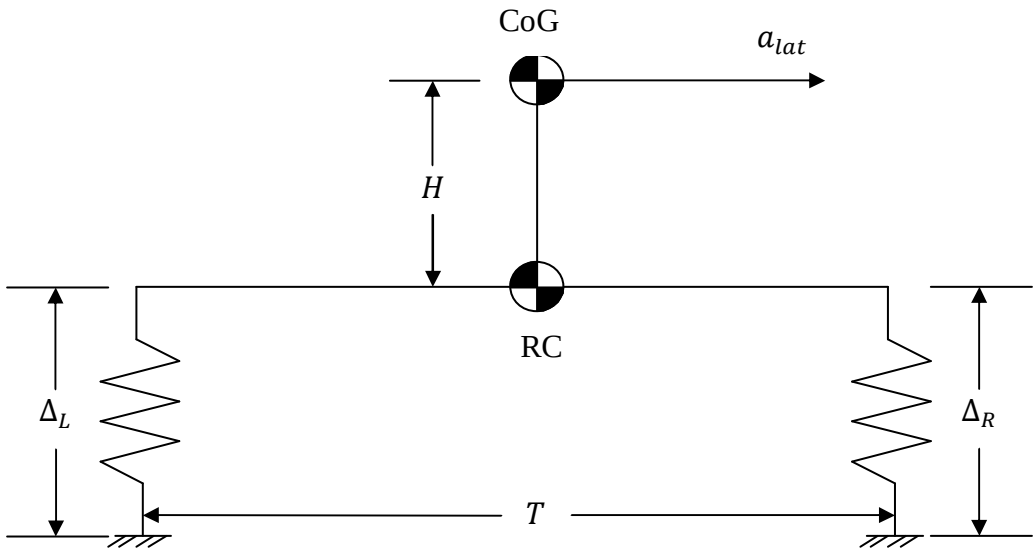

Figure 6-3: Schematic used for bypass velocity calculation

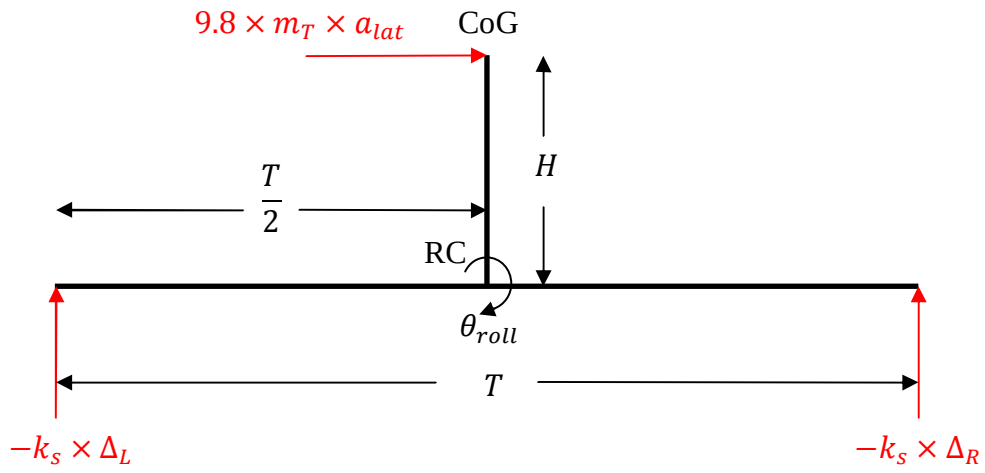

Figure 6-4: Free body diagram used to determine bypass velocities. Forces are shown in red

Using the free body diagram of Figure 6-4 as a starting point, the roll rate of the vehicle can be calculated.

The spring rate is the sum of the spring rate at the front and rear of the vehicle.

$$k_s = k_{s1} + k_{s2} \tag{6.1}$$

Because of the assumptions that vehicle is symmetric, the roll centre occurs along the centreline of the vehicle and that the angle of rotation of the sprung mass small, the following relationships can be defined:

$$\Delta_L = -\Delta_R = \theta_{roll} \times \frac{T}{2} \tag{6.2}$$

another other important relation is:

$$H = CoGH - RCH = 0.495 - 0.295 = 0.3 \tag{6.3}$$

Setting the sum of the moments about the roll centre to be equal to zero gives

$$-k_s \Delta_L \frac{T}{2} + 9.8 \times m_T a_{lat} H + k_s \Delta_R \frac{T}{2} = 0 \tag{6.4}$$

which can be simplified

$$-k_s \theta_{roll} \frac{T}{2} \frac{T}{2} + 9.8 \times m_T a_{lat} H - k_s \theta_{roll} \frac{T}{2} \frac{T}{2} = 0 \tag{6.5}$$

$$9.8 \times m_T a_{lat} H = k_s \theta_{roll} \frac{T^2}{2} \tag{6.6}$$

$$\frac{\theta_{roll}}{a_{lat}} = \frac{19.6 \times m_T H}{k_s T^2} \tag{6.7}$$

Given the values in Table 6-4, the roll rate can be determined in units of radians per unit of g-force.

$$\frac{\theta_{roll}}{a_{lat}} = 0.0319\ rad.g^{-1} \tag{6.8}$$

From the data for the maximum lateral acceleration, the maximum roll of the vehicle may be determined

$$\theta_{roll_{max}} = 0.0440\ rad \tag{6.9}$$

This gives a maximum displacement at the springs

$$\Delta_{L_{max}} = -\Delta_{R_{max}} = \frac{T}{2}\tan\left(\theta_{roll_{max}}\right) \tag{6.10}$$

$$\Delta_{L_{max}} = 35.2\ mm \tag{6.11}$$

From the time taken, the maximum velocity due to roll of the sprung mass is calculated

$$\dot{\Delta}_{L_{max}} = \frac{\Delta_{L_{max}}}{t_{0\rightarrow max}} \tag{6.12}$$

$$\dot{\Delta}_{L_{max}} = 24.1\ mm.s^{-1} \tag{6.13}$$

Equation (6.13) describes the maximum velocity of the damper assuming that the damper acts directly above, and vertical to, the centre of the wheel hub. To determine the velocity of the actual damper, this number must be multiplied by the motion ratio.

Recalling that the motion ratios are 0.63 and 1 for the front and rear dampers respectively;

$$\dot{\Delta}_{FD_{max}} = 15.2\ mm.s^{-1} \tag{6.14}$$

$$\dot{\Delta}_{RD_{max}} = 24.1\ mm.s^{-1} \tag{6.15}$$

Recall that the motivation for calculating these values was to find an estimate of the maximum velocity of the dampers due to rolling of the sprung mass of the vehicle. The intention was to set the bypass velocity at this value and utilise a higher damping ratio in the slower region of the curve to control the body roll. In reality, a V8 Supercar damper uses bypass velocities which are considerably higher than those that have been calculated here. One of the reasons for this is due to the large mass of a V8 Supercar, a higher bypass velocity is used to work the tyre harder, to generate more heat and better grip. The treatment of this is beyond the scope of this thesis, so the default bypass velocities that are included in the V8 Supercar model of ChassisSim will be used. These values are presented in Table 6-2. Although the values calculated for $\dot{\Delta}_{FD_{max}}$ and $\dot{\Delta}_{RD_{max}}$ do not relate directly to bypass velocities in the case of V8 Supercars, they are still necessary for the damper histogram analysis of section 6.3.

Table 6-2: V8 Supercar damper bypass velocities

	Bypass Velocity in Bump (mm/s)	Bypass Velocity in Rebound (mm/s)
Front Damper	100	50
Rear Damper	50	100

6.2 Lap Time Analysis

6.2.1 Linear Damping

Now that bypass velocity for the damper has been defined, it is necessary to find a way to make accurate quantitative comparisons between different configurations. Using the seven post shaker rig to repeat the CPL analysis from section 5.2 is unlikely to be sufficient. This is because in this analysis mode, the road inputs are identical and simultaneous in each of the four tyres. This may result in some low frequency pitching of the vehicle's sprung mass, as determined in Figure 3-6, however it does not take into account the roll of the sprung mass due to the lateral g-forces on the vehicle. As this is one of the fundamental reasons for using a dual rate damper, another method of comparison is necessary. For this, a lap time simulation will be used. This will also allow the effect of the different bump profiles and configurations of corners at the individual tracks to be taken account of. The track that will be used for this analysis is Willowbank Raceway in Queensland. There are two main reasons for this.

1. This is used as a test track for many V8 Supercar teams meaning that its bump characteristics are well defined and are typical of Australian V8 Supercar Circuits.
2. The simulation on this track executes much more quickly than most of the other tracks. Given that each simulation can take anywhere up to 3 minutes to complete, this becomes an important factor for this thesis where hundreds of individual simulations are required.

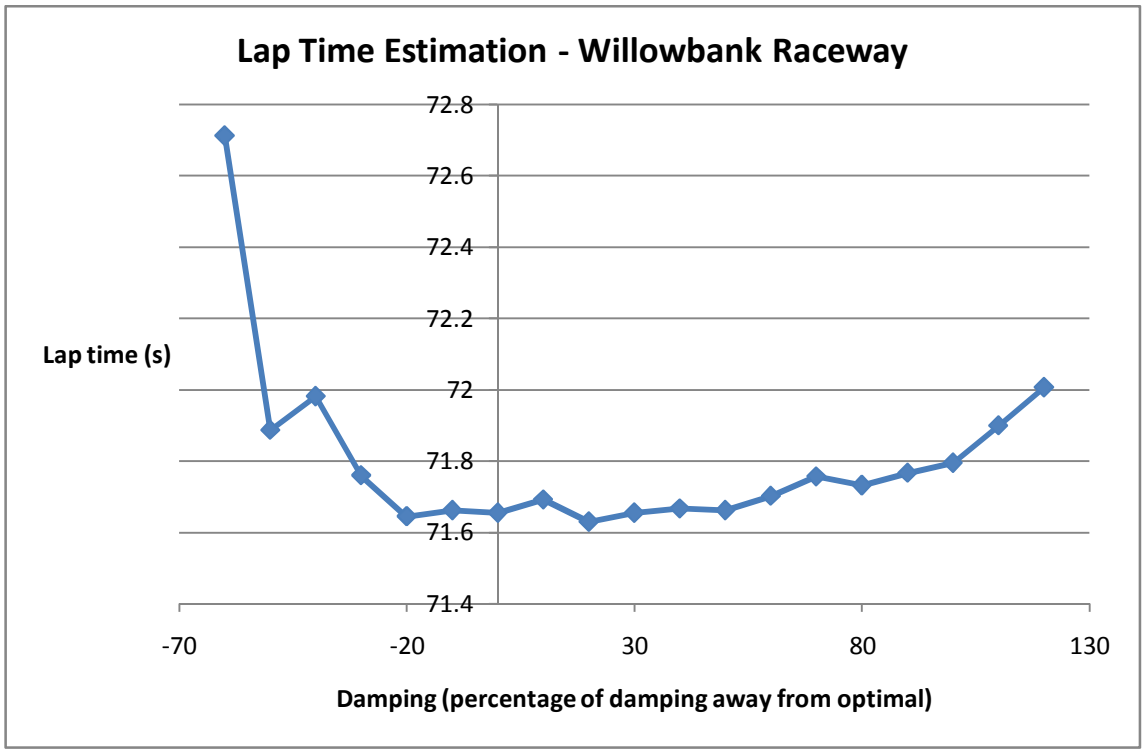

Figure 6-5: The effect of moving damping characteristics away from the CPL optimal values on ChassisSim predicted lap time

The first step of this analysis is to use linear dampers, like those already studied, on this track. This will show how closely the CPL analysis translates across to the road profile for this particular track. It will also act as a good starting point for the iterative process

that will need to be carried out. The results of these simulations are plotted in Figure 6-5. This graph was created by starting with the values for front and rear damping coefficients that were determined to be optimal according to the CPL analysis of section 5.2. These were 3200 Ns/m at the front and 2000 Ns/m at the rear. These values were then varied by the same percentage as shown by the abscissa of the graph, and the predicted lap time obtained.

The first thing to notice from Figure 6-5 is that the fastest lap time occurs when the damping coefficients are 20% greater than those determined to be optimal by way of the seven post shaker rig analysis. This result is expected, as the seven post shaker rig analysis neglects the effect of lateral g-force induced body motions, which have been explained as requiring a higher damping ratio to control. A surprising result from this graph is that altering the damping in the region from -20% through to +50% results in less than a 0.1 of a second difference, which in practice is an unlikely result.

To give some perspective on these lap times, the top eight qualifying times from the V8 Supercar meeting at this track in July of 2008 are given in Table 6-3. This shows that the fastest lap time was 70.7351 seconds, and that there was less than 0.2 seconds between the best qualifier and qualifying in eighth place.

Table 6-3: Results from V8 Supercars qualifying 9/7/08 [23]

Position	Driver	Fastest Lap Time	Gap
1	James Courtney	1:10.7351	0
2	Mark Winterbottom	1:10.7438	0:00.0087
3	Russell Ingall	1:10.8066	0:00.0715
4	Craig Lowndes	1:10.8503	0:00.1152
5	Mark Skaife	1:10.8887	0:00.1536
6	Garth Tander	1:10.9096	0:00.1745
7	Will Davison	1:10.9279	0:00.1928
8	Jason Richards	1:10.9303	0:00.1952

6.2.2 Lap time with BPV

A non-linear analysis can now be conducted using the optimal results from the linear case as a starting point, once again by taking an iterative approach. Some of the initial values of interest are presented in Table 6-4. At this stage, the damping coefficients are assumed to be equal in both bump and rebound.

Table 6-4: Initial values of damping coefficients and bypass velocity

Damper	Low Speed Damping Coefficient (Ns/m)	High Speed Damping Coefficient (Ns/m)	Bypass Velocity Bump (mm/s)	Bypass Velocity Rebound (mm/s)
Front	3840	3840	100	50
Rear	2400	2400	50	100

The iterations begin with the front damper by varying its low speed damping coefficient, while holding all the other parameters constant. The results of this lap time simulation are presented in Figure 6-6. The general shape of this graph agrees with what is expected, both from practical experience, and the mathematical reasoning explained throughout this thesis. The optimal damping point for the low speed region at the front is 7000 Ns/m, which is higher than what was predicted for a linear damper.

There are, however, a few concerning features about this graph. Firstly, there is a considerable amount of "noise" and peakiness in the results. Once again, over a very large region of damping coefficients there is only a very small variation in lap times, which does agree well with what is known in practice.

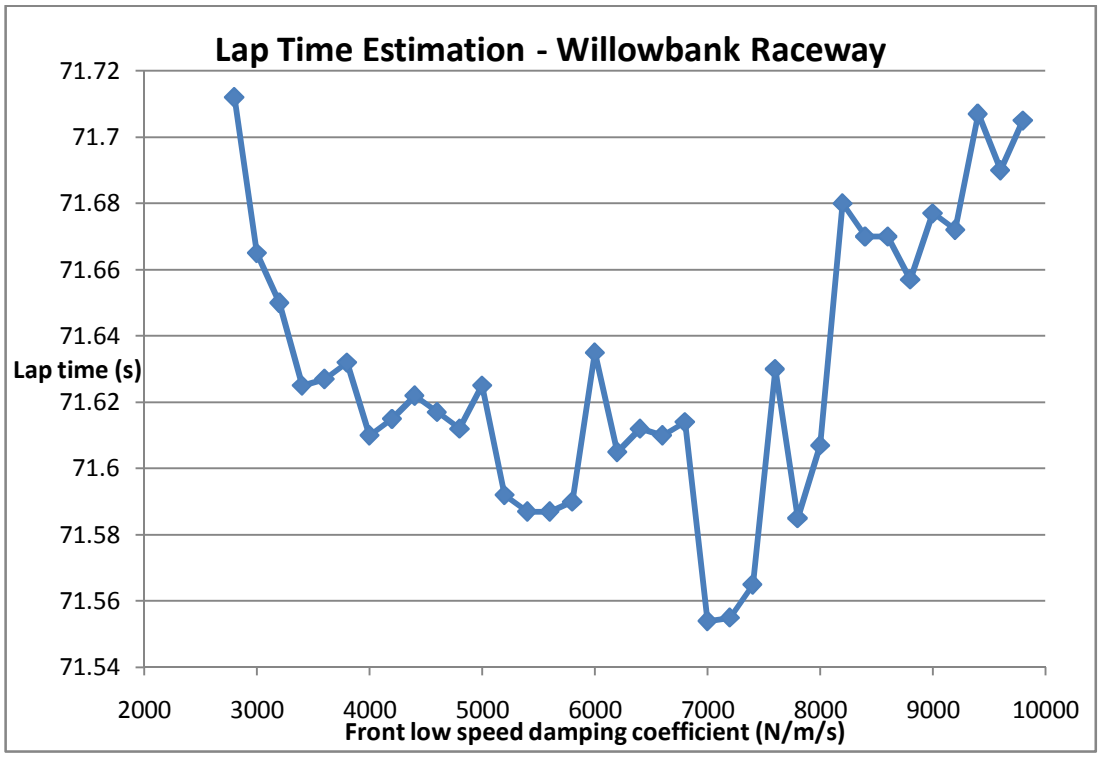

Figure 6-6: Effect of variation of low speed damping coefficient at front on predicted lap times

Because the slope of the damper curve is now much steeper in the low speed region, the height of the curve at the bypass velocity is now much higher. Despite the fact that the high speed damping curve has not changed its slope, it now has an offset which means that the damper force is much higher for a given velocity than it was before the low speed region was altered. This is best demonstrated by comparing Figure 6-7 with Figure 6-8. These are screenshots of the damper curves created by the ChassisSim damper properties toolbox. Figure 6-7 shows a linear damper, while Figure 6-8 demonstrates the effect of increasing the low speed region of the curve. For example, in the bump region, the damper force as 450 mm/s has increased from 4354 N to 5123 N. Note also that the numbers in this toolbox are not the same as those that have been used in the analysis to this point. This is because until now, all of the analysis has been completed assuming that the dampers and springs are acting directly at the wheel, which is also known as the "wheel rate model". In this program, these numbers have been converted to the actual values at the damper and spring, by taking into account the motion ratio. The treatment of this was described in section 1.3.3.

Bearing this in mind, the high speed damping ratio must now be readjusted. Holding the low speed damping coefficient at its new-found optimal value of 7000 Ns/m, the effect of varying the high speed damping coefficient on lap time is plotted in Figure 6-9. Again, it is clear in this figure that the lap time prediction is under estimating the effect of varying the damper properties. Also, the amount of noise in the results is very large in comparison to the variation in the value of the results themselves.

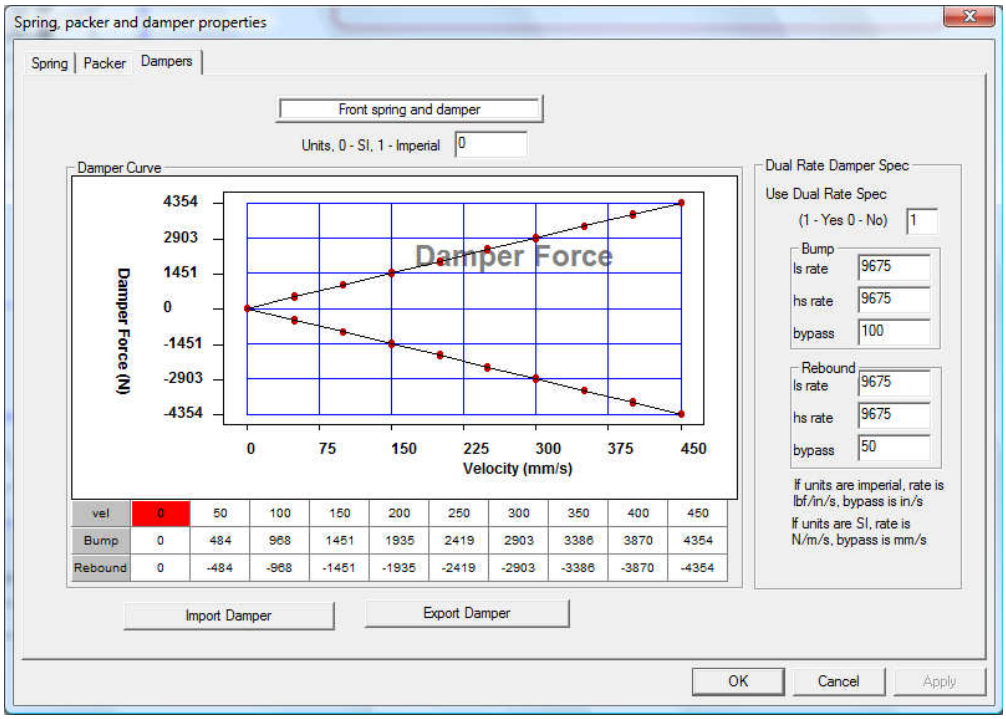

Figure 6-7: ChassisSim damper property toolbox with linear damper

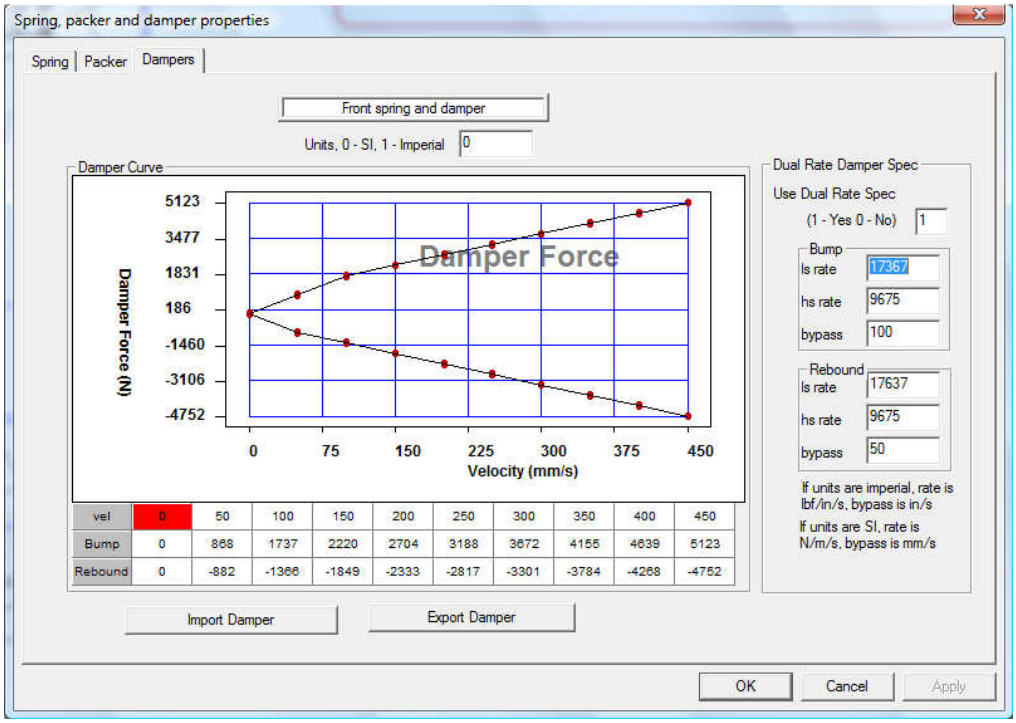

Figure 6-8: The effect of variation of low speed damping properties on the high speed region of the curve

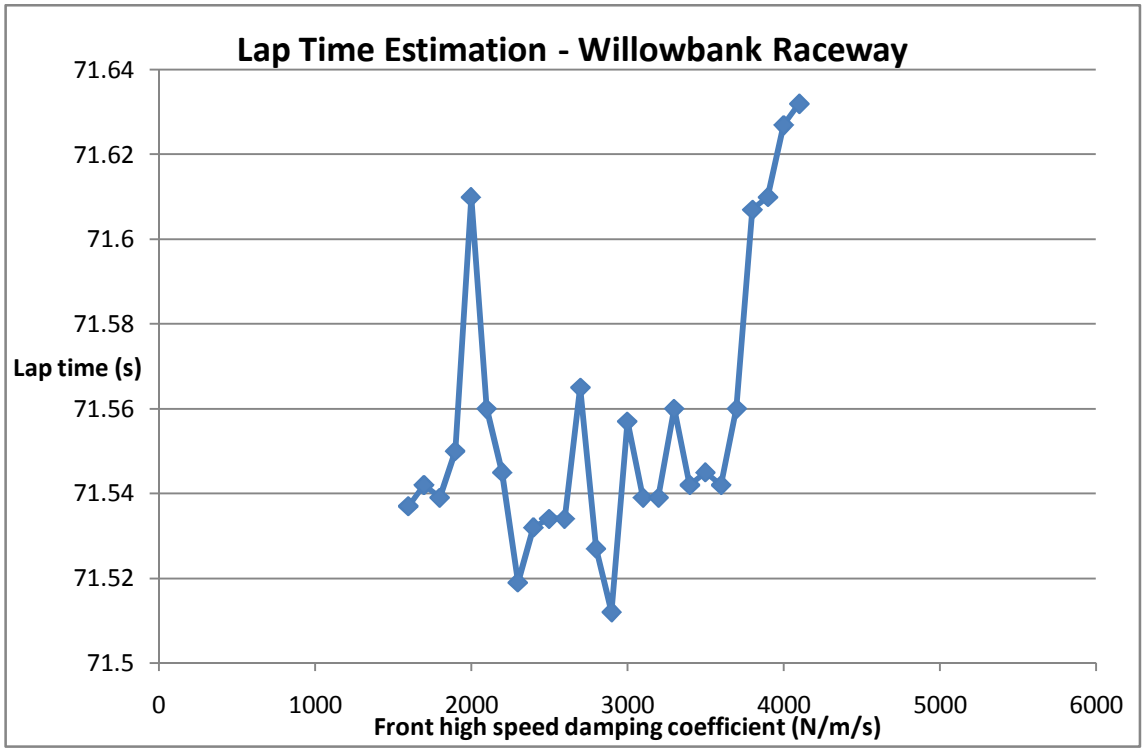

Figure 6-9: Effect of readjusting the high speed damping coefficient on predicted lap times

It is apparent that this method of analysis is extremely time consuming, and labour intensive. Also the results being obtained are confusing. This method of damper optimsiation is unsuitable for the needs of a V8 Supercar team.

6.2.3 Optimisation Toolbox

Another tool which comes with the ChassisSim package is the optimisation toolbox. This toolbox allows the user to input a range of damping parameters to be explored, shown in Figure 6-10. It then runs a number of subroutines to determine the damper

curves which will result in the fastest lap time. This toolbox can also be used to optimise other parameters of the vehicle, such as spring rates and aerodynamic balance, however these will not be considered as they are beyond the scope of this thesis. Their optimisation can be switched off by entering zeros in the appropriate boxes.

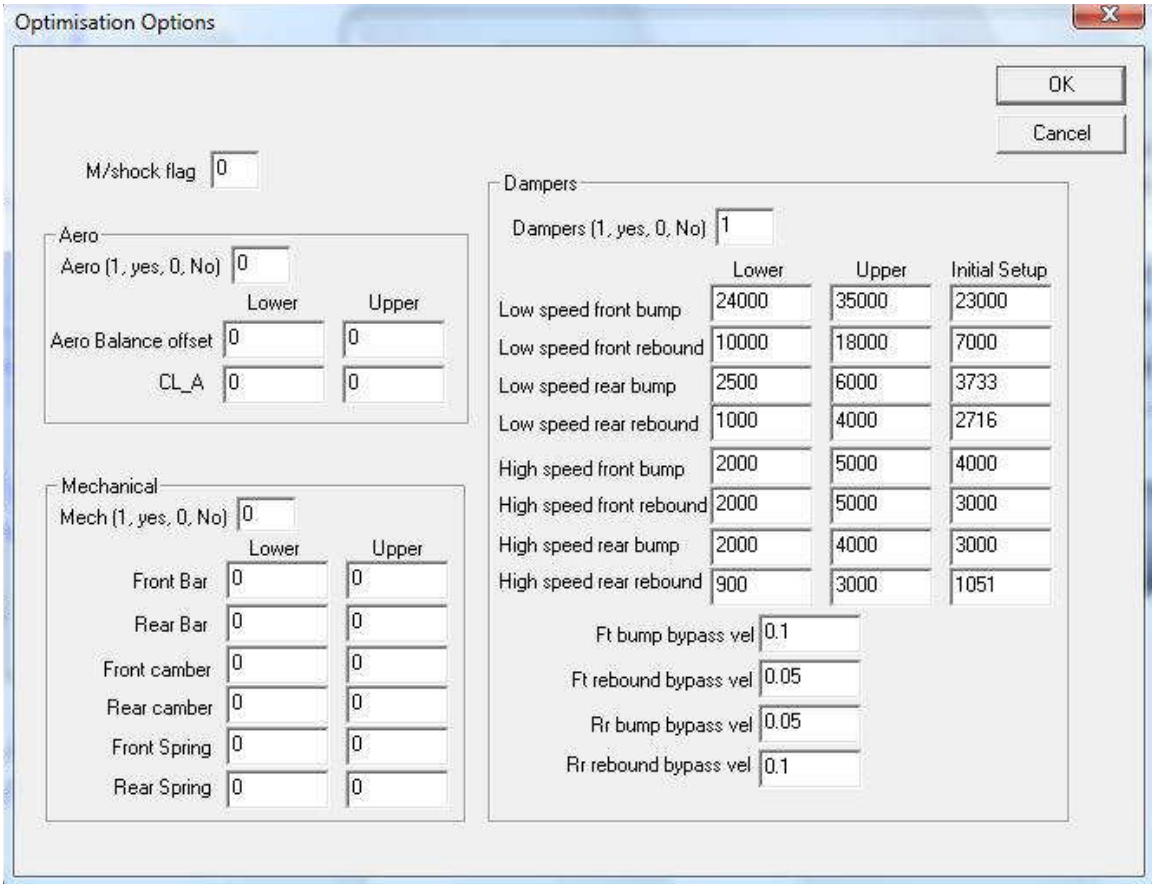

Figure 6-10: The ChassisSim optimisation toolbox interface

After running an optimisation of the dampers for the default V8 Supercar at Willowbank Raceway, ChassisSim predicts that the damping coefficients provided in Table 6-5 will produce the fastest lap time, of 71.324 seconds. The values given in Table 6-5 are as they would apply to the actual damper. To continue to analyse this

vehicle as a wheel rate model, the damping coefficients as they apply at the wheel are required. Table 6-6 shows the damping coefficients as they apply at the wheel, by taking into account the effect of motion ratio.

Table 6-5: Results of optimisation for Willowbank Raceway. Note that these are the values as they apply at the damper.

	Bump		Rebound	
	Low Speed Damping Coefficient (Ns/m)	High Speed Damping Coefficient (Ns/m)	Low Speed Damping Coefficient (Ns/m)	High Speed Damping Coefficient (Ns/m)
Front	30857	3004	11410	2667
Rear	3733	3396	2716	1051

Table 6-6: Results of optimisation of dampers for Willowbank Raceway. These are the values as they apply at the wheel.

	Bump		Rebound	
	Low Speed Damping Coefficient (Ns/m)	High Speed Damping Coefficient (Ns/m)	Low Speed Damping Coefficient (Ns/m)	High Speed Damping Coefficient (Ns/m)
Front	12247	1192	4529	1059
Rear	3733	3396	2716	1051

These values result in the front and rear damper curves of Figure 6-11 and Figure 6-12. These curves are only presented as they would apply at the damper, because this is where the adjustments are made. That is to say, that although the wheel rate model is often used to simplify the analysis, the race engineer is ultimately only interested in how to tune the actual damper. It is now apparent that the reason that the lap time analysis of section 6.2.2 gave such confusing results is because the optimal damping coefficients do not occur within the range of values that were being studied.

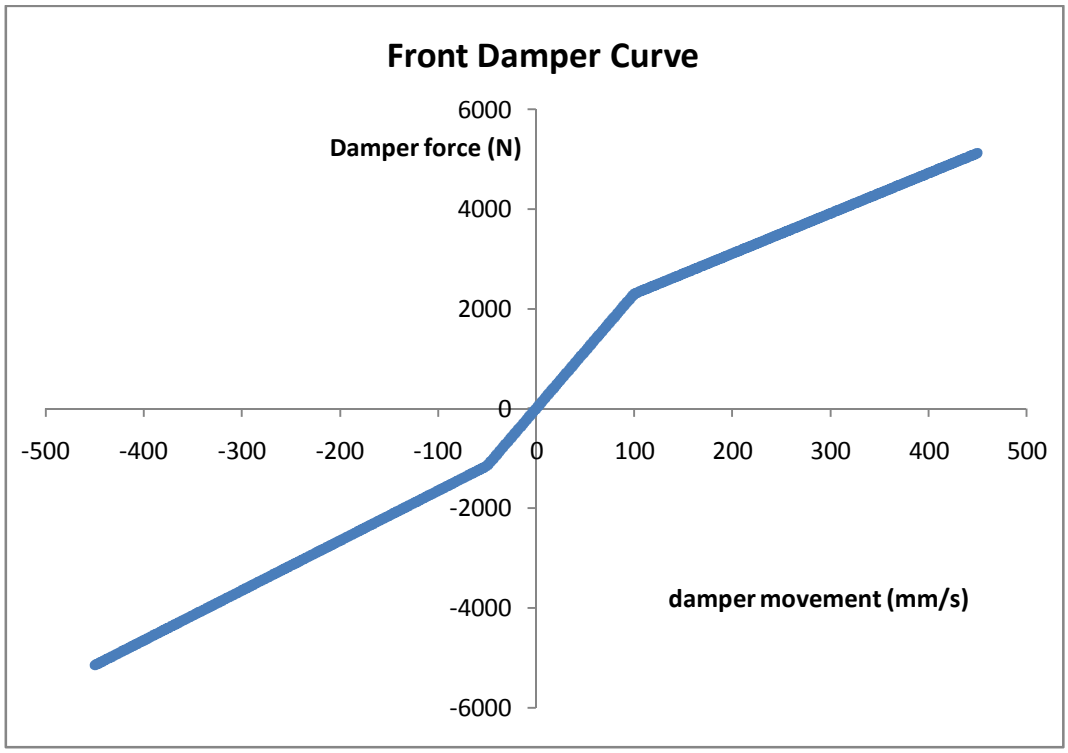

Figure 6-11: Front damper curve created by ChassisSim optimisation toolbox

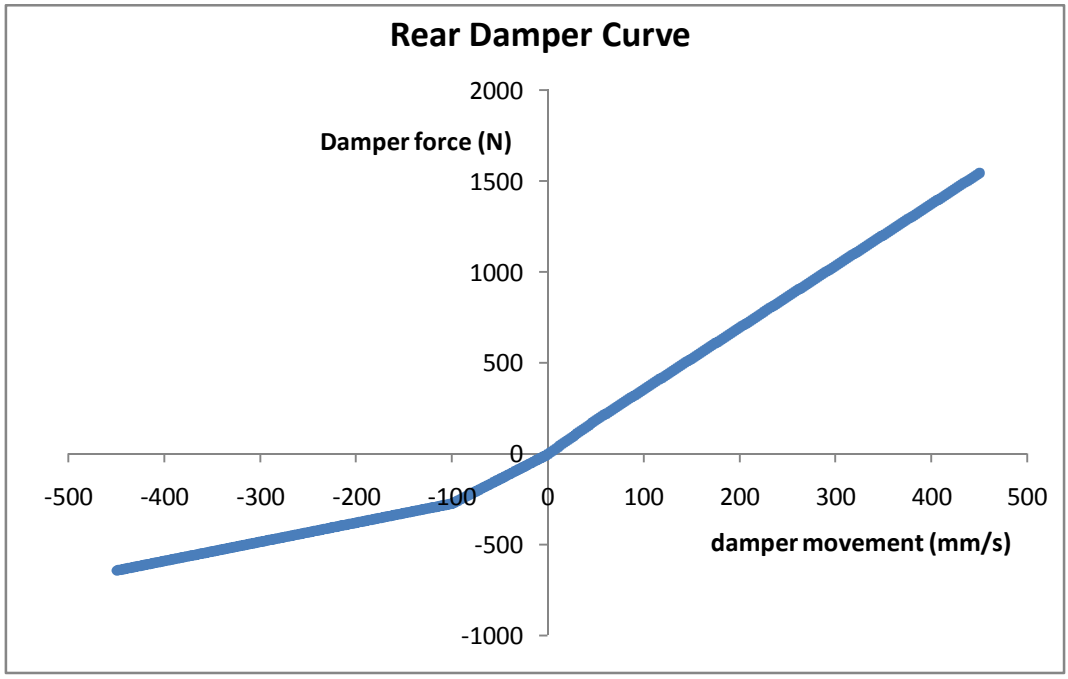

Figure 6-12: Rear damper curve created by ChassisSim optimisation toolbox

6.3 Damper histogram analysis

There are a number of reasons why the lap time prediction may not be the best estimation of a vehicles performance. For instance, the lap time simulation makes assumptions about the skill of the driver. That is, the driver is assumed to be driving the vehicle at the limit of traction of the tyres at all times. In reality, it is not possible for a driver to do this. Instead it is important that the vehicle is not just theoretically fast, but also able to be *driven* fast. Other factors include the fact that the set-up that produces the fastest simulated lap may be unacceptably harsh on tyres, causing them to wear extremely quickly, creating a poorly performing car in later laps. Alternatively, this set-up may not work the tyres hard enough, meaning that they do not generate enough heat to operate at their peak efficiency.

Because of all these factors, it is still necessary to evaluate the data that is produced from the simulated lap, in a somewhat empirical manner. The damper traces can be analysed to ensure that they fit the characteristics known from empirical experience to be optimal, and if they are not at their optimal values, empirical rules can be used to remedy this. This is where the concept of a "damper histogram" becomes important.

Due to the peculiarities of a V8 Supercar, such as its high unsprung mass and relatively skinny tires, it has been found in practice that the optimal shape of the damper curves for a V8 Supercar don't strictly relate to what has been suggested as optimal in the mathematical analysis of this thesis. Instead, engineers of V8 Supercars rely on somewhat empirical rules to analyse their dampers from the vehicle's logged data. The concept of damper histogram analysis was discussed by Nowlan [8]. This uses a series of semi empirical rules to tune the dampers to their optimal point. A damper histogram is presented as the histogram of the damper's velocity throughout a lap. The values of maximum damper velocity due to roll, that were calculated in section 6 are necessary for performing a damper histogram analysis, as it is known from practice that a V8 Supercar will perform best when the velocity of the front damper is slower than this value for 20% of the lap in both bump and rebound. It is also desired that the overall shape of the histogram is a symmetric bell curve. These values are applicable at the front of a V8 Supercar. At this stage there is no published data which describes the optimal damper histograms for the rear dampers of a V8 Supercar. This is most likely due to the peculiarity of its suspension geometry, and the fact that it carries a relatively high unsprung mass compared to other race cars.

To begin the damper histogram analysis, an initial estimate of damping coefficients is required. Damper histogram analysis is best defined for the front suspension, so these are what will form the primary focus of this chapter. The rear dampers will be set at the values found by the ChassisSim optimisation toolbox in section 6.2.3 to be best.

For the front damping, the dampers will initially be assumed linear. The best estimate of linear damper was made in section 5.2, and this gave optimal damping coefficients of 3840 Ns/m at the front wheels.

The damper histograms in this thesis have been created using MATLAB. An example of the .m file used to create these is given in Appendix B.5. To determine the damper velocity, the damper position trace is differentiated for each individual time step of the ChassisSim output. The damper histogram is calculated using values at the damper, as opposed to at the wheel. This means that the effect of motion ratio must be accounted for. Treatment of this was covered in section 1.3.3. Recalling that the motion ratios for this vehicle are 0.63 at the front and 1 at the rear, the initial damping coefficients of the actual dampers are presented in Table 6-7.

The damper histograms for this vehicle completing a lap of Willowbank Raceway are presented in Figure 6-13. A couple of important points need to be noted about these graphs. Firstly, the scale along the x-axis and the size of the information bins are different between the front and the rear dampers. This is because the lower motion ratio at the front, means that the damper velocities at the front are confined to a smaller

range. Secondly, the data peaks at the histogram's extremities refer to all the remaining data outside of the range that has been graphed.

Table 6-7: Initial damping coefficients for damper histogram analysis

	Bump		Rebound	
	Low Speed Damping Coefficient (Ns/m)	High Speed Damping Coefficient (Ns/m)	Low Speed Damping Coefficient (Ns/m)	High Speed Damping Coefficient (Ns/m)
Front	9674	9674	9674	9674
Rear	3733	3396	2716	1051

The first thing to notice is that the percentage of time in the low speed region in both bump and rebound is much lower than the 20% required. With this in mind, either the low speed regions of the curve can be increased, or the high speed decreased.

In this case, a little of each can be done, which results in Table 6-8 as the values for the next iteration. These parameters, once run through a simulated lap using ChassisSim, and then though the MATLAB damper histogram .m file, result in the damper histograms for the front dampers in Figure 6-14. The low speed percentages are still too low, and there is some asymmetry beginning to develop in the shape of the curves.

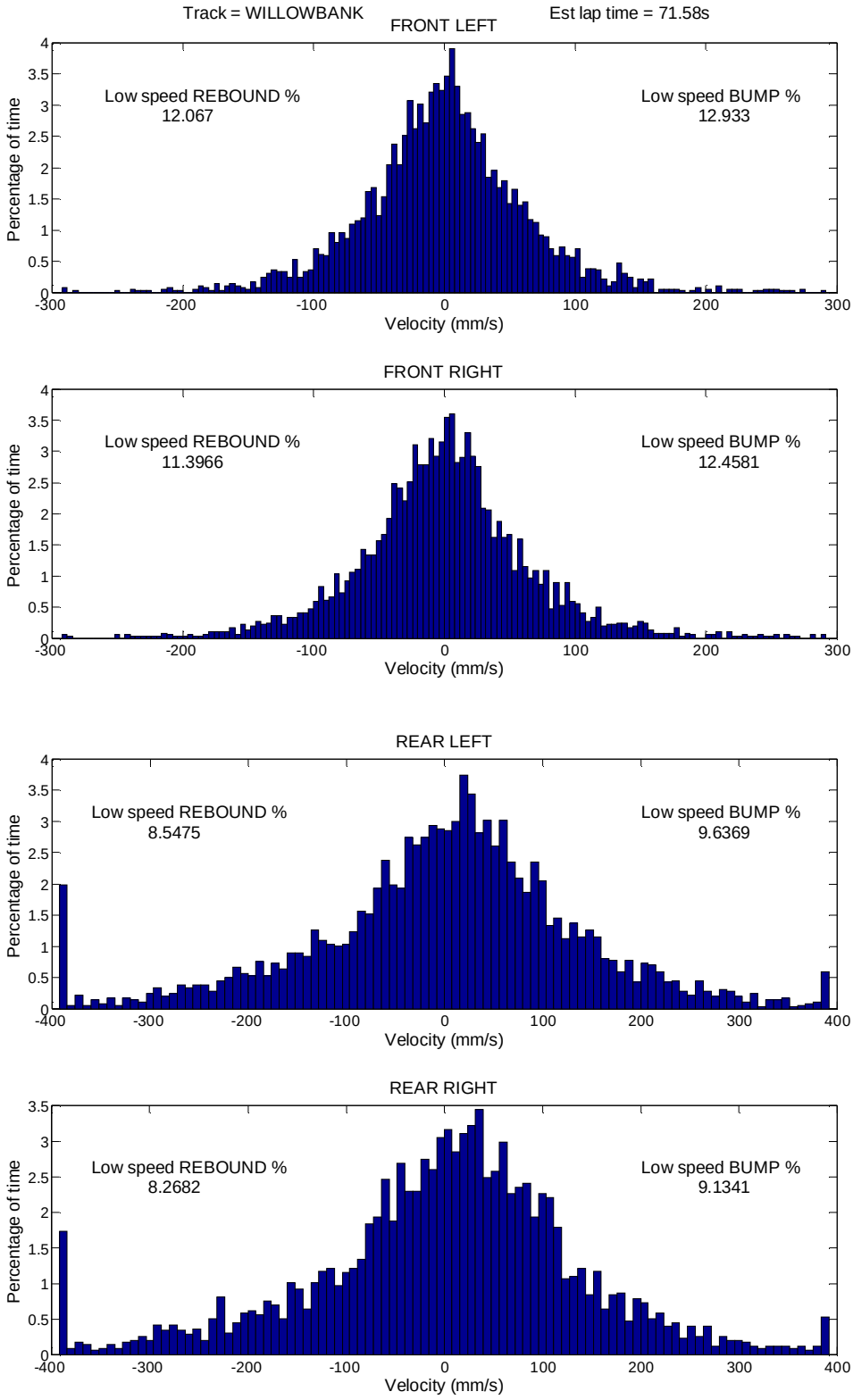

Figure 6-13: Damper histograms with initial damping coefficients

Table 6-8: Values for damper histogram analysis, second iteration values

	Bump		Rebound	
	Low Speed Damping Coefficient (Ns/m)	High Speed Damping Coefficient (Ns/m)	Low Speed Damping Coefficient (Ns/m)	High Speed Damping Coefficient (Ns/m)
Front	16000	8062	16000	8062
Rear	3733	3396	2716	1051

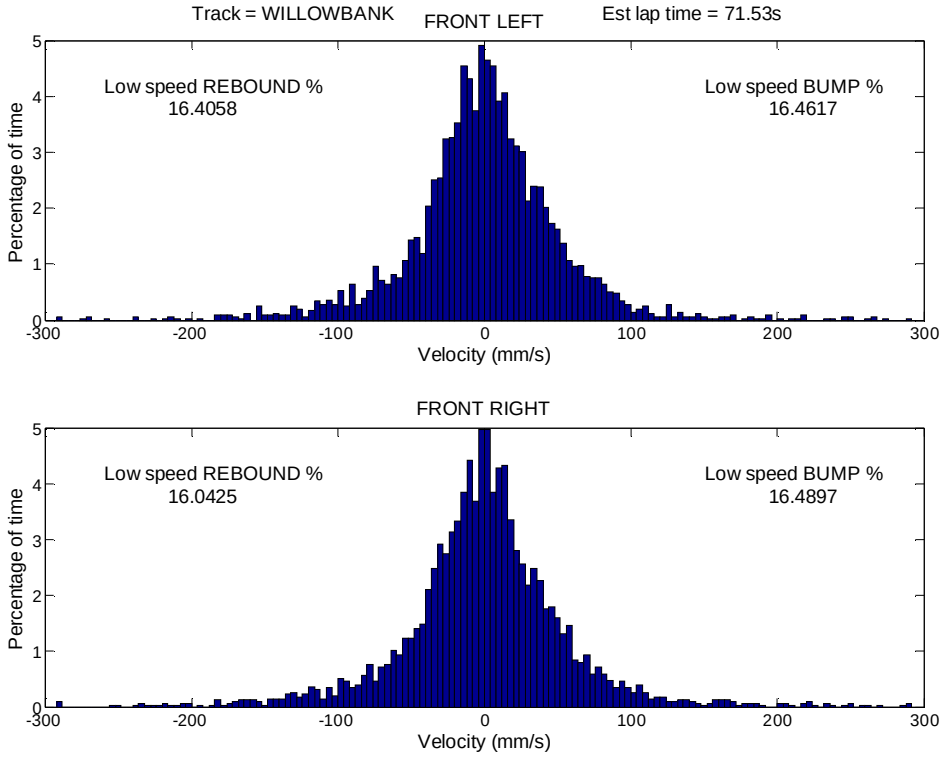

Figure 6-14: Damper histograms, second iteration

This procedure is repeated until the desired shape of the damper histogram is obtained. For this vehicle, at this track, the optimal damping coefficients obtained via damper histogram analysis of the front suspension are presented in Table 6-9. The shape of the damper curve is shown in Figure 6-15 and the histograms of this are shown in Figure 6-16.

Table 6-9: Final damper histogram analysis values

	Bump		Rebound	
	Low Speed Damping Coefficient (Ns/m)	High Speed Damping Coefficient (Ns/m)	Low Speed Damping Coefficient (Ns/m)	High Speed Damping Coefficient (Ns/m)
Front	23000	8062	23000	10000
Rear	3733	3396	2716	1051

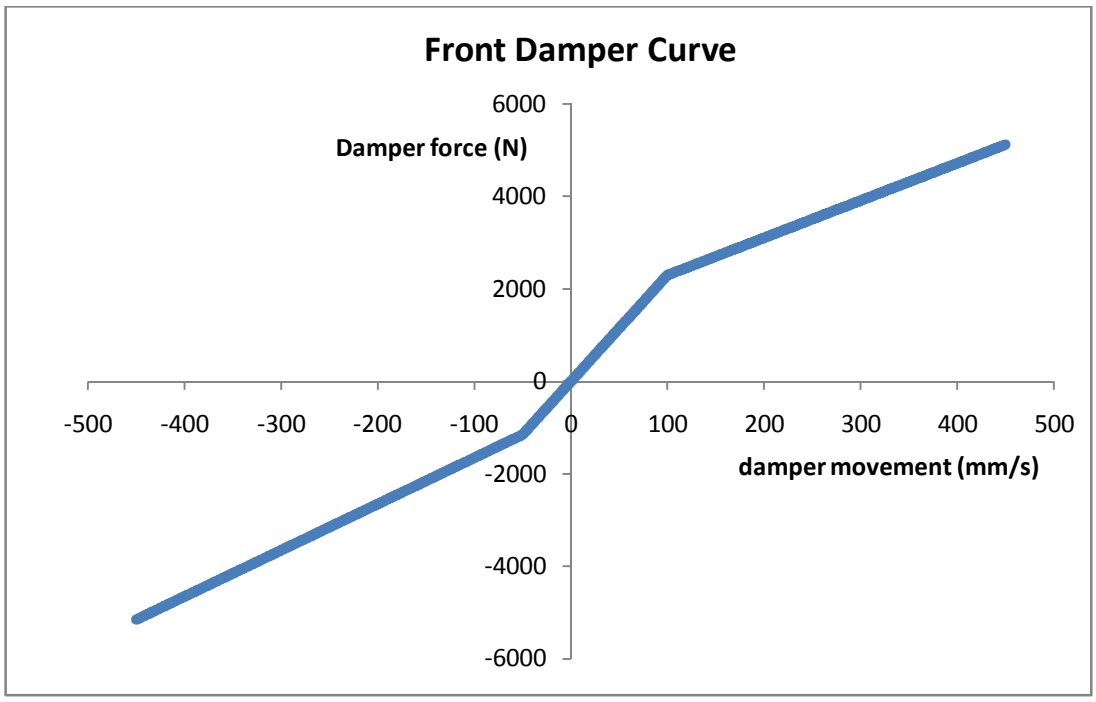

Figure 6-15: Front damper curve after damper histogram analysis

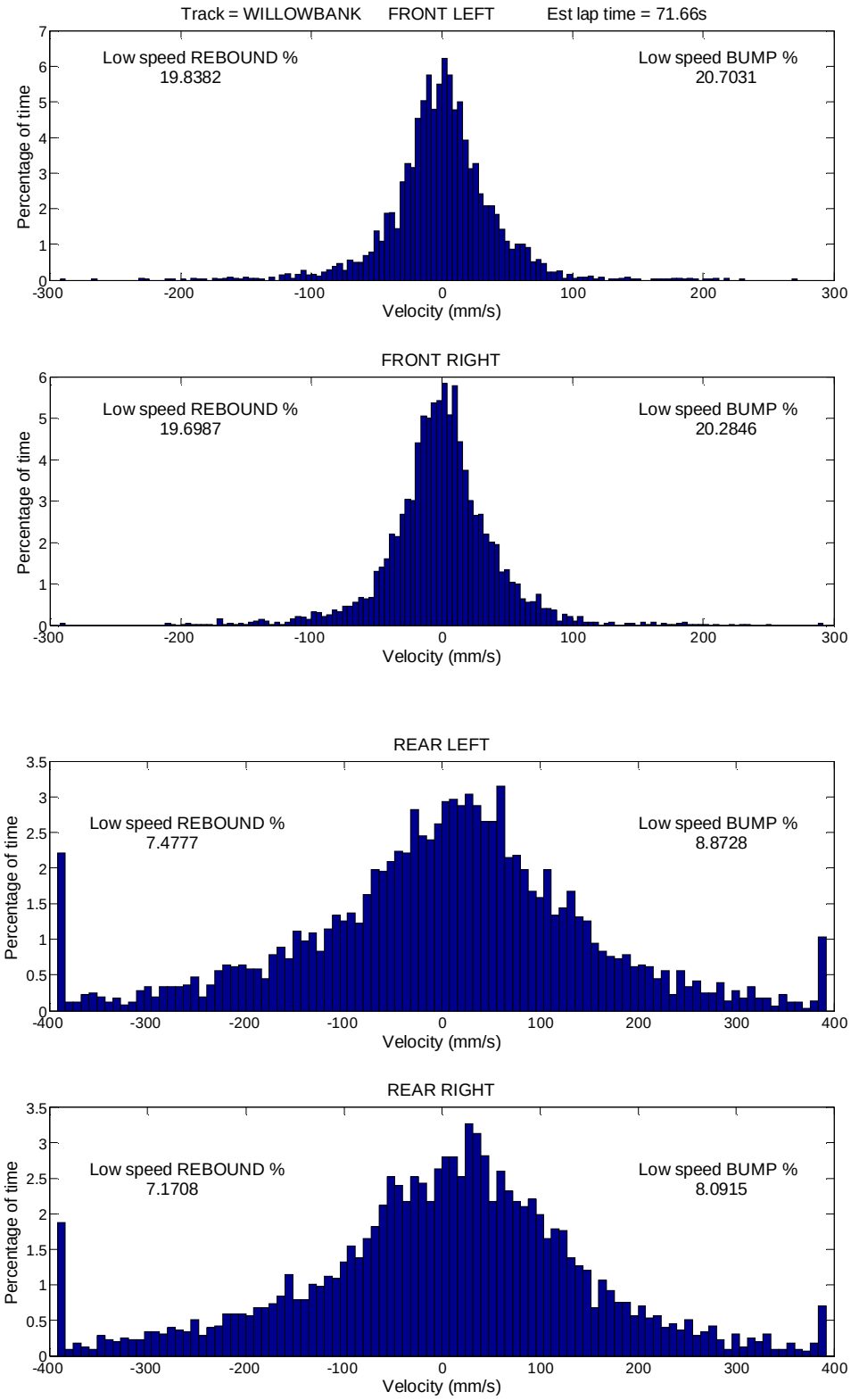

Figure 6-16: Final damper histograms

Chapter 7 – Comparison of damper selection methods

Now that four different methods of selecting the optimal dampers for the vehicle have been examined, some comparisons will be made between the different methods, to try to determine which of these will be best. These methods, as they have been applied to this thesis, can be broken into two different categories: linear and non-linear.

7.1 Linear Damping

V8 Supercars do not use linear damping, and as such the linear damping methods used in this thesis cannot be applied in order to find the optimal dampers. That said there are a few important things that can be noted from the linear damper study of this thesis, the results of which are summarised in Table 7-1.

Table 7-1: Comparison of linear damping coefficients at the wheel

	Evaluation Criterion		CPL Analysis		Linear Lap Time Approximation	
Chapter	4		5.2		6.2.1	
	Damping Coefficient (Ns/m)	Damping Ratio	Damping Coefficient (Ns/m)	Damping Ratio	Damping Coefficient (Ns/m)	Damping Ratio
Front	4250	0.49	3200	0.37	3840	0.44
Rear	3000	0.38	2000	0.25	2400	0.3

The first thing to note is the difference in damping ratio between the results obtained by the evaluation criterion, and those from the CPL analysis. This occurs because of the inclusions of extra complexities such as aerodynamic loads in the CPL analysis. Also, the CPL analysis uses a different sweep of sine waves as an input to that of the evaluation criterion. This highlights the importance of using accurate input parameters to a simulated vehicle model. It also shows how seemingly small changes of one or two of the vehicle's characteristics can have quite a dramatic effect on the way that the vehicle performs.

It should also be noted that the evaluation criterion and CPL analysis both underestimate the damping ratio required. This occurs because both of these analyses make the assumption that the vehicle is travelling in a straight line, and therefore body roll is unlikely to occur. When travelling around a circuit, however, body roll is a significant issue, and needs to be controlled by a higher damping ratio. This is why the damping ratios of the linear lap time approximation in Table 7-1 are higher than those obtained through CPL analysis alone.

7.2 Non-Linear Damping

A summary of optimal non-linear damping ratios for the front of the vehicle that are obtained by the methods outlined in this thesis are presented in Table 7-2. This table also contains the damping ratios which have been suggested by Nowlan [8]. The damper curves that these damping ratios require are compared in Figure 7-1. From this figure, it can be seen that different analysis methods result in different optimal damper

curves. It is necessary to make a decision about which method is most appropriate for a given circumstance.

Table 7-2: Comparison of damping ratios at the front obtained by various methods

Front Damper		Nowlan [8]	Lap time optimisation	Damper histogram
Bump	Low Speed	0.5-1.2	1.41	1.05
	High Speed	0.3-0.4	0.14	0.37
Rebound	Low Speed	0.3-0.7	0.52	1.05
	High Speed	0.3-0.4	0.12	0.46

The first point to notice is that lap time optimisation using the ChassisSim optimisation toolbox is extremely computationally intensive. It usually requires several hundred individual laps to be simulated, each of which can take up to approximately 4 minutes, depending on which track is being simulated and the speed of the computer. This means, that most optimisations usually take between 10 and 20 hours to complete. Although the optimisation is a great tool for setting some base values for the dampers, it cannot be used during the race meeting itself, due to time constraints.

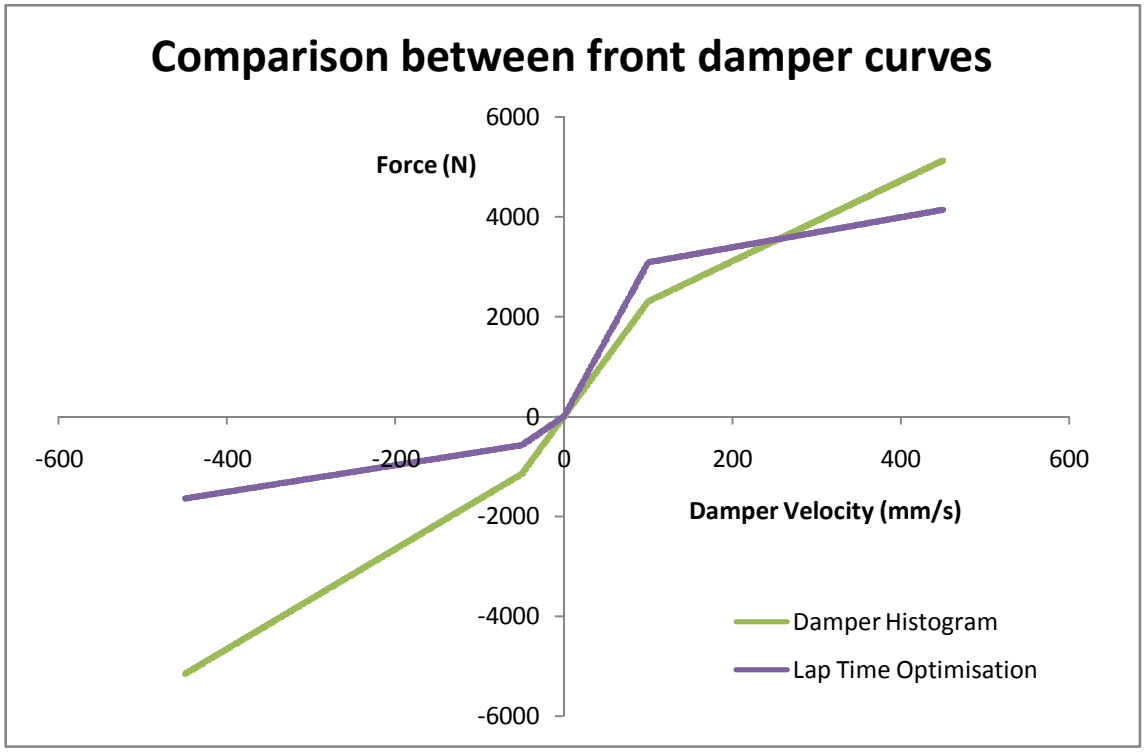

Figure 7-1: Comparison of front damper curves obtained by different methods

At the actual race meeting, conditions will change by the hour, requiring adjustments to the vehicles parameters such as spring rates and aerodynamic balance. These adjustments will change the shape of the ideal damper, so a much more efficient method of optimising the damper curves is required. This is why the method of damper histogram analysis was created. By knowing what shape the damper histogram should be, the engineer can tune the damper until it takes this shape. Previous to simulation packages such as ChassisSim being available, the engineer would simply take a "guess" at what adjustment should be made. ChassisSim allows the engineer to run as many laps as required to ensure the histograms are correct before the actual vehicle even begins the race.

The damper histogram analysis of this thesis has been confined only to the front dampers. This is because the optimal shape of the histogram for the front has already been defined. To perform this analysis at the rear would require the team to look at the damper histograms of its actual logged data of the rear damper from laps at various circuits where the vehicle performed well. From this, patterns could be found and rules defined for the optimal shape of the rear damper histograms. Because race car teams are typically quite secretive, the appropriate logged data could not be collected for analysis within this thesis.

Figure 7-2 shows the front damper histograms using the dampers suggested by running the optimisation toolbox for Willowbank Raceway. Despite the fact that this configuration resulted in the fastest simulated lap, it is seen from a damper histogram analysis that these dampers are not ideal. This histogram is skewed towards the bump side of the curve, with too much damping occurring in the low speed bump region, and too little occurring in the low speed rebound. This is also apparent from Figure 7-1, where the damping force of the damper obtained through lap time optimisation is very low in rebound.

There are a number of explanations for this. For instance, simply obtaining the fastest single lap may come at the cost of the vehicles performance over the duration of the race, if the vehicle wears out the tyres unnecessarily quickly. Also, increasing the damping coefficients can increase the amount of heat generated by the tyre, which may increase the tyre's performance. Finally, in obtaining the lap times, ChassisSim assumes that the driver's skill is such that the vehicle is driven at the limit of traction at all times.

By using extremely low damping ratios, as is the case in these lap time optimised dampers, it may create an unpredictable vehicle where it is simply beyond the skill level of the driver to remain at the limit of traction.

It is for all of these reasons that the damper histogram analysis is used by race teams, and is the best way of using the capabilities of a simulation package such as ChassisSim.

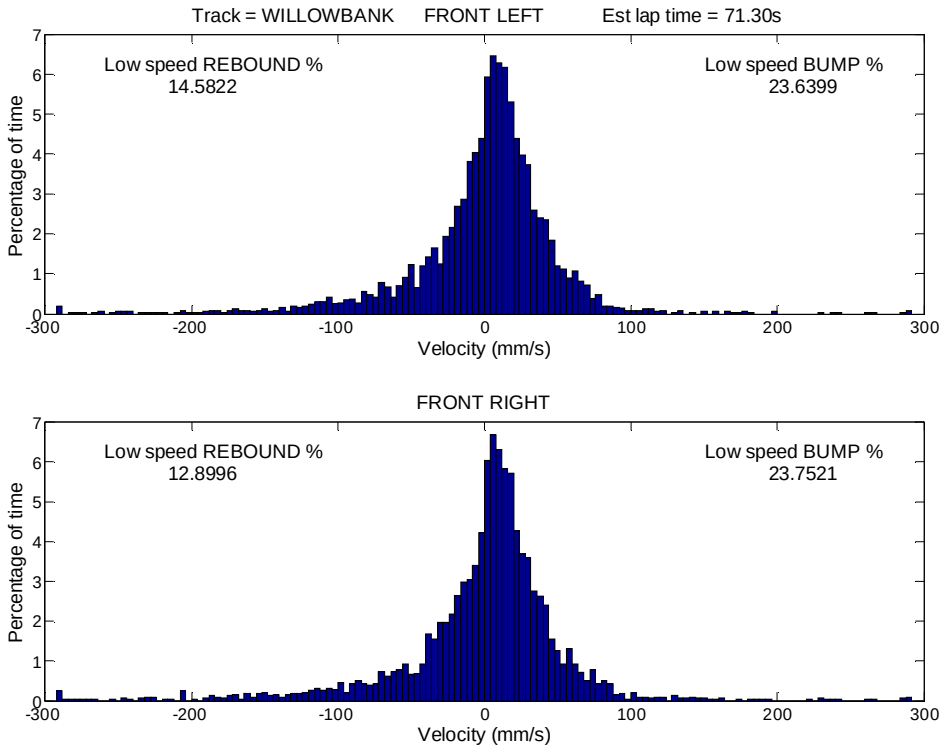

Figure 7-2: Damper histogram of front damper for lap time optimised results

Chapter 8 – Conclusion

8.1 Conclusion

The objectives of this thesis were to demonstrate and evaluate a variety of different methods which can be used to optimise the damping characteristics of a V8 Supercar, and this is what has been done.

The way in which dampers can affect a vehicle is often misunderstood and confusing. This paper has exemplified this, as each of the different damper optimisation tools and procedures have given quite different results to what is seemingly the same problem. Therefore it is very important that the race car's engineer has a good understanding of the dynamics of the system, so that they can critically evaluate the results that are obtained. This paper has provided the tools to do just that. Computer simulation will not replace the role of the vehicle's engineer, as experience is still required in order to correctly interpret the results, and translate these to a competitive race car.

What has been sought throughout this paper is to find the best method of choosing damper curves. Most methods are iterative procedures, the best of which is damper histogram analysis. This is because it does not just rely on the mathematics of the system, but also accounts for other less quantifiable objectives, such as maintaining driveability of the vehicle, and creating adequate heat in the tyres. It is also one of the quicker analyses to perform, which can be very important during a race meeting.

Damper histogram analysis can be performed using the logged data of the vehicle, however this can be quite cumbersome. A much better method of achieving this is through the use of an accurate vehicle dynamics program such as ChassisSim. This program allows optimisation of the dampers before arriving at the track. This means that the limited testing and practice time available to race teams can be put to better use by studying a different area of the vehicle.

By employing the techniques studied in this thesis, race teams can not only save a lot of money by reducing the amount of track testing required, but they can also put themselves at a big advantage relative to their competitors for the race meeting by arriving with a car which is already at close to optimal damper se-tup.

8.2 Future Work

After more than 100 years of research, the tuning of a race car's dampers is still considered by many to be more of an art than a science. As such, there is a lot of scope for future research in this field.

Following on from this thesis in particular, future work needs to be carried out to further increase the understanding of the optimal characteristics for a damper histogram. This may mean collecting data of histograms of the rear dampers of a V8 Supercar, and attempting to find patterns in these. It may also mean conducting a mathematical

analysis to further justify the damper histogram rules that are already being used for the front of a V8 Supercar.

Another emerging area of race car damping is the concept of frequency selective dampers. These rely on the fact that undesirable body motions occur at a lower frequency than the motions of the tyre following the road. By being frequency selective, these dampers can supply a higher damping force to minimise body roll, and a much lower force to allow high frequency movements. To this date, very little research has been conducted on these, and there is a limited amount known about whether these can be used to improve vehicle performance.

References

[1] Zhang, Z., Yu, J., "Design Process of a Double Wish-Bone Suspension" *Proceedings of the 2008 SAE Interntional Powertrains, Fuels and Lubricants Congress*, Shanghai, China, 23-25 June 2008.

[2] 2008, V8 Supercars, "V8 Supercar Operations Manual", *The Official Website of V8 Supercars Australia*. [Online] [Cited: 10th October 2008] http://www.v8supercars.com.au/content/tech/v8_supercar_operations_manual_/.

[3] Dixon, J.C., *The Shock Absorber Handbook*, John Wiley and Sons, West Sussex 2007.

[4] Karnopp, D., "Active and Semi-Active Vibration Isolation", *Journal of Mechanical Design*, **117**, 177-185 (1995)

[5] Ahmed, A.K.W., "An Equivalent Linearization Technique for the Frequency Response Analysis of Asymmetric Dampers", *Journal of Sound and Vibration*, **153**, 537-542 (1992)

[6] Liu, Y., Shang, J., Yu, F., Li, H., "Test and Simulation of Nonlinear Dynamic Response for the Twin-Tube Hydraulic Shock Absorber", *Proceedings of the SAE 2002 World Congress*, Detroit, Michigan, 4-7 March 2002.

[7] Shawkatul, I.A.S.M., Ahmed, A.K.W., "A Comparative Study of Advanced Suspension Dampers for Vibration and Shock Isolation Performance of a Road Vehicle", *Proceedings of the 2006 SAE World Congress*, Detroit, Michigan, 3-6 April 2006.

[8] Nowlan, D., "Finding the Sweet Spot", *International Journal of Motorsport Engineering*, **18**(2), 52-58 (2008).

[9] Kowalski, D., Rao, M.D., Blough, J., Gruenberg, S., Griffiths, D., "The Effects of Different Input Excitation on the Dynamic Characterization of an Automotive Shock Absorber", *Proceedings of the 2001 Noise and Vibration Conference*, Traverse City, Michigan, 30 April - 3 May, 2001.

[10] Milliken, W. F., Milliken, D. L., *Race Car Vehicle Dynamics*, Society of Automotive Engineers, Warrendale, PA, 1995.

[11] Adams, H., *Chassis Engineering: Chassis Design, Building and Tuning for High Performance Handling,* The Bexley Publishing Group, New York, 1993.

[12] Candelpergher, A.G.M., Vetturi, D., "Development of a New Software for Racecar Suspension Kinematics", *Proceedings of the 2002 SAE Conference and Exhibition*, Indianapolis, Indianna, 2-5 December 2002.

[13] Gobbi, M., Mastinu, G., "Analytical Description and Optimization of the Dynamic Behaviour of Passively Suspended Road Vehicles", *Journal of Sound and Vibration*, **245**(3), 457-481 (2001).

[14] Ledesma, R., "Ride Performance Comparison of Trailer Suspension Systems Using Computational Methods", *Proceedings of the International Truck and Bus Exhibition*, Detroit, Michigan, 18-20 November 2002.

[15] Sugasawa, F., et al., "Electronically Controlled Shock Absorber System Used as a Road Sensor which Utilizes Supersonic Waves", *Society of Automotive Engineers* SAE Paper No. 851652, Warrendale, PA (1985).

[16] van Kasteel, R., Cheng-guo, W., Lixin, Q., Jin-zhao, L., Wen-zhang, Z., "A New Shock Absorber Model with an Application in Vehicle Dynamics Studies", *Proceedings of the 2003 SAE International Truck and Bus Meeting and Exhibition*, Fort Worth, Texas. 10-12 November 2003.

[17] Andrén, P., "Power Spectral Density Approximation of Longitudinal Road Profile", *International Journal of Vehicle Design* **40**, 2-14, (2006).

[18] Tamboli, J.A., Joshi, S.G., "Optimum Design of a Passive Suspension System of a Vehicle Subjected to Actual Random Road Excitations", Journal of Sound and Vibration, **219**(2), 193-205 (1999).

[19] Kowalczyk, H., "Damper Tuning with the use of a Seven Post Shaker Rig", *Proceedings of the SAE 2002 World Congress*, Detroit, Michigan, 4-7 March 2002.

[20] Kelly, J., Kwalczyk, H., Oral, H., "Track Simulation and Vehicle Characterization with 7 Post Testing", *Proceedings of the 2002 SAE Motorsports Engineering Conference and Exhibition*, Indianapolis, Indianna, 2-5 December 2002.

[21] Dylejko, P. "Optimisation of a Vehicle Suspension System Subject to Stochastic Excitation" Bachelor of Engineering (Mechanical), James Cook University.

[22] Nowlan, D., "Shake, Rattle and Roll", *International Journal of Motorsport Engineering*, **18**(4), 50-54 (2008).

[23] 2008 Series. *V8 Supercars Australia*. [Online] [Cited: 10th October 2008] http://www.v8supercars.com.au/v8data/2008/evnt_264/raceresult.asp?ssn=2008&ind=M&rid=881&eid=264&ts=&rDesc=Qualifying&rDay=Saturday%20%20&keepThis=true&TB_iframe=true&height=400&width=800.

[24] Deakin, A., Shovlin, A., Brooks, P., Crolla, D., "Design of a Single Seater Racing Car Suspension System. Dearborn", *Proceedings of the Motorsports Engineering Conference and Exposition*, Michigan, 16-19 November 1998.

[25] Haque, M.M., Ahmend, A.K., Sankar, S., "Simulation of Displacement Sensitive Non-Linear Dampers via Integral Formulation of Damping Force", *Journal of Sound and Vibration*, **187**(1), 95-109 (1995).

Appendix A: Excerpt from "V8 Supercars Operations Manual Rules" [2]

C 9.4 Shock Absorbers

All Cars competing in the VCS must only be fitted with any of the Shock absorbers designated in the following table:

Brand	Model			
Ohlins	TT44	TTX 40*	TT40	TTX40* MkII
Penske	8760	8765	8770	TSD-02*
Sachs**	Formula Matrix	Formula Matrix TRD*		
Koni	2822			

* Shaft through design

** Teams using the Formula Matrix must utilise the adjuster block with Part No. 001706999019

The specified Shock Absorbers will be identified by the means of detailed drawings, photographs and specifications held by TEGA/V8 Supercars.

NOTE: For clarification all shock absorbers listed must function as the manufacturer intended. Any device or part or modification which changes it functionality will deem it illegal.

The Shock Absorbers must comply with the following requirements:

9.4.1 Adjustment of any shock absorber from the cockpit is forbidden;

9.4.2 All damper units must function independently of each other, i.e. no connections are permitted between units;

9.4.3 Material may be removed from MacPherson strut towers solely in order to facilitate the use of adjustable shock absorbers;

9.4.4 The shock absorber mounts on the body/chassis may be relocated within a 20 mm radius of the approved point except where MacPherson strut suspension is specified;

9.4.5 Where MacPherson Strut suspension is specified, the shock absorber mounts must remain fixed as stated in the relevant VSD;

9.4.6 The use of electronically adjustable shock absorbers is forbidden;

9.4.7 Only one (1) shock absorber per wheel is permitted; and

9.4.8 Only four (4) shock absorber characteristics that can be adjusted from the outside of each shock absorber are permitted, but this number does not include shock absorber gas pressure adjustment.

9.4.9 For the Ford Falcon BA/BF and the Holden Commodore VY/VZ/VE models only:

9.4.9.1 The shock absorbers will be deemed to pivot and mount to the body/chassis at the same point. The location of this point must comply with all other parts of Rule C 9.4, and

9.4.9.2 The coil springs fitted to the front and rear suspension must only be mounted on the shock absorber in a "coil over" configuration, and

9.4.9.3 The shock absorber / spring assembly fitted to the front suspension must be mounted to the body/chassis as detailed in Rule C 9.4 and must attach directly to the lower wishbone.

9.4.9.4 The shock absorber / spring assembly fitted to the rear suspension must be mounted to the body/chassis as detailed in Rule C 9.4 and must attach directly to the rear axle assembly.

Appendix B: MATLAB Script

This appendix contains examples of some of the MATLAB .m files that were written in order to complete this thesis. This is not a comprehensive list of every .m file used, the remainder usually requiring only minor modifications from those presented here.

B.1 Create FRF for unsprung mass of quarter car model

```
% This MATLAB .m file determines the frequency response function of the
% unsprung mass for the 2DOF quarter car model. It graphs the results as a
% function of amplitude of response against frequency of road profile
% displacements. It will graph the response with four different damping
% coefficients, and also calculate and report the damping ratios.

clear all

% Spring and mass variables that can be altered by user

ms=345;     % Sprung mass (kg)
mu=50;      % Unsprung mass (kg)
ks=55000;   % Spring rate of suspension (N/m)
ku=305000;  % Spring rate of tyre (N/m)

% The damping coefficients (N/m/s) that can be altered by user
c1=3484;
c2=4356;
c3=5227;
c4=6098;

cu=0; % Damping coefficient of tyre (N/m/s)


% Find the damping ratios
DRC1= (c1/(2*ms))*(sqrt(ms/ks));
DRC2= (c2/(2*ms))*(sqrt(ms/ks));
DRC3= (c3/(2*ms))*(sqrt(ms/ks));
DRC4= (c4/(2*ms))*(sqrt(ms/ks));


% Solve the frequency response of the system
f=[0:0.01:15];
p=size(f);
for n=1:p(2)

  w(n)=2*pi*(f(n));

  G(n)=abs(((-ms*(w(n))^2+ks+c1*j*w(n))*(ku+j*w(n)*cu))/((-mu*(w(n))^2+...
      ku+ks+j*w(n)*(cu+c1))*(-ms*(w(n))^2+ks+c1*j*w(n))-(ks+c1*j*w(n))^2));
  H(n)=abs(((-ms*(w(n))^2+ks+c2*j*w(n))*(ku+j*w(n)*cu))/((-mu*(w(n))^2+...
      ku+ks+j*w(n)*(cu+c2))*(-ms*(w(n))^2+ks+c2*j*w(n))-(ks+c2*j*w(n))^2));
  K(n)=abs(((-ms*(w(n))^2+ks+c3*j*w(n))*(ku+j*w(n)*cu))/((-mu*(w(n))^2+...
      ku+ks+j*w(n)*(cu+c3))*(-ms*(w(n))^2+ks+c3*j*w(n))-(ks+c3*j*w(n))^2));
```

```
  L(n)=abs(((-ms*(w(n))^2+ks+c4*j*w(n))*(ku+j*w(n)*cu))/((-mu*(w(n))^2+...
      ku+ks+j*w(n)*(cu+c4))*(-ms*(w(n))^2+ks+c4*j*w(n))-(ks+c4*j*w(n))^2));
end

%Plot the results
h=plot(f,G,f,H,f,K,f,L);
set(h,'linewidth',4);
xlabel('Frequency of Base Excitation (Hz)','FontSize',18);
ylabel('Transmissibility','FontSize',18);
grid on;
h_legend=legend(['Damping Ratio = ',num2str(DRC1,'%.2f')],...
    ['Damping Ratio = ',num2str(DRC2,'%.2f')],...
    ['Damping Ratio = ',num2str(DRC3,'%.2f')],...
    ['Damping Ratio = ',num2str(DRC4,'%.2f')]);
set(h_legend,'FontSize',16);
h_title=title...
    ('Ratio of amplitude of unsprung mass to amplitude of road profile');
set(h_title,'FontSize',20);
h_axis=gca;
set(h_axis,'FontSize',16);
```

B.2 Create FRF for front unsprung mass of half car model

```
% This MATLAB file determines the frequency response function of the
% front unsprung mass for the 4DOF half car model. It graphs the results as a
% function of amplitude of response against frequency of road profile
% displacements. It will graph the response with four different damping
% coefficients, and also calculate and report the damping ratios.

clear all

% Mass variables that can be altered by user
ms=630; % Unsprung mass of half of vehicle
mu1=50; % Sprung mass of front wheel and suspension elements
mu2=83; % Sprung mass of rear wheel and suspension elements
Is=250; % Moment of inertia about centre of gravity
wdf=0.518; % Weight distribution at the front


% Vehicle length
lf=1.3; % horizontal distance between C of G and front suspension
lb=1.5; % horizontal distance between C of G and rear suspension

% Spring variables that can be altered by user
k1s=55000;   % Spring rate front suspension (N/m)
k2s=55000;   % Spring rate rear suspension (N/m)
k1u=305000; % Spring rate front tyre (N/m)
k2u=305000;  % Spring rate rear tyre (N/m)

% Damping coefficients that can be altered by user for each of the four
% cases

% Front
c1s1=3000;
c1s2=4500;
c1s3=6000;
c1s4=7500;
```

```
% Rear
c2s1=3000;
c2s2=4500;
c2s3=6000;
c2s4=7500;

c1u=0; % Damping Coefficient front tyre (N/m/s)
c2u=0; % Damping Coefficient rear tyre (N/m/s)


% Solve for FRF of case 1
c1s=c1s1;
c2s=c2s1;

%Find damping ratios
DRCF1=(c1s/(2*ms*wdf))*(sqrt(ms*wdf/(k1s)));
DRCR1=(c2s/(2*ms*(1-wdf)))*(sqrt(ms*(1-wdf)/(k2s)));

f=[0:0.01:30];
p=size(f);
for n=1:p(2)

    w(n)=2*pi*(f(n));

    % Matrix elements
    a11=-mu1*(w(n))^2+k1u+k1s+j*w(n)*(c1u+c1s);
    a12=0;
    a13=-k1s-j*w(n)*c1s;
    a14=k1s*lf+j*w(n)*c1s*lf;
    a21=0;
    a22=-mu2*(w(n))^2+k2u+k2s+j*w(n)*(c2u+c2s);
    a23=-k2s-j*w(n)*c2s;
    a24=-k2s*lb-j*w(n)*c2s*lb;
    a31=-k1s-j*w(n)*c1s;
    a32=-k2s-j*w(n)*c2s;
    a33=-ms*(w(n))^2+k1s+k2s+j*w(n)*(c1s+c2s);
    a34=-k1s*lf+k2s*lb+j*w(n)*(c2s*lb-c1s*lf);
    a41=k1s*lf+j*w(n)*c1s*lf;
    a42=-k2s*lb-j*w(n)*c2s*lb;
    a43=-k1s*lf+k2s*lb+j*w(n)*(c2s*lb-c1s*lf);
    a44=-Is*(w(n))^2+k1s*lf^2+k2s*lb^2+j*w(n)*(c1s*lf^2+c2s*lb^2);
    z1=k1u+j*w(n)*c1u;
    z2=k2u+j*w(n)*c2u;

    G(n)=abs((z1*a22*a33*a44-z1*a22*a34*a43-z1*a32*a23*a44+...
        z1*a32*a24*a43+z1*a42*a23*a34-z1*a42*a24*a33+z2*a32*a13*a44-...
        z2*a32*a14*a43-z2*a42*a13*a34+z2*a42*a14*a33)/(a11*a22*a33*a44-...
        a11*a22*a34*a43-a11*a32*a23*a44+a11*a32*a24*a43+...
        a11*a42*a23*a34-a11*a42*a24*a33-a31*a22*a13*a44+...
        a31*a22*a14*a43+a31*a42*a13*a24-a31*a42*a14*a23+...
        a41*a22*a13*a34-a41*a22*a14*a33-a41*a32*a13*a24+a41*a32*a14*a23));

end

% Case 2
c1s=c1s2;
c2s=c2s2;
DRCF2=(c1s/(2*ms*wdf))*(sqrt(ms*wdf/(k1s)));
DRCR2=(c2s/(2*ms*(1-wdf)))*(sqrt(ms*(1-wdf)/(k2s)));

f=[0:0.01:30];
p=size(f);
for n=1:p(2)

    w(n)=2*pi*(f(n));
```

```
    % Matrix elements
    a11=-mu1*(w(n))^2+k1u+k1s+j*w(n)*(c1u+c1s);
    a12=0;
    a13=-k1s-j*w(n)*c1s;
    a14=k1s*lf+j*w(n)*c1s*lf;
    a21=0;
    a22=-mu2*(w(n))^2+k2u+k2s+j*w(n)*(c2u+c2s);
    a23=-k2s-j*w(n)*c2s;
    a24=-k2s*lb-j*w(n)*c2s*lb;
    a31=-k1s-j*w(n)*c1s;
    a32=-k2s-j*w(n)*c2s;
    a33=-ms*(w(n))^2+k1s+k2s+j*w(n)*(c1s+c2s);
    a34=-k1s*lf+k2s*lb+j*w(n)*(c2s*lb-c1s*lf);
    a41=k1s*lf+j*w(n)*c1s*lf;
    a42=-k2s*lb-j*w(n)*c2s*lb;
    a43=-k1s*lf+k2s*lb+j*w(n)*(c2s*lb-c1s*lf);
    a44=-Is*(w(n))^2+k1s*lf^2+k2s*lb^2+j*w(n)*(c1s*lf^2+c2s*lb^2);
    z1=k1u+j*w(n)*c1u;
    z2=k2u+j*w(n)*c2u;

    H(n)=abs((z1*a22*a33*a44-z1*a22*a34*a43-z1*a32*a23*a44+...
        z1*a32*a24*a43+z1*a42*a23*a34-z1*a42*a24*a33+z2*a32*a13*a44-...
        z2*a32*a14*a43-z2*a42*a13*a34+z2*a42*a14*a33)/(a11*a22*a33*a44-...
        a11*a22*a34*a43-a11*a32*a23*a44+a11*a32*a24*a43+...
        a11*a42*a23*a34-a11*a42*a24*a33-a31*a22*a13*a44+...
        a31*a22*a14*a43+a31*a42*a13*a24-a31*a42*a14*a23+...
        a41*a22*a13*a34-a41*a22*a14*a33-a41*a32*a13*a24+a41*a32*a14*a23));
end

%Case 3
c1s=c1s3;
c2s=c2s3;
DRCF3=(c1s/(2*ms*wdf))*(sqrt(ms*wdf/(k1s)));
DRCR3=(c2s/(2*ms*(1-wdf)))*(sqrt(ms*(1-wdf)/(k2s)));

f=[0:0.01:30];
p=size(f);
for n=1:p(2)

    w(n)=2*pi*(f(n));

    % Matrix elements
    a11=-mu1*(w(n))^2+k1u+k1s+j*w(n)*(c1u+c1s);
    a12=0;
    a13=-k1s-j*w(n)*c1s;
    a14=k1s*lf+j*w(n)*c1s*lf;
    a21=0;
    a22=-mu2*(w(n))^2+k2u+k2s+j*w(n)*(c2u+c2s);
    a23=-k2s-j*w(n)*c2s;
    a24=-k2s*lb-j*w(n)*c2s*lb;
    a31=-k1s-j*w(n)*c1s;
    a32=-k2s-j*w(n)*c2s;
    a33=-ms*(w(n))^2+k1s+k2s+j*w(n)*(c1s+c2s);
    a34=-k1s*lf+k2s*lb+j*w(n)*(c2s*lb-c1s*lf);
    a41=k1s*lf+j*w(n)*c1s*lf;
    a42=-k2s*lb-j*w(n)*c2s*lb;
    a43=-k1s*lf+k2s*lb+j*w(n)*(c2s*lb-c1s*lf);
    a44=-Is*(w(n))^2+k1s*lf^2+k2s*lb^2+j*w(n)*(c1s*lf^2+c2s*lb^2);
    z1=k1u+j*w(n)*c1u;
    z2=k2u+j*w(n)*c2u;

    K(n)=abs((z1*a22*a33*a44-z1*a22*a34*a43-z1*a32*a23*a44+...
        z1*a32*a24*a43+z1*a42*a23*a34-z1*a42*a24*a33+z2*a32*a13*a44-...
        z2*a32*a14*a43-z2*a42*a13*a34+z2*a42*a14*a33)/(a11*a22*a33*a44-...
```

```
        a11*a22*a34*a43-a11*a32*a23*a44+a11*a32*a24*a43+...
        a11*a42*a23*a34-a11*a42*a24*a33-a31*a22*a13*a44+...
        a31*a22*a14*a43+a31*a42*a13*a24-a31*a42*a14*a23+...
        a41*a22*a13*a34-a41*a22*a14*a33-a41*a32*a13*a24+a41*a32*a14*a23));
end

% Case 4
c1s=c1s4;
c2s=c2s4;
DRCF4=(c1s/(2*ms*wdf))*(sqrt(ms*wdf/(k1s)));
DRCR4=(c2s/(2*ms*(1-wdf)))*(sqrt(ms*(1-wdf)/(k2s)));

f=[0:0.01:30];
p=size(f);
for n=1:p(2)

    w(n)=2*pi*(f(n));

    % Matrix elements
    a11=-mu1*(w(n))^2+k1u+k1s+j*w(n)*(c1u+c1s);
    a12=0;
    a13=-k1s-j*w(n)*c1s;
    a14=k1s*lf+j*w(n)*c1s*lf;
    a21=0;
    a22=-mu2*(w(n))^2+k2u+k2s+j*w(n)*(c2u+c2s);
    a23=-k2s-j*w(n)*c2s;
    a24=-k2s*lb-j*w(n)*c2s*lb;
    a31=-k1s-j*w(n)*c1s;
    a32=-k2s-j*w(n)*c2s;
    a33=-ms*(w(n))^2+k1s+k2s+j*w(n)*(c1s+c2s);
    a34=-k1s*lf+k2s*lb+j*w(n)*(c2s*lb-c1s*lf);
    a41=k1s*lf+j*w(n)*c1s*lf;
    a42=-k2s*lb-j*w(n)*c2s*lb;
    a43=-k1s*lf+k2s*lb+j*w(n)*(c2s*lb-c1s*lf);
    a44=-Is*(w(n))^2+k1s*lf^2+k2s*lb^2+j*w(n)*(c1s*lf^2+c2s*lb^2);
    z1=k1u+j*w(n)*c1u;
    z2=k2u+j*w(n)*c2u;

    L(n)=abs((z1*a22*a33*a44-z1*a22*a34*a43-z1*a32*a23*a44+...
        z1*a32*a24*a43+z1*a42*a23*a34-z1*a42*a24*a33+z2*a32*a13*a44-...
        z2*a32*a14*a43-z2*a42*a13*a34+z2*a42*a14*a33)/(a11*a22*a33*a44-...
        a11*a22*a34*a43-a11*a32*a23*a44+a11*a32*a24*a43+...
        a11*a42*a23*a34-a11*a42*a24*a33-a31*a22*a13*a44+...
        a31*a22*a14*a43+a31*a42*a13*a24-a31*a42*a14*a23+...
        a41*a22*a13*a34-a41*a22*a14*a33-a41*a32*a13*a24+a41*a32*a14*a23));
end

% Plot the results
h=plot(f,G,f,H,f,K,f,L);
set(h,'linewidth',4);
xlabel('Frequency of Base Excitation (Hz)','FontSize',18);
ylabel('Transmissibility','FontSize',18);
grid on;
h_legend=legend(['CdF = ',num2str(c1s1),'N/m',', CdR = ',num2str(c2s1),...
    'N/m','; DRF = ',num2str(DRCF1,'%.2f'),', DRR = ',...
    num2str(DRCR1,'%.2f')],['CdF = ',num2str(c1s2),'N/m',', CdR = ',...
    num2str(c2s2),'N/m','; DRF = ',num2str(DRCF2,'%.2f'),', DRR = ',...
    num2str(DRCR2,'%.2f')],['CdF = ',num2str(c1s3),'N/m',', CdR = ',...
    num2str(c2s3),'N/m','; DRF = ',num2str(DRCF3,'%.2f'),', DRR = ',...
    num2str(DRCR3,'%.2f')],['CdF = ',num2str(c1s4),'N/m',', CdR = ',...
    num2str(c2s4),'N/m','; DRF = ',num2str(DRCF4,'%.2f'),', DRR = ',...
    num2str(DRCR4,'%.2f')],'Location', 'SouthWest');
set(h_legend,'FontSize',16);
h_title=title...
('Ratio of amplitude of front unsprung mass to road profile displacements');
```

```
set(h_title,'FontSize',20);
h_axis=gca;
set(h_axis,'FontSize',16);
```

B.3 Evaluation criterion for half car model versus damping coefficient

```
% This .m file evaluates and plots the value of the "evaluation criterion"
% (R) for the half car model over a range of different damping
% coefficients. By choosing the damper with the lowest value of R, we will
% obtain maximum road holding performance for this system.
% It makes the assumption that the damping coefficient at the front and
% rear are equal.
clear all

% Model variables
ms=630;     % Sprung mass (kg)
mu1=50;      % Unsprung mass front (kg)
mu2=83;     % Unsprung mass rear (kg)
k1s=55000;   % Suspension spring rate front (N/m)
k2s=55000;      % Suspension spring rate rear (N/m)
k1u=305000;  % Spring rate of front tyre (N/m)
k2u=305000;  % Spring rate of rear tyre (N/m)
c1u=0;       % Damping coefficient of front tyre (N/m/s)
c2u=0;      % Damping coefficient of rear tyre (N/m/s)
lf=1.3;     % horizontal distance between C of G and front suspension
lb=1.5;     % horizontal distance between C of G and rear suspension
Is=250;     % Moment of inertia about centre of gravity
wdf=0.518;  % Weight distribution at the front
a=46.85*10^-4;   % Road roughness coefficient
b=0.19;          % Wavelength distribution coefficient

% Solve for R for each value of shock absorber damping coefficient
d=[1000:20:8000];
q=size(d);
h=0.01;


% Find R-value of front tyre
for m=1:q(2)
    cs(m)=d(m);
    tsum=0;

    c1s=cs(m);
    c2s=cs(m);

    hz=[1:0.01:25];
    p=size(hz);

    for n=1:p(2)

        f(n)=hz(n)-1;
        w(n)=2*pi*(f(n));

        % Matrix elements
        a11=-mu1*(w(n))^2+k1u+k1s+j*w(n)*(c1u+c1s);
        a12=0;
        a13=-k1s-j*w(n)*c1s;
        a14=k1s*lf+j*w(n)*c1s*lf;
        a21=0;
```

```
        a22=-mu2*(w(n))^2+k2u+k2s+j*w(n)*(c2u+c2s);
        a23=-k2s-j*w(n)*c2s;
        a24=-k2s*lb-j*w(n)*c2s*lb;
        a31=-k1s-j*w(n)*c1s;
        a32=-k2s-j*w(n)*c2s;
        a33=-ms*(w(n))^2+k1s+k2s+j*w(n)*(c1s+c2s);
        a34=-k1s*lf+k2s*lb+j*w(n)*(c2s*lb-c1s*lf);
        a41=k1s*lf+j*w(n)*c1s*lf;
        a42=-k2s*lb-j*w(n)*c2s*lb;
        a43=-k1s*lf+k2s*lb+j*w(n)*(c2s*lb-c1s*lf);
        a44=-Is*(w(n))^2+k1s*lf^2+k2s*lb^2+j*w(n)*(c1s*lf^2+c2s*lb^2);
        z1=k1u+j*w(n)*c1u;
        z2=k2u+j*w(n)*c2u;

        G(n)=a*exp(-b*f(n));
        Z1bar(n)=sqrt(-(a/b)*(exp(-b*(f(n)+(h/2)))-exp(-b*(f(n)-(h/2)))));

        %FRF of front unsprung mass
        Z(n)=abs((z1*a22*a33*a44-z1*a22*a34*a43-z1*a32*a23*a44+...
        z1*a32*a24*a43+z1*a42*a23*a34-z1*a42*a24*a33+z2*a32*a13*a44-...
        z2*a32*a14*a43-z2*a42*a13*a34+z2*a42*a14*a33)/(a11*a22*a33*a44-...
        a11*a22*a34*a43-a11*a32*a23*a44+a11*a32*a24*a43+...
        a11*a42*a23*a34-a11*a42*a24*a33-a31*a22*a13*a44+...
        a31*a22*a14*a43+a31*a42*a13*a24-a31*a42*a14*a23+...
        a41*a22*a13*a34-a41*a22*a14*a33-a41*a32*a13*a24+a41*a32*a14*a23));

        Z2bar(n)=Z(n)*Z1bar(n);
        sum1=(Z1bar(n)-Z2bar(n))^2;
        tsum=tsum+sum1;

    end

    answw(m)=sqrt(tsum);
    resf(m)=(answ(m)*k1u)/((ms*wdf+mu1)*9.18);

end

% Find R-value of rear tyre
for m=1:q(2)

    cs(m)=d(m);
    tsum=0;
    c1s=cs(m);
    c2s=cs(m);

    hz=[1:0.01:25];
    p=size(hz);
    for n=1:p(2)

        f(n)=hz(n)-1;
        w(n)=2*pi*(f(n));

        % Matrix elements
        a11=-mu1*(w(n))^2+k1u+k1s+j*w(n)*(c1u+c1s);
        a12=0;
        a13=-k1s-j*w(n)*c1s;
        a14=k1s*lf+j*w(n)*c1s*lf;
        a21=0;
        a22=-mu2*(w(n))^2+k2u+k2s+j*w(n)*(c2u+c2s);
        a23=-k2s-j*w(n)*c2s;
        a24=-k2s*lb-j*w(n)*c2s*lb;
        a31=-k1s-j*w(n)*c1s;
        a32=-k2s-j*w(n)*c2s;
        a33=-ms*(w(n))^2+k1s+k2s+j*w(n)*(c1s+c2s);
        a34=-k1s*lf+k2s*lb+j*w(n)*(c2s*lb-c1s*lf);
```

```
        a41=k1s*lf+j*w(n)*c1s*lf;
        a42=-k2s*lb-j*w(n)*c2s*lb;
        a43=-k1s*lf+k2s*lb+j*w(n)*(c2s*lb-c1s*lf);
        a44=-Is*(w(n))^2+k1s*lf^2+k2s*lb^2+j*w(n)*(c1s*lf^2+c2s*lb^2);
        z1=k1u+j*w(n)*c1u;
        z2=k2u+j*w(n)*c2u;

        G(n)=a*exp(-b*f(n));
        Z1bar(n)=sqrt(-(a/b)*(exp(-b*(f(n)+(h/2)))-exp(-b*(f(n)-(h/2)))));

        % FRF of rear unsprung mass
        Z(n)=abs((z1*a31*a23*a44-z1*a31*a24*a43-z1*a41*a23*a34+...
        z1*a41*a24*a33+z2*a11*a33*a44-z2*a11*a34*a43-z2*a31*a13*a44+...
        z2*a31*a14*a43+z2*a41*a13*a34-z2*a41*a14*a33)/(a11*a22*a33*a44-...
        a11*a22*a34*a43-a11*a32*a23*a44+a11*a32*a24*a43+...
        a11*a42*a23*a34-a11*a42*a24*a33-a31*a22*a13*a44+...
        a31*a22*a14*a43+a31*a42*a13*a24-a31*a42*a14*a23+...
        a41*a22*a13*a34-a41*a22*a14*a33-a41*a32*a13*a24+...
        a41*a32*a14*a23));

        Z2bar(n)=Z(n)*Z1bar(n);
        sum1=(Z1bar(n)-Z2bar(n))^2;
        tsum=tsum+sum1;

    end

    answ(m)=sqrt(tsum);
    resr(m)=(answ(m)*k2u)/((ms*(1-wdf)+mu2)*9.18);

end


% Plot the results
h=plot(d,resf,d,resr);
set(h,'linewidth',4);
xlabel('Damping coefficient (N/m/s)','FontSize',18);
ylabel('Evaluation Criterion (R)','FontSize',18);
grid on;
h_title=title('"Evaluation Criterion" for half car model');
set(h_title,'FontSize',20);
h_legend=legend('Front Tyre','Rear Tyre');
set(h_legend,'FontSize',16);
h_axis=gca;
set(h_axis,'FontSize',16);
```

B.4 Use evaluation criterion to optimise damping at the front

```
% This .m file uses a set value for the damping coefficient of the rear
% shock absorber, and evaluates the value of 'R' while the front shock
% absorber is varied.
clear all

% Model variables
ms=630;     % Sprung mass (kg)
mu1=50;      % Unsprung mass front (kg)
mu2=83;     % Unsprung mass rear (kg)
k1s=55000;   % Suspension spring rate front (N/m)
k2s=55000;      % Suspension spring rate rear (N/m)
k1u=305000;  % Spring rate of front tyre (N/m)
```

```
k2u=305000;  % Spring rate of rear tyre (N/m)
c1u=0;       % Damping coefficient of front tyre (N/m/s)
c2u=0;      % Damping coefficient of rear tyre (N/m/s)
lf=1.3;     % horizontal distance between C of G and front suspension
lb=1.5;     % horizontal distance between C of G and rear suspension
Is=250;     % Moment of inertia about centre of gravity
wdf=0.518;  % Weight distribution at the front
a=46.85*10^-4;   % Road roughness coefficient
b=0.19;          % Wavelength distribution coefficient

c2s=3000;       % Damping coefficient rear suspension


% Solve for R for each value of shock absorber damping coefficient
d=[1000:20:8000];
q=size(d);
h=0.01;


% Find R-value of front tyre
for m=1:q(2)
    cs(m)=d(m);
    tsum=0;

    c1s=cs(m);


    hz=[1:0.01:25];
    p=size(hz);

    for n=1:p(2)

        f(n)=hz(n)-1;
        w(n)=2*pi*(f(n));

        % Matrix elements
        a11=-mu1*(w(n))^2+k1u+k1s+j*w(n)*(c1u+c1s);
        a12=0;
        a13=-k1s-j*w(n)*c1s;
        a14=k1s*lf+j*w(n)*c1s*lf;
        a21=0;
        a22=-mu2*(w(n))^2+k2u+k2s+j*w(n)*(c2u+c2s);
        a23=-k2s-j*w(n)*c2s;
        a24=-k2s*lb-j*w(n)*c2s*lb;
        a31=-k1s-j*w(n)*c1s;
        a32=-k2s-j*w(n)*c2s;
        a33=-ms*(w(n))^2+k1s+k2s+j*w(n)*(c1s+c2s);
        a34=-k1s*lf+k2s*lb+j*w(n)*(c2s*lb-c1s*lf);
        a41=k1s*lf+j*w(n)*c1s*lf;
        a42=-k2s*lb-j*w(n)*c2s*lb;
        a43=-k1s*lf+k2s*lb+j*w(n)*(c2s*lb-c1s*lf);
        a44=-Is*(w(n))^2+k1s*lf^2+k2s*lb^2+j*w(n)*(c1s*lf^2+c2s*lb^2);
        z1=k1u+j*w(n)*c1u;
        z2=k2u+j*w(n)*c2u;

        G(n)=a*exp(-b*f(n));
        Z1bar(n)=sqrt(-(a/b)*(exp(-b*(f(n)+(h/2)))-exp(-b*(f(n)-(h/2)))));

        %FRF of front unsprung mass
        Z(n)=abs((z1*a22*a33*a44-z1*a22*a34*a43-z1*a32*a23*a44+...
        z1*a32*a24*a43+z1*a42*a23*a34-z1*a42*a24*a33+z2*a32*a13*a44-...
        z2*a32*a14*a43-z2*a42*a13*a34+z2*a42*a14*a33)/(a11*a22*a33*a44-...
        a11*a22*a34*a43-a11*a32*a23*a44+a11*a32*a24*a43+...
        a11*a42*a23*a34-a11*a42*a24*a33-a31*a22*a13*a44+...
        a31*a22*a14*a43+a31*a42*a13*a24-a31*a42*a14*a23+...
```

```
        a41*a22*a13*a34-a41*a22*a14*a33-a41*a32*a13*a24+a41*a32*a14*a23));

        Z2bar(n)=Z(n)*Z1bar(n);
        sum1=(Z1bar(n)-Z2bar(n))^2;
        tsum=tsum+sum1;

    end

    answ(m)=sqrt(tsum);
    resf(m)=(answ(m)*k1u)/((ms*wdf+mu1)*9.18);

end



% Plot the results
h=plot(d,resf);
set(h,'linewidth',4);
xlabel('Damping coefficient (N/m/s)','FontSize',18);
ylabel('R','FontSize',18);
grid on;
h_title=title('"Evaluation Criterion" for half car model');
set(h_title,'FontSize',20);
str='R value of front tyre';
str2=['With damping coefficient of rear suspension set at ' num2str(c2s)...
 ' N/m/s'];
h_legend=legend(strvcat(str,str2));
set(h_legend,'FontSize',16);
h_axis=gca;
set(h_axis,'FontSize',16);
```

B.5 Create damper histograms from ChassisSim logged data

```
clear all

%Loads the ChassisSim output file
load wbank_1.txt

%Loads vectors from ChassisSim output file
% 2 = time in seconds
% 7 = front left damper position in mm
% 8 = front right damper position in mm
% 9 = rear left damper position in mm
% 10 = rear right damper position in mm
time = wbank_1(:,2);
FL = wbank_1(:,7);
FR = wbank_1(:,8);
RL = wbank_1(:,9);
RR = wbank_1(:,10);
```

```
%Set the bypass velocities (in mm/s)
bpvf=15.2;
bpvr=24.1;

%FRONT LEFT

%Differentiates damper position discretely for each time step to
%create velocity vector
length=size(time);
tot=length(1);
total=tot-1;

for n=1:total;
    vel(n)=(FL(n+1)-FL(n))/(time(n+1)-time(n));
end
vel(tot)=0;

%draws histogram
figure(1);
subplot(2,1,1);
s=-290:4:290;
[N, X] = hist(vel, s);
h=bar(X, (N./sum(N))*100,1);
title('FRONT LEFT','fontsize',16);
xlabel('Velocity (mm/s)','fontsize',16);
ylabel('Percentage of time','fontsize',16);
h_axis=gca;
set(h_axis,'FontSize',14);

xpos=xlim;
ypos=ylim;

%finds and reports percentage of low speed bump
lsb=-(bpvf/2):bpvf:(bpvf*1.5);
[N, X] = hist(vel, lsb);
LSBP=(N(2)/sum(N))*100;
str='Low speed BUMP %';
str2=['            ' num2str(LSBP)];
text(xpos(2)-150,ypos(2)-1,strvcat(str,str2),'fontsize',16);


%finds and reports percentage low speed rebound
lsr=-(bpvf*1.5):bpvf:(bpvf/2);
[N, X] = hist(vel, lsr);
LSRP=(N(2)/sum(N))*100;
str='Low speed REBOUND %';
str2=['            ' num2str(LSRP)];
text(xpos(1)+40,ypos(2)-1,strvcat(str,str2),'fontsize',16);

lapt=time(tot);
text(-170,4.5,['Track = WILLOWBANK                                    '...
    '        Est lap time = ',num2str(lapt,'%.2f'),'s'
],'fontsize',16);
```

```
%Differentiates damper position discretely for each time step to
%create velocity vector


for n=1:total;
    vel(n)=(FR(n+1)-FR(n))/(time(n+1)-time(n));
end
vel(tot)=0;


%draws histogram
subplot(2,1,2);
s=-290:4:290;
[N, X] = hist(vel, s);
h=bar(X, (N./sum(N))*100,1);


title('FRONT RIGHT','fontsize',16);
xlabel('Velocity (mm/s)','fontsize',16);
ylabel('Percentage of time','fontsize',16);
h_axis=gca;
set(h_axis,'FontSize',14);

xpos=xlim;
ypos=ylim;

%finds and reports percentage of low speed bump
lsb=-(bpvf/2):bpvf:(bpvf*1.5);
[N, X] = hist(vel, lsb);
LSBP=(N(2)/sum(N))*100;
str='Low speed BUMP %';
str2=['            ' num2str(LSBP)];
text(xpos(2)-150,ypos(2)-1,strvcat(str,str2),'fontsize',16);


%finds and reports percentage low speed rebound
lsr=-(bpvf*1.5):bpvf:(bpvf/2);
[N, X] = hist(vel, lsr);
LSRP=(N(2)/sum(N))*100;
str='Low speed REBOUND %';
str2=['            ' num2str(LSRP)];
text(xpos(1)+40,ypos(2)-1,strvcat(str,str2),'fontsize',16);


%Differentiates damper position discretely for each time step to
%create velocity vector
for n=1:total;
    vel(n)=(RL(n+1)-RL(n))/(time(n+1)-time(n));
end
vel(tot)=0;


%draws histogram
figure(2);
subplot(2,1,1);
s=-290:4:290;
```

```
[N, X] = hist(vel, s);
h=bar(X, (N./sum(N))*100,1);


title('REAR LEFT','fontsize',16);
xlabel('Velocity (mm/s)','fontsize',16);
ylabel('Percentage of time','fontsize',16);
h_axis=gca;
set(h_axis,'FontSize',14);

xpos=xlim;
ypos=ylim;

%finds and reports percentage of low speed bump
lsb=-(bpvr/2):bpvr:(bpvr*1.5);
[N, X] = hist(vel, lsb);
LSBP=(N(2)/sum(N))*100;
str='Low speed BUMP %';
str2=['            ' num2str(LSBP)];
text(xpos(2)-150,ypos(2)-1,strvcat(str,str2),'fontsize',16);


%finds and reports percentage low speed rebound
lsr=-(bpvr*1.5):bpvr:(bpvr/2);
[N, X] = hist(vel, lsr);
LSRP=(N(2)/sum(N))*100;
str='Low speed REBOUND %';
str2=['            ' num2str(LSRP)];
text(xpos(1)+40,ypos(2)-1,strvcat(str,str2),'fontsize',16);


%Differentiates damper position discretely for each time step to
%create velocity vector
for n=1:total;
    vel(n)=(RR(n+1)-RR(n))/(time(n+1)-time(n));
end
vel(tot)=0;


%draws histogram
subplot(2,1,2);
s=-290:4:290;
[N, X] = hist(vel, s);
h=bar(X, (N./sum(N))*100,1);


title('REAR RIGHT','fontsize',16);
xlabel('Velocity (mm/s)','fontsize',16);
ylabel('Percentage of time','fontsize',16);
h_axis=gca;
set(h_axis,'FontSize',14);

xpos=xlim;
ypos=ylim;

%finds and reports percentage of low speed bump
```

```
lsb=-(bpvr/2):bpvr:(bpvr*1.5);
[N, X] = hist(vel, lsb);
LSBP=(N(2)/sum(N))*100;
str='Low speed BUMP %';
str2=['            ' num2str(LSBP)];
text(xpos(2)-150,ypos(2)-1,strvcat(str,str2),'fontsize',16);

%finds and reports percentage low speed rebound
lsr=-(bpvr*1.5):bpvr:(bpvr/2);
[N, X] = hist(vel, lsr);
LSRP=(N(2)/sum(N))*100;
str='Low speed REBOUND %';
str2=['            ' num2str(LSRP)];
text(xpos(1)+40,ypos(2)-1,strvcat(str,str2),'fontsize',16);
```